Efficient numerical methods
for the Biot poroelasticity system
in multilayered domains

Anna Naumovich

Vom Fachbereich Mathematik
der Universität Kaiserslautern
zur Verleihung des akademischen Grades

Doktor der Naturwissenschaften
(Doctor rerum naturalium, Dr. rer. nat.)

genehmigte Dissertation

1. Gutachter: Priv.-Doz. Dr. Oleg Iliev
2. Gutachter: Prof. Dr. Gabriel Wittum

Datum der Disputation: 02.05.2007

D 386

Acknowledgements

No man is an island, entire of itself
Every man is a piece of the continent, a part of the main ...
– John Donne

This PhD thesis is the result of three years of work, which would be impossible without the help, support and encouragement of several people. Here, I have the opportunity to express my gratitude to them.

First of all, I would like to thank Priv.-Doz. Dr. Oleg Iliev from the Fraunhofer ITWM[1] and Prof. Peter Matus from the Institute of Mathematics of NASB[2] for giving me the opportunity of doing my PhD in Kaiserslautern.

I am very grateful to my PhD supervisor Oleg Iliev, who has always been open for discussions, and was continuously supplying this work with ideas, invaluable comments and reasonable criticism. I have profited a great deal from his experience while being his PhD student.

Many thanks to Prof. Francisco Lisbona and Prof. Francisco Gaspar for the hospitality during my two weeks visit to the University of Zaragoza. Sincere thanks to Prof. Francisco Gaspar for his help and invaluable feedback on the aspects of this thesis. I owe him lots of gratitude for a fruitful collaboration and continuous support during these three years.

Special gratitude goes to Prof. Raytcho Lazarov from Texas A&M[3] University for many interesting and inspiring discussions, which lead me to deeper understanding of the subject.

I thank my colleagues from the Department Flows and Complex Structures of the Fraunhofer ITWM for friendly and supportive environment.

I would like to express my deepest gratitude to my family for unconditional love and support. I warmly thank my friends George, Monika, Alfonso, Irina, Jevgenij and Natallia for being with me in good and bad times.

---

[1]Institut für Techno- und Wirtschaftsmathematik
[2]National Academy of Sciences of Belarus
[3]Agriculture and Mechanics

Table of Contents

Chapter 1

Introduction

1.1　Background

The presence of a moving fluid in a porous medium affects its mechanical response. In the same time, the change in the mechanical state of the porous skeleton influences the behavior of the fluid inside the pores. These two coupled deformation-diffusion phenomena lie at the heart of the theory of poroelasticity. More precisely, the two key phenomena can be summarized as following:

- fluid-to-solid coupling: occurs when a change in the fluid pressure or fluid mass induces a deformation of the porous skeleton.

- solid-to-fluid coupling: occurs when modifications in the stress of the porous skeleton induce change in fluid pressure or fluid mass.

In accordance with these two phenomena, the fluid-filled porous medium acts in a time-dependent manner. Indeed, suppose that the porous medium is compressed – this will result in an increment of the fluid pressure inside the pores and consequent fluid flow. The time dependence of the fluid pressure (i.e. dissipation of the fluid pressure through the diffusive fluid flux according to the Darcy law) will induce a time dependence of the poroelastic stresses, which in turn will respond back to the fluid pressure field. Obviously, the model of such process is time dependent and, if the inertial forces are neglected, it can be considered as quasi-static.

One should underline the importance of the two-way coupling in the theory of poroelasticity. The earliest theories (see, e.g., pioneer work of Terzaghi [61]), accounted for the fluid-to-solid coupling only. In this case, the problem is mathematically much easier. It can be decoupled and solved in two stages, separately for the flow and for the stress fields. This kind of theory can model successfully some of the poroelastic processes in the case of highly compressible fluids such as air. However, when one deals with slightly compressible (or incompressible)

fluids, the solid-to-fluid coupling cannot be neglected since the changes in stress field can influence significantly the pore pressure. Maurice Biot was the first who, by means of phenomenological approach, developed a detailed mathematical theory of poroelasticity [12] which successfully incorporated the both basic phenomena mentioned above. The model proposed by Biot was subsequently re-derived via homogenization [2], [18] and mixture theory [15], [47], [56], what placed the Biot theory on a rigorously founded fundamental basis.

The theory of poroelasticity has applications to many fields in science and engineering, e.g., soil consolidation [12], [11], [19], [22], [43], [57], [60], [63], filtration [5], [9], biological soft tissue modelling [4], [24], [31], [57], including bone, cartilage, skin, arterial walls, etc. Due to the fact that often natural as well as industrial porous materials have inhomogeneous structure (which can be, in particular, layered), the need in modelling of poroelastic processes in such media is aroused by many practical applications. Examples of such media can be layered soil profiles, biological tissues or filtering materials.

1.2   Biot model

The classical quasi-static Biot poroelasticity system describes coupled elastic deformations and diffusive flow in porous medium. Porous medium is supposed to be fully saturated by a slightly compressible fluid, or almost saturated with incompressible fluid. The material comprising the porous medium is supposed to be incompressible, which means that deformations in the medium occur due to the deformations of the porous skeleton (e.g., local rearrangements of the grains with localized slipping and rolling, if the material is granular).

Suppose that the porous medium occupies the domain Ω with boundary Γ. Then the Biot model, which describes poroelastic process in Ω, can be written as a system of partial differential equations for the unknown fluid pressure $p(x,t)$ and displacement vector of the porous medium $\mathbf{u}(x,t)$, consisting of the equilibrium equation and the diffusion equation:

$$- \nabla \cdot \mathbf{S} + \nabla p = 0,$$
$$\frac{\partial}{\partial t}\left(\phi\beta p + \nabla \cdot \mathbf{u}\right) + \nabla \cdot \mathbf{V} = f(\mathbf{x}, t), \quad \mathbf{x} \in \Omega, \tag{1.1}$$

where

$$\mathbf{S} = \mu\left(\nabla\mathbf{u} + (\nabla\mathbf{u})^T\right) + \lambda\nabla \cdot \mathbf{u}\,\mathbf{I}$$

is a second order symmetric stress tensor (expressing the Hook's law), and

$$\mathbf{V} = -\frac{\kappa}{\eta}\nabla p,$$

is the fluid velocity vector (expressing the Darcy law), λ (dilation moduli) and μ (shear moduli) are Lamé coefficients of the porous medium, ϕ is the porosity,

β is the compressibility of the fluid, κ is the permeability of the porous medium, η is the viscosity of the fluid, $\mathbf{I}$ is the unit tensor, and $f(\mathbf{x}, t)$ is a source term, which describes e.g., injection process or extraction process.

The coupling first order terms in the system have the following meaning: the term ∇p in the first equation results from the additional stress in the medium coming from the fluid pressure, the term $\nabla \cdot \mathbf{u}$ in the second equation represents the additional fluid content due to local volume change.

The Biot system should be supplemented with relevant boundary and initial conditions that have clear physical meaning. For example, the pressure $p = g$ can be prescribed on part of the boundary Γ_D and "no-flow" condition $\mathbf{V} \cdot \mathbf{n} = 0$ ($\mathbf{n}$ standing for the unit normal vector to Γ, pointing outside the domain Ω) on the rest of the boundary Γ_N. For the displacement we may have $\mathbf{u} = 0$ on Γ_0 and $\mathbf{S} \cdot \mathbf{n} = \mathbf{g}$ on Γ_t that corresponds to the cases when the elastic body is clamped on Γ_0 and have prescribed traction force on Γ_t. However, one should mention that a problem with exclusively Neumann boundary conditions, namely traction and fluid flux, is ill-posed.

For the initial condition, the value $\phi\beta p + \nabla \cdot \mathbf{u}$ (what corresponds to the variation of the fluid content) at $t = 0$ should be specified.

Detailed theoretical analysis, including the well-posedness, uniqueness and existence of the solution of the Biot system can be found, for example, in [58].

1.3   Interface conditions for the Biot model

When the poroelastic processes have to be modeled in the layered porous medium, the theory must account for the discontinuities of the parameters which characterize the layers. This gives rise to the so-called interface problem for the Biot model. It means that, apart from the model itself, initial and boundary conditions, certain continuity conditions which link the solutions in the respective subdomains should be posed at the interfaces between the layers. These conditions must have a clear physical background and, moreover, be consistent with the Biot model itself.

Suppose that Γ_I is the interface between the layers of the porous medium with different properties. Several physical assumptions give rise to the conditions on Γ_I.

Under the assumption that, despite the deformation and movement of the interface, no solid mass is transported across it, the no-jump condition for the normal component of the displacement of the porous skeleton is imposed. The assumption that the subdomains do not slip with respect to each other imposes that displacements of the porous skeleton in the directions tangential to the interface are continuous across the interface. From these two assumptions, the

continuity of the displacement vector across the interface follows:

$$[\mathbf{u}] = 0, \quad \mathbf{x} \in \Gamma_I,$$

Mass conservation of the fluid phase requires the interface condition

$$[\mathbf{V} \cdot \mathbf{n}] = 0, \quad \mathbf{x} \in \Gamma_I,$$

which is the continuity of the normal component of the fluid flux across the interface. Since the deformation in the porous medium is not produced by the stress in the porous skeleton alone, but by the fluid pressure as well, the stress conservation across the interface should be written for the porous medium as a whole in the form

$$[(\mathbf{S} - p\mathbf{I}) \cdot \mathbf{n}] = 0, \quad \mathbf{x} \in \Gamma_I.$$

Under the assumption of perfect hydraulic contact, the fluid pressure p is continuous across the interface

$$[p] = 0, \quad \mathbf{x} \in \Gamma_I,$$

and this reduces the stress continuity condition to the following condition:

$$[\mathbf{S} \cdot \mathbf{n}] = 0, \quad \mathbf{x} \in \Gamma_I.$$

Summarizing, we come to the following set of the continuity conditions (see, e.g., [10, sec. 2.7.3], [14], [36]):

$$[\mathbf{u}] = 0, \ [p] = 0, \ [\mathbf{S} \cdot \mathbf{n}] = 0, \ [\mathbf{V} \cdot \mathbf{n}] = 0, \quad \mathbf{x} \in \Gamma_I. \tag{1.2}$$

In the formulae above, $\mathbf{n}$ stands for the unit normal vector to the interface and $[q]$ designates the difference between the values of the quantity q on the both sides of the interface ($q = \mathbf{u}$, p, etc.).

As it is shown in [36], the set of interface conditions (1.2) can also be derived directly from the Biot equations if they are written for a general inhomogeneous medium. The interface conditions obtained in this way are shown to be the only ones that are fully consistent with the validity of the Biot equations throughout the poroelastic continuum.

1.4   Review of the discretization methods

Due to the complexity of the Biot system, analytical solutions in closed form are available only in very special cases (see, e.g., [38], [63], [8], [7], [39]). Certainly, the situation gets complicated in the case of inhomogeneous porous media. Therefore, numerical methods are commonly used for solving the respective initial-boundary value problems.

The choice of the numerical method for the discretization of the poroelasticity system is not so obvious. The finite element method currently dominates in solving poroelasticity system, especially when dealing with complex domains or adaptive grids (see, e.g., [43], [48], [42], [45], [51], [40], [68]). Boundary element method was implemented in poroelasticity using the Laplace transform and the time stepping technique (see. e.g., [20], [21], [3], [25], [50]). Several attempts have been made to solve the system using the method of potentials (see, e.g., [13], [53], [46]). There are as well certain works on poroelasticity that apply finite difference method ([6], [9], [34], [33]). However, solutions generated by finite elements and finite differences on collocate grids often exhibit non-physical oscillations at the early stages of the time stepping (i.e., close to the initial state). To avoid this difficulty certain discretization on staggered grids have been suggested and theoretically analyzed in [34], [33] in the case when the coefficients of the poroelasticity system are smooth.

The situation is more complicated when the coefficients of the system have discontinuities along material interfaces, e.g., multilayered porous media, especially when it is essential to capture the solution near the interface in an accurate way.

Although finite element methods can be applied to the interface problems, however, they usually work on grids which resolve the interfaces (an exception is [28], where elliptic interface problems are considered), fact that imposes certain restriction on the method. Moreover, even when the grids resolve the interfaces, standard finite element methods do not provide good approximation for the flux variables. On the other hand, there is variety of successful finite difference and finite volume approaches, where the interfaces are allowed to cross the grid cells (see, e.g., [37], [44], [65], [29] and references therein).

The discretization of one-dimensional Biot model with discontinuous coefficients is derived and then analyzed in [49], [27]. Approximation of the fluxes and stresses near the interface of discontinuity was done there by means of a harmonic averaging of the coefficients. Such approach for second order elliptic equations has been developed in the 60's by Samarskii and summarized in his monograph [54]. However, this kind of approach is not applicable for the poroelasticity system in the multidimensional case due to the appearance of mixed derivatives in the elasticity part of the system.

1.5 Motivation for a multigrid method

After the discretization of a partial differential equation (PDE) or a system of PDEs, one is often left with a large sparse system of linear algebraic equations, which has to be solved. These systems are often very large since, in order to

achieve the desired accuracy of the solution, a large number of grid points is needed for the discretization. This number is especially big if the PDEs are solved in the three dimensional spaces. The solution of the respective linear system is often computationally very expansive, and requires large computational time even on the most advanced modern computers. Hence, the development of efficient solvers for such systems is of a great importance. Iterative methods for solving large sparse linear systems gained a great popularity in the recent years. However, it is well-known, that convergence of many of the classical iterative methods (like Gauss-Seidel, etc.) deteriorates when the number of unknowns increases, what often makes these methods inefficient for large systems. This fact gives a strong motivation for the development of the so-called optimal iterative solvers. For such solvers, the number of arithmetic operations needed to solve the considered problem is proportional to the number of unknowns of this problem. This means that the convergence of such solvers does not depend on the number of unknowns (or, equivalently, on the discretization grid size, if the discretized PDE is to be solved). Multigrid methodology (see, e.g. [30], [17], [64], [16]) allows one to construct efficient linear solvers for a large class of problems, including discretized elliptic PDEs (or systems of PDEs). Special extensions of the standard multigrid, including a very careful adjustment of the multigrid components, are needed to treat successfully systems which arise from the discretization of problems with strongly discontinuous coefficients. But as soon as the adjustment is done, fast convergence, which is independent of the size of the jumps, can be achieved.

1.6   Main goals and structure of the thesis

This work concerns with deriving and analyzing algorithms for the quasi-static Biot poroelasticity system in bounded multilayered domains in one and three dimensions. The main goals of the thesis are:

- in one dimension - to derive and theoretically analyze finite volume discretization of the Biot model and to efficiently solve the obtained system of linear algebraic equations.

- in three dimensions - to derive the finite volume discretization of the Biot model and to develop and apply an efficient multigrid solver for the produced system of linear algebraic equations.

The thesis is organized as follows:

In **Chapter 2**, the one-dimensional Biot model is considered. The finite volume discretization, which accounts for the discontinuous coefficients, is presented here. The obtained finite difference scheme is theoretically investigated and detailed convergence analysis is presented here as well. Next, the derivation of modified finite volume difference schemes that use the equations to improve the approximation near the interface is shown. Several numerical experiments based on the derived discretizations are performed to confirm the theory.

In **Chapter 3**, finite volume discretization of the three dimensional Biot model is presented. Here, the discretization is described in details - introduction of the control volumes on the staggered grids, integration of the governing equations and transformation of the volumetric integrals into the surface integrals; derivation of the interpolating polynomials, which are then used to obtain approximations for the fluxes. Numerical experiments, which represent convergence of the obtained discretization, are presented in the end of the Chapter.

In **Chapter 4**, we describe development of a multigrid solver for the discretized Biot model obtained in Chapter 3. This Chapter emphasizes the proper derivation of the inter-grid transfer operators. In the end, results of several numerical experiments are presented. In these experiments, convergence of the multigrid solvers based on different inter-grid transfer operators is investigated and compared to each other. In the end, real poroelastic process taking place in the two-layered porous medium is modelled by the Biot system, which is then discretized and solved with the multigrid solver.

Finally, some conclusions are drawn.

Chapter 2

Biot model in one dimension

In this chapter, the one-dimensional Biot model with discontinuous coefficients is considered. The finite difference scheme is derived by means of the finite volume method. Then, detailed theoretical analysis of the obtained discrete model is performed. Error estimates, which established convergence rates for both the pressure and the displacement unknowns are derived. Besides, modified and more accurate discretizations that give second order convergence of the fluxes are derived as well. Finally, numerical experiments of model problems that supplement the theoretical considerations conclude the chapter.

2.1 Problem formulation and its finite difference approximation

2.1.1 Continuous problem

In one dimension, the domain of consideration Ω is an interval $(0, L)$, the boundary Γ is $\{0, L\}$ and the model (1.1) is written in the following way:

$$
\begin{aligned}
-\frac{\partial}{\partial x}\left((\lambda + 2\mu)\frac{\partial u}{\partial x}\right) + \frac{\partial p}{\partial x} &= 0, \ x \in (0, L), \ t \in (0, T], \\
\frac{\partial}{\partial t}\left(\phi\beta p + \frac{\partial u}{\partial x}\right) - \frac{\partial}{\partial x}\left(\frac{\kappa}{\eta}\frac{\partial p}{\partial x}\right) &= q(x, t), \ x \in (0, L), \ t \in (0, T].
\end{aligned}
\tag{2.1}
$$

In its classical formulation, the one-dimensional Biot model describes, e.g., fluid flow and skeleton deformation caused by the constant vertical load applied on the top of the column of soil, which is bounded with rigid and impermeable bottom and lateral walls, and a top wall which is free to drain. The following boundary and initial conditions (the space axis is directed downward) supplement this model:

$$
p = 0, \ (\lambda + 2\mu)\frac{\partial u}{\partial x} = -s_0, \ \text{if } x = 0,
\tag{2.2}
$$

what means that the upper boundary is free to drain and a load with the value

s_0 is applied on it;

$$u = 0, \quad \frac{\partial p}{\partial x} = 0, \text{ if } x = L, \tag{2.3}$$

what corresponds to a rigid and impermeable lower boundary. Initial condition

$$\phi\beta p + \frac{\partial u}{\partial x} = 0, \text{ for } t = 0 \tag{2.4}$$

means that the variation in water content is zero in the beginning of the process.

Now, let us consider the case when the porous medium is not homogeneous but has a layered structure, each layer being characterized by different porosity, permeability, and Lamé coefficients. For the simplicity of presentation, let us restrict ourself to the case of only two layers, as depicted in the Figure 2.1.
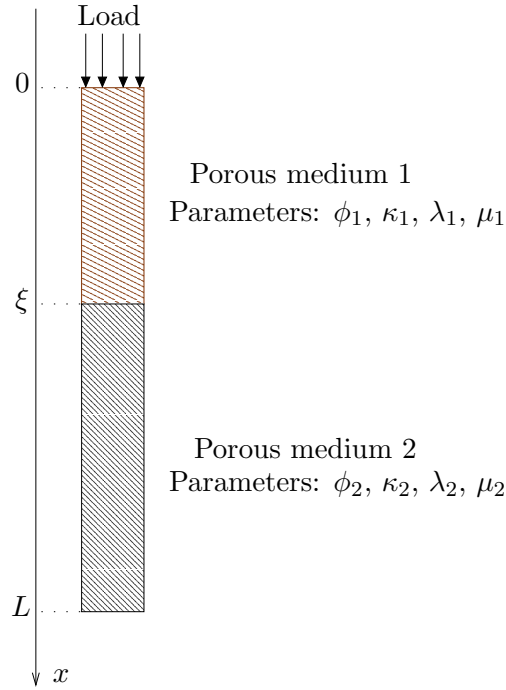
Figure 2.1: Model problem in one dimension: sketch of the domain.

In the case of the considered two-layered medium, coefficients of the governing equations are discontinuous across the interface ξ:

$$\lambda(\mathbf{x}) = \left\{ \begin{array}{ll} \lambda_1 & z < \xi, \\ \lambda_2 & z > \xi, \end{array} \right. \qquad \mu(\mathbf{x}) = \left\{ \begin{array}{ll} \mu_1 & z < \xi, \\ \mu_2 & z > \xi, \end{array} \right.$$

$$\kappa(\mathbf{x}) = \left\{ \begin{array}{ll} \kappa_1 & z < \xi, \\ \kappa_2 & z > \xi, \end{array} \right. \qquad \phi(\mathbf{x}) = \left\{ \begin{array}{ll} \phi_1 & z < \xi, \\ \phi_2 & z > \xi. \end{array} \right.$$

To complete the model, continuity conditions on the interface between different layers should supplement the system. In the assumption of a perfect contact,

the interface conditions look as follows:

$$[u] = 0, \ [p] = 0, \tag{2.5}$$

which express continuity of the displacement and of the fluid pressure across the interface. Also, one has:

$$[S] = 0, \ [V] = 0, \tag{2.6}$$

which mean continuity of the stress of the porous skeleton

$$S(x,t) = (\lambda + 2\mu)\frac{\partial u}{\partial x}, \tag{2.7}$$

and continuity of the fluid flux

$$V(x,t) = -\frac{\kappa}{\eta}\frac{\partial p}{\partial x}. \tag{2.8}$$

In the formulae (2.5), (2.6) $[\, q \,] = q|_{z=\xi+0} - q|_{z=\xi-0}$.

Now, the following dimensionless dependent and independent functions are introduced:

$$x := \frac{x}{L}, \quad \xi := \frac{\xi}{L}, \quad t := \frac{(\lambda_0 + 2\mu_0)\kappa_0 t}{\eta L^2}, \quad p := \frac{p}{s_0}, \quad u := \frac{(\lambda_0 + 2\mu_0)u}{s_0 L},$$

$$\nu := \frac{\lambda + 2\mu}{\lambda_0 + 2\mu_0}, \qquad \kappa := \frac{\kappa/\eta}{\kappa_0/\eta_0}, \quad a = \phi\beta(\lambda_0 + 2\mu_0), \quad f(x,t) = \frac{L^2\eta}{s_0\kappa_0}q(x,t).$$

Here the characteristic length L and certain reference values for the permeability, Lamé coefficients, etc. are used. Then, the governing equations together with the boundary, initial, and interface conditions can be transformed to dimensionless form:

$$
\begin{aligned}
-\frac{\partial}{\partial x}\left(\nu\frac{\partial u}{\partial x}\right) + \frac{\partial p}{\partial x} &= 0, \ x \in (0,1), \ t \in (0,T], \\[2mm]
\frac{\partial}{\partial t}\left(ap + \frac{\partial u}{\partial x}\right) - \frac{\partial}{\partial x}\left(\kappa\frac{\partial p}{\partial x}\right) &= f(x,t), \ x \in (0,1), \ t \in (0,T], \\[2mm]
\nu\frac{\partial u}{\partial x} = -1, \ p = 0, &\qquad \text{if } x = 0, \ t \in [0,T], \\[2mm]
u = 0, \ \kappa\frac{\partial p}{\partial x} = 0, &\qquad \text{if } x = 1, \ t \in [0,T], \\[2mm]
ap + \frac{\partial u}{\partial x} = 0, &\qquad \text{if } t = 0, \ x \in (0,1), \\[2mm]
[u] = 0, \ \left[\nu\frac{\partial u}{\partial x}\right] = 0, \ [p] = 0, \ \left[\kappa\frac{\partial p}{\partial x}\right] = 0, &\qquad \text{for } x = \xi, \ t \in [0,T].
\end{aligned}
\tag{2.9}
$$

Further, the possible discontinuities of the dimensionless coefficients at $x = \xi$ are distinguished:

$$\nu(x) = \begin{cases} \nu_1(x) & x < \xi, \\ \nu_2(x) & x > \xi, \end{cases} \qquad \kappa(x) = \begin{cases} \kappa_1(x) & x < \xi, \\ \kappa_2(x) & x > \xi, \end{cases}$$
$$a(x) = \begin{cases} a_1(x) & x < \xi, \\ a_2(x) & x > \xi. \end{cases} \tag{2.10}$$

For the convenience of the theoretical analysis, the problem (2.9) is transformed into a problem with homogeneous boundary conditions, by doing the following substitution:

$$u(x,t) := u(x,t) + x - 1.$$

According to this substitution, the problem (2.9) is reformulated as following:

$$-\frac{\partial}{\partial x}\left(\nu\frac{\partial u}{\partial x}\right) + \frac{\partial p}{\partial x} = 0, \ x \in (0,1), \ t \in (0,T],$$

$$\frac{\partial}{\partial t}\left(ap + \frac{\partial u}{\partial x}\right) - \frac{\partial}{\partial x}\left(\kappa\frac{\partial p}{\partial x}\right) = f(x,t), \ x \in (0,1), \ t \in (0,T],$$

$$\nu\frac{\partial u}{\partial x} = 0, \ p = 0, \qquad \text{if} \ \ x = 0, \ t \in [0,T],$$

$$u = 0, \ \kappa\frac{\partial p}{\partial x} = 0, \qquad \text{if} \ \ x = 1, \ t \in [0,T],$$

$$ap + \frac{\partial u}{\partial x} = 1, \qquad \text{if} \ \ t = 0, \ x \in (0,1),$$

$$[u] = 0, \ \left[\nu\frac{\partial u}{\partial x}\right] = 0, \ [p] = 0, \ \left[\kappa\frac{\partial p}{\partial x}\right] = 0, \qquad \text{for} \ \ x = \xi, \ t \in [0,T].$$
$$\tag{2.11}$$

2.1.2 Grids and notations for finite differences and discrete norms

The interval $(0,1)$ is split into $N > 1$ equal subintervals of size

$$h = \frac{2}{2N-1}.$$

To overcome stability difficulties, which often arise when the discretization of the Biot model is done on the collocate grids, the use of staggered grids was proposed in [34]. Two different spatial grids (so-called staggered grids), $\overline{\omega}_p$ to discretize the pressure equation and $\overline{\omega}_u$ to discretize the displacement equation, are employed:

$$\overline{\omega}_p = \{x_i : \ x_i = ih, \ i = 0, \ldots, N-1\},$$
$$\overline{\omega}_u = \{x_{i-0.5} : \ x_{i-0.5} = x_i - 0.5h, \ i = 1, \ldots, N\}.$$

Further, the grids ω_p and ω_u are also used:

$$\omega_p = \{x_i \in \overline{\omega}_p, \ i = 1, \dots, N-1\},$$
$$\omega_u = \{x_{i-0.5} \in \overline{\omega}_u, \ i = 1, \dots, N-1\}.$$

A grid in time with a step-size τ is also defined:

$$\omega_T = \{t_n : \ t_n = n\tau, \ n = 1, 2, \dots, M\}.$$

The sketch of the grids is depicted in Fig.2.2. One may look at these grids as designed to represent the values of the pressure p at the grid points $x_i \in \overline{\omega}_p$ and the values of the displacement u at the midpoints $x_{i-0.5} \in \overline{\omega}_u$ of the subintervals (x_{i-1}, x_i). According to these grids, position of the interface ξ could be represented in the form

$$\xi = x_{i_{int}-0.5} + \theta h, \tag{2.12}$$

where $0 < i_{int} < N$ is an integer and $0 \leq \theta < 1$.
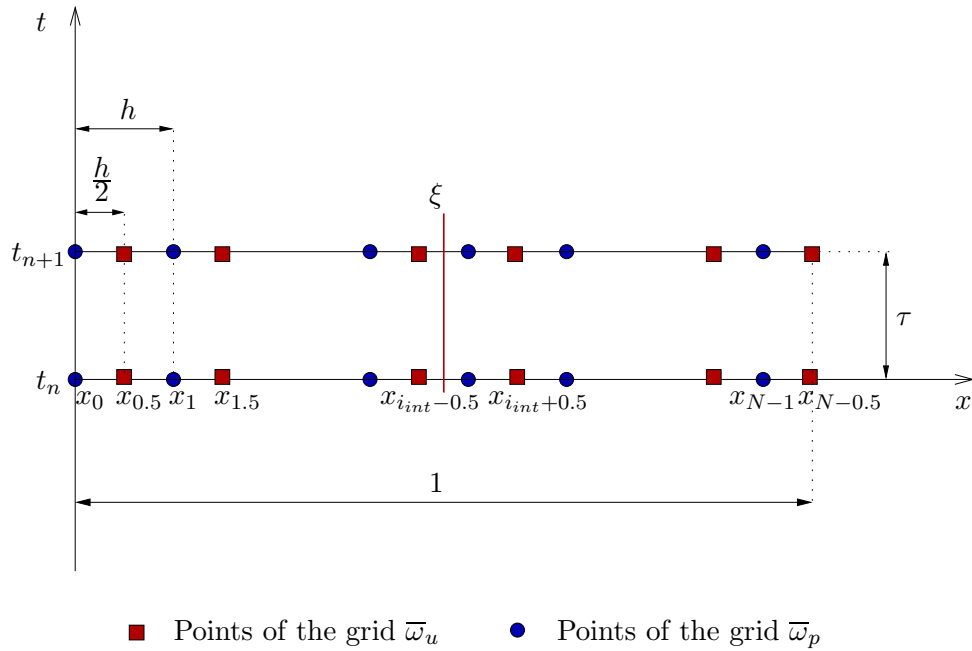

Figure 2.2: Staggered grid in one dimension.

Now, the following shorthand notations for discrete functions, defined on $\overline{\omega}_p \times \omega_T$ and $\overline{\omega}_u \times \omega_T$, respectively, are introduced:

$$u := u^n := u_i^n := u(x_{i-0.5}, t_n),$$
$$p := p^n := p_i^n := p(x_i, t_n),$$
$$p^\sigma := \sigma p^{n+1} + (1-\sigma)p^n,$$
$$\hat{p} := p^{n+1}.$$

Then, the Hilbert space $H_{\overline{\omega}_p}$ of discrete functions $p = (p_0, p_1, ..., p_{N-1})$ defined on the grid $\overline{\omega}_p$ and the Hilbert space $H_{\overline{\omega}_u}$ of functions $u = (u_1, u_2, ..., u_N)$ defined on the grid $\overline{\omega}_u$, are introduced. The respective inner products and norms in these spaces are

$$(p, q)_{\overline{\omega}_p} = \sum_{i=0}^{N-1} h p_i q_i, \ \parallel p \parallel_{\overline{\omega}_p} = (p, p)_{\overline{\omega}_p}^{\frac{1}{2}},$$

$$(u, v)_{\overline{\omega}_u} = \sum_{i=1}^{N} h u_i v_i, \ \parallel u \parallel_{\overline{\omega}_u} = (u, u)_{\overline{\omega}_u}^{\frac{1}{2}}.$$

Hilbert spaces H_{ω_p} and H_{ω_u} of grid functions $p = (p_1, p_2, ..., p_{N-1})$ and $u = (u_1, u_2, ..., u_{N-1})$ defined on the grids ω_p and ω_u respectively with following inner products and norms

$$(p, q)_{\omega_p} = \sum_{i=1}^{N-1} h p_i q_i, \ \parallel p \parallel_{\omega_p} = (p, p)_{\omega_p}^{\frac{1}{2}},$$

$$(u, v)_{\omega_u} = \sum_{i=1}^{N-1} h u_i v_i, \ \parallel u \parallel_{\omega_u} = (u, u)_{\omega_u}^{\frac{1}{2}}$$

are employed as well. Further, the standard notation for the first order backward and forward finite differences on a uniform mesh will be used (see, e.g.. [54]):

$$p_x := p_{x,i} = (p(x_{i+1}) - p(x_i))/h,$$
$$p_{\bar{x}} := p_{\bar{x},i} = (p(x_i) - p(x_{i-1}))/h.$$

Inspecting these expressions one can see that they represent central differences with respect to the points in ω_u and therefore they can be considered as quantities defined on the mesh ω_u. In a similar way one can define

$$u_x := u_{x,i} = (u(x_{i+0.5}) - u(x_{i-0.5}))/h,$$
$$u_{\bar{x}} := u_{\bar{x},i} = (u(x_{i-0.5}) - u(x_{i-1.5}))/h,$$

which represent central differences with respect to the points in ω_p and could be considered as quantities defined on the mesh ω_p.

Finally, the finite differences in time are defined:

$$u_t := u_t^n := u_t(x_{i-0.5}, t_n) = (u_i^{n+1} - u_i^n)/\tau, \ \ x_{i-0.5} \in \omega_u,$$
$$p_t := p_t^n := p_t(x_i, t_n) = (p_i^{n+1} - p_i^n)/\tau, \ \ x_i \in \omega_p.$$

2.1.3   Finite difference scheme

The differential problem (2.11) is approximated by finite volume method. First, the Biot equations are rewritten in the following way:

$$-\frac{\partial S}{\partial x} + \frac{\partial p}{\partial x} = 0, \ x \in (0,1), \ t \in (0, T],$$

$$\frac{\partial}{\partial t}\left(ap + \frac{\partial u}{\partial x}\right) + \frac{\partial V}{\partial x} = f(x,t), \ x \in (0,1), \ t \in (0, T], \tag{2.13}$$

where $S(x,t)$ and $V(x,t)$ are one-dimensional components of stress of the solid and velocity of the fluid, defined by the formulae (3.2) and (3.3), respectively.

Now, the first equation from (2.13) is integrated over the interval (x_{i-1}, x_i):

$$-\int_{x_{i-1}}^{x_i} \frac{\partial S}{\partial x} dx + \int_{x_{i-1}}^{x_i} \frac{\partial p}{\partial x} dx = 0, \tag{2.14}$$

and the second equation over the interval $(x_{i-0.5}, x_{i+0.5})$:

$$\int_{x_{i-0.5}}^{x_{i+0.5}} \frac{\partial}{\partial t}\left(ap + \frac{\partial u}{\partial x}\right) dx + \int_{x_{i-0.5}}^{x_{i+0.5}} \frac{\partial V}{\partial x} dx = \int_{x_{i-0.5}}^{x_{i+0.5}} f(x,t) dx. \tag{2.15}$$

Now, in accordance with the interface conditions (2.5), (2.6), some integrals from (2.14), (2.15) can be rewritten as:

$$\int_{x_{i-1}}^{x_i} \frac{\partial S}{\partial x} dx = S(x_i) - S(x_{i-1}), \quad \int_{x_{i-0.5}}^{x_{i+0.5}} \frac{\partial V}{\partial x} dx = V(x_{i+0.5}) - V(x_{i-0.5}),$$

$$\int_{x_{i-1}}^{x_i} \frac{\partial p}{\partial x} dx = p(x_i) - p(x_{i-1}), \quad \int_{x_{i-0.5}}^{x_{i+0.5}} \frac{\partial u}{\partial x} dx = u(x_{i+0.5}) - u(x_{i-0.5}). \tag{2.16}$$

Using the rectangular quadratic formula, one can write

$$\int_{x_{i-0.5}}^{x_{i+0.5}} \frac{\partial}{\partial t}(ap) dx \approx \frac{\partial p}{\partial t}(x_i) \int_{x_{i-0.5}}^{x_{i+0.5}} a(x) dx \approx a_i \frac{p_{i+1} - p_i}{\tau},$$

where

$$a_i = \int_{x_{i-0.5}}^{x_{i+0.5}} a(x) dx. \tag{2.17}$$

In order to approximate the fluxes $S(x)$ and $V(x)$ in the formulae (2.16) in the necessary grid points, one integrates the equation

$$\frac{S(x)}{\nu} = \frac{\partial u}{\partial x}$$

over the interval $(x_{i-0.5}, x_{i+0.5})$, and the equation

$$\frac{V(x)}{\kappa} = -\frac{\partial p}{\partial x}$$

over the interval (x_{i-1}, x_i). This yields the following integral equations:

$$\int_{x_{i-0.5}}^{x_{i+0.5}} \frac{S(x)}{\nu} dx = \int_{x_{i-0.5}}^{x_{i+0.5}} \frac{\partial u}{\partial x} dx, \quad \int_{x_{i-1}}^{x_i} \frac{V(x)}{\kappa} dx = -\int_{x_{i-1}}^{x_i} \frac{\partial p}{\partial x} dx.$$

Then, applying formulae of approximate integrating, one can transform these equations in the following way:

$$S(x_i) \int\limits_{x_{i-0.5}}^{x_{i+0.5}} \frac{dx}{\nu(x)} \approx u_{i+0.5} - u_{i+0.5}, \quad V(x_{i-0.5}) \int\limits_{x_{i-1}}^{x_i} \frac{dx}{\kappa(x)} \approx -(p_i - p_{i-1}).$$

From these two formulae, approximating expressions for fluxes can be found:

$$S(x_i) \approx S_i = \nu_i \frac{u_{i+0.5} - u_{i-0.5}}{h}, \quad V(x_{i-0.5}) \approx V_i = -\kappa_i \frac{p_i - p_{i-1}}{h}.$$

where

$$\nu_i = \nu^H(x_i) = \left(\frac{1}{h} \int\limits_{x_{i-0.5}}^{x_{i+0.5}} \frac{dx}{\nu(x)} \right)^{-1}, \quad \kappa_i = \kappa^H(x_{i-0.5}) = \left(\frac{1}{h} \int\limits_{x_{i-1}}^{x_i} \frac{dx}{\kappa(x)} \right)^{-1}. \tag{2.18}$$

Expressions in (2.18) are called formulae of the harmonic averaging. For more details, see [54, Chapter 3, pp.150–155] or [26].

After the substitution of approximate expressions for all the integrals into balance equations (2.14) and (2.15), weighted discretization in time with the weight parameter σ is applied. This procedure produces a finite difference scheme, which is a discrete analogue of the problem (2.11). Using non-index notations, this scheme for the discrete approximate solution $u = u_i^n$ at point $(x_{i-0.5}, t_n) \in \omega_u \times \omega_T$ and $p = p_i^n$ at grid point $(x_i, t_n) \in \omega_p \times \omega_T$ can be written in the following way:

$$-\frac{\nu}{h}\hat{u}_x + \hat{p}_{\bar{x}} = 0 \ , \quad x = x_{0.5} \ (i = 1), \ \ t \in \omega_T,$$

$$-(\nu\hat{u}_{\bar{x}})_x + \hat{p}_{\bar{x}} = 0 \ , \quad x = x_{i-0.5} \in \omega_u \backslash \{x_{0.5}\} \ (i = 2, \dots, N-1), \ \ t \in \omega_T,$$

$$(ap + u_x)_t - (\kappa p_{\bar{x}}^\sigma)_x = f^\sigma, \quad x = x_i \in \omega_p \backslash \{x_{N-1}\} \ (i = 1, \dots, N-2), \ \ t \in \omega_T,$$

$$(ap + u_x)_t - \frac{\kappa}{h}p_{\bar{x}}^\sigma = f^\sigma, \quad x = x_{N-1} \ (i = N-1), \ \ t \in \omega_T,$$

$$p_0 = 0, \ \ u_N = 0, \quad t \in \omega_T,$$

$$ap + u_x = 1, \quad x = x_i \in \bar{\omega}_p \ (i = 1, \dots, N-1), \ \ t = 0, \tag{2.19}$$

where coefficients a, κ, and ν are calculated according to the formulae (2.17) and (2.18) and the right hand side f is defined as:

$$f_i(t) = \frac{1}{h} \int\limits_{x_{i-0.5}}^{x_{i+0.5}} f(x,t)dx. \tag{2.20}$$

2.1.4 Operator form of the difference scheme

The discrete divergence operator $D : H_{\omega_u} \to H_{\omega_p}$ is defined in the following way:

$$(Du, p)_{\omega_p} = \sum_{i=1}^{N-2} (u(x_{i+0.5}) - u(x_{i-0.5}))p(x_i) - u(x_{N-1.5})p(x_{N-1}), \ \forall u \in H_{\omega_u}, \forall p \in H_{\omega_p}.$$

The discrete gradient operator $G : H_{\omega_p} \to H_{\omega_u}$ is defined as following:

$$(Gp, u)_{\omega_u} = p(x_1)u(x_{0.5}) + \sum_{i=2}^{N-1} (p(x_i) - p(x_{i-1}))u(x_{i-0.5}), \ \forall p \in H_{\omega_p}, \forall u \in H_{\omega_u}.$$

The right hand sides of these formulae give rise to bilinear forms on the spaces of discrete functions and define linear operators, which could be expressed in a component form as:

$$x_i \in \omega_p : \ (Du)_i = (Du)(x_i)$$
$$= \begin{cases} u_{x,i} := (u(x_{i+0.5}) - u(x_{i-0.5}))/h, & \text{for } i = 1, \dots, N-2, \\ -u(x_{N-1.5})/h, & \text{for } i = N-1; \end{cases}$$

$$\tag{2.21}$$

$$x_{i-0.5} \in \omega_u : \ (Gp)_i = (Gp)(x_{i-0.5})$$
$$= \begin{cases} p(x_1)/h, & \text{for } i = 1, \\ p_{\bar{x},i} := (p(x_i) - p(x_{i-1}))/h, & \text{for } i = 2, \dots, N-1. \end{cases}$$

Using summation by parts, one can easily show that for any discrete functions $u \in H_{\omega_u}$ and $p \in H_{\omega_p}$, the operators G and D are adjoint to each other in the sense that

$$(Gp, u)_{\omega_u} = -(p, Du)_{\omega_p}.$$

The operators, which represent multiplication by a scalar grid functions a, ν and κ defined by (2.17) and (2.18) in the spaces H_{ω_p} and H_{ω_u}, are defined as following:

$$Q : H_{\omega_p} \to H_{\omega_p} : \quad a \in H_{\omega_p}, \quad (Qp, q)_{\omega_p} = (ap, q)_{\omega_p} \ \ \forall p, q \in H_{\omega_p},$$
$$N : H_{\omega_p} \to H_{\omega_p} : \quad \nu \in H_{\omega_p}, \quad (Np, q)_{\omega_p} = (\nu p, q)_{\omega_p}, \ \ \forall p, q \in H_{\omega_p},$$
$$K : H_{\omega_u} \to H_{\omega_u} : \quad \kappa \in H_{\omega_u}, \quad (Ku, v)_{\omega_u} = (\kappa u, v)_{\omega_u}, \ \ \forall u, v \in H_{\omega_u}.$$

Finally, the operators A and B are introduced:

$$A : H_{\omega_u} \to H_{\omega_u} : \quad A = -GND,$$
$$B : H_{\omega_p} \to H_{\omega_p} : \quad B = -DKG.$$

It is obvious from the definition that the operators A and B are self-adjoint and positive definite in the inner products of the spaces H_{ω_u} and H_{ω_p}, respectively, and therefore they define new norms:

$$\|u\|_A = (u, u)_A^{\frac{1}{2}} = (Au, u)_{\omega_u}^{\frac{1}{2}}, \quad \|p\|_B = (p, p)_B^{\frac{1}{2}} = (Bp, p)_{\omega_p}^{\frac{1}{2}}.$$

The discrete operators defined above are invertible, the inverse operators are also self-adjoint and positive definite, and thus they also define norms. For the further analysis, some properties of the operators and operator norms introduced above, should be emphasized. These properties are given in the following lemma:

Lemma 2.1.1. *For any* $v \in H_{\omega_u}$ *and* $q \in H_{\omega_p}$, *the following inequalities are valid:*

$$\|Dv\|_{\omega_p} \leq c_\nu \|v\|_A, \quad \|Gq\|_{A^{-1}} \leq c_\nu \|q\|_{\omega_p},$$

$$\|Gq\|_{\omega_u} \leq c_\kappa \|q\|_B, \quad \|Dv\|_{B^{-1}} \leq c_\kappa \|v\|_{\omega_u}, \quad (2.22)$$

$$\|q\|_{\omega_p} \leq \sqrt{2} c_\kappa \|q\|_B, \quad \|v\|_{\omega_u} \leq \sqrt{2} c_\nu \|v\|_A,$$

where $c_\nu = \left(\min_{x \in \omega_p}\{\nu(x)\}\right)^{-1/2}$ *and* $c_\kappa = \left(\min_{x \in \omega_p}\{\kappa(x)\}\right)^{-1/2}$.

Proof. The proof of these inequalities follows form the definition of the operators D, G, A and B. By the definition of the A-norm of $v \in H_{\omega_u}$, one can write:

$$\|v\|_A^2 = (Av, v)_{\omega_u} = (-GNDv, v)_{\omega_u} = (NDv, Dv)_{\omega_p}^{\frac{1}{2}} \geq \min_{x \in \omega_p}\{\nu(x)\}(Dv, Dv)_{\omega_p},$$

which proves the first inequality. The other inequalities are obtained in the same manner. Note that the last two inequalities follow easily from the above consideration and from the discrete analogs of Poincare inequality (see, e.g. [54, p. 110–114]): $\|q\|_{\omega_p}^2 \leq 2(Gp, Gp)_{\omega_u}$. $\square$

Using the above notations, the difference scheme (2.19) can be written in an operator form: find $u^{n+1} \in H_{\omega_u}$ and $p^{n+1} \in H_{\omega_p}$ such that

$$Au^{n+1} + Gp^{n+1} = 0, \ n = 0, 1, \ldots, M - 1,$$

$$(Qp^n + Du^n)_t + Bp^\sigma = f^\sigma, \ n = 0, 1, \ldots, M - 1, \quad (2.23)$$

$$Qp^0 + Du^0 = 1, \ n = 0.$$

For smooth coefficients (e.g. single layered porous media), second order convergence in operator norms is proven in [34]. Here, a theoretical analysis of the convergence rate of the difference scheme (2.23) in the case of discontinuous coefficients is presented.

2.2 Analysis of the scheme with harmonic averaging of the coefficients

2.2.1 Stability of the finite difference scheme

The scheme for problem with discontinuous coefficients will be studied in the framework of the operator theory of finite difference schemes (see, e.g. [54, 55]).

The following proposition, which is a straightforward reformulation of the similar proposition from [34], establishes the stability of the scheme and will be used throughout this paper for deriving a priori error estimates:

Proposition 2.2.1. *If $\sigma \geq 0.5$, then the solution of the difference scheme (2.23) satisfies the following relation for any $n \geq 0$*

$$\|u^{n+1}\|_A^2 + \|p^{n+1}\|_Q^2 \leq \|u^n\|_A^2 + \|p^n\|_Q^2 + \frac{\tau}{2}\|f^\sigma\|_{B^{-1}}^2. \qquad (2.24)$$

Now, the errors in the displacement and the pressure are introduced:

$$z^n(x) = u^n(x) - u(x, t_n), \quad x \in \omega_u \quad \text{and} \quad r^n(x) = p^n(x) - p(x, t_n), \quad x \in \omega_p.$$

Obviously, the error functions z and r satisfy $r_0^{n+1} = 0$, $z_N^{n+1} = 0$ and solve the following finite difference problem:

$$
\begin{aligned}
Az^{n+1} + Gr^{n+1} &= \psi_1^{n+1}, \quad n = 0, 1, ..., M-1, \\
(Qr^n + Dz^n)_t + Br^\sigma &= \psi_2^{n+1}, \quad n = 0, 1, ..., M-1, \\
Qr^0 + Dz^0 &= \psi_2^0,
\end{aligned}
\qquad (2.25)
$$

where the discrete functions $\psi_1^{n+1} \in H_{\omega_u}$ and $\psi_2^{n+1} \in H_{\omega_p}$ are approximation (local truncation) errors for the first and second equations, respectively.

Lemma 2.2.1. *The following presentation of the local truncation error is valid:*

$$\psi_1^{n+1} = G\eta_1^{n+1}, \quad \psi_1^{n+1} \in H_{\omega_u}, \quad \eta_1 \in H_{\omega_p}, \qquad (2.26)$$

with $\quad \eta_{1,i}^{n+1} = \eta_1^{n+1}(x_i) = \nu_i u_{\bar{x},i+1}^{n+1} - \nu(x_i)\dfrac{\partial u}{\partial x}(x_i, t_{n+1})$, *and*

$$\psi_2^{n+1} = D\eta_2^n + \tilde{\psi}_2^{n+1}, \quad \tilde{\psi}_2^{n+1} \in H_{\omega_p}, \quad \eta_2 \in H_{\omega_u}, \qquad (2.27)$$

where

$$\eta_2^n(x_{i-0.5}) = \eta_{2,i}^n = (\kappa_i p_{\bar{x},i}^\sigma - u_{t,i}^n) - \left(\kappa\frac{\partial p}{\partial x} - \frac{\partial u}{\partial t}\right)(x_{i-0.5}, t_{n+0.5}), \qquad (2.28)$$

$$\tilde{\psi}_{2,i}^n = a_i p_{i,t}^n - \frac{1}{h} \int\limits_{x_{i-0.5}}^{x_{i+0.5}} \frac{\partial}{\partial t}\left(ap(x, t_{n+0.5})\right)dx - \left(f_i^\sigma - \frac{1}{h}\int\limits_{x_{i-0.5}}^{x_{i+0.5}} f(x, t_{n+0.5})dx\right) \quad (2.29)$$

Proof. The above representation of the truncation error follows easily from the corresponding "balance" equations. Namely, the first equation (2.11) for $t = t_{n+1}$ is integrated over one interval of the mesh ω_u. Similarly, the second equation (2.11) at $t = t_{n+\frac{1}{2}}$ is integrated over one cell of the mesh ω_p. As a result, (2.26), (2.27), (2.28) and (2.29) are obtained. $\qquad \square$

If the coefficients of the problem are smooth, it is easy to show that ψ_1^n and ψ_2^n are $O(h^2 + \tau^{m_\sigma})$, where $m_\sigma = 1$ if $\sigma \neq 0.5$ and $m_\sigma = 2$ if $\sigma = 0.5$. Thus, error estimate follows easily from the stability of the scheme. In the case of interfaces the situation needs more refined analysis. Below two cases: arbitrary location of the interface position with respect to grid points and interface at a grid point, are presented.

2.2.2   Error estimate for an arbitrary position of the interface

In this case, the parameter θ in the representation $\xi = x_{i_{int}-0.5} + \theta h$ can take any value between 0 and 1. Namely, the following can be proven:

Proposition 2.2.2. *Assume that the solution $u(x,t)$ and $p(x,t)$ of the problem (2.11) is sufficiently smooth for $t > 0$ in each of the subintervals $(0, \xi)$ and $(\xi, 1)$ and u^0 and p^0 are $O(h^{\frac{3}{2}})$ approximations of $u(x,0)$ and $p(x,0)$, respectively. Then the finite difference scheme (2.23) is convergent and the following a priori error estimate holds:*

$$\|p^n - p(t_n)\|_{\omega_p} + \|u^n - u(t_n)\|_A \le C(h^{3/2} + \tau^{m_\sigma}), \qquad (2.30)$$

with a constant C independent of h and τ, $m_\sigma = 1$ if $\sigma > 0.5$ and $m_\sigma = 2$ if $\sigma = 0.5$.

Proof. First step will be to establish estimates for the errors z and r, introduced in (2.25). For any fixed n, displacement error $z = z^n$ is split in the following way

$$z = z_1 + z_2, \quad \text{where} \quad Az_1 = \psi_1. \qquad (2.31)$$

Then, using this and the equation $Az_{1,t} = \psi_{1,t}$, one gets

$$\|z_1\|_A = \|\psi_1\|_{A^{-1}}, \quad \text{and} \quad \|z_{1,t}\|_A \le C\|\psi_{1,t}\|_{A^{-1}}. \qquad (2.32)$$

Since the approximation error ψ_1 can be represented in the form (2.26), from Lemma 2.1.1 one has $\|\psi_1\|_{A^{-1}} \le c_\nu \|\eta_1\|_{\omega_p}$. Using Taylor expansion, one can easily see that $\eta_{1,i} = O(h^2)$ for all $i \ne n$ and $\eta_{1,n} = O(h)$, so $\|\eta_1\|_{\omega_p} = O(h^{3/2})$. Similar estimates are valid for the discrete time derivatives of η. Hence, from (2.32), it follows:

$$\|z_1\|_A \le \|\psi_1\|_{A^{-1}} = O(h^{3/2}) \quad \text{and} \quad \|z_{1,t}\|_A \le C\|\psi_{1,t}\|_{A^{-1}} = O(h^{3/2}). \qquad (2.33)$$

Consider now the problems for r^n and z_2^n:

$$\begin{aligned}
&Az_2^{n+1} + Gr^{n+1} = 0 \ , \ \ n = 0, 1, ..., M-1, \\
&(Qr^n + Dz_2^n)_t + Br^\sigma = \psi_2^{n+1} - Dz_{1,t}^n \ , \ \ n = 0, 1, ..., M-1
\end{aligned} \qquad (2.34)$$

If $\sigma \ge 0.5$, it follows from (2.24):

$$\|z_2^{n+1}\|_A^2 + \|r^{n+1}\|_Q^2 \le \|z_2^0\|_A^2 + \|r^0\|_Q^2 + \frac{\tau}{2} \sum_{k=0}^n \left(\|\psi_2^{k+1}\|_{B^{-1}}^2 + \|Dz_{1t}^k\|_{B^{-1}}^2 \right) \ (2.35)$$
$$n = 0, \dots, M-1.$$

Consider local truncation error ψ_2. It can be represented in the form (2.27), (2.28), where for $\theta \le 0.5$, one has

$$\begin{aligned}
\eta_{2,i} = O(h^2 + \tau^{m_\sigma}) \ \text{ if } \ i \ne n, \\
\eta_{2,i} = O(h + \tau^{m_\sigma}) \ \text{ if } \ i = n,
\end{aligned}$$

whereas for $\theta > 0.5$:

$$\eta_{2,i} = O(h^2 + \tau^{m_\sigma}) \quad \text{if} \quad i \neq n+1,$$
$$\eta_{2,i} = O(h + \tau^{m_\sigma}) \quad \text{if} \quad i = n+1.$$

Furthermore, from (2.29), one can see that $\tilde{\psi}_2 = O(h^2 + \tau^{m_\sigma})$.

Then the estimate $\|\tilde{\psi}_2\|_{\omega_p} \leq \sqrt{2} c_\kappa \|\tilde{\psi}_2\|_B$ of Lemma 2.1.1 produces $\|\tilde{\psi}_2\|_{B^{-1}} \leq \sqrt{2} c_\kappa \|\tilde{\psi}_2\|_{\omega_p}$ and taking into account the estimates for η_2 and $\tilde{\psi}_2$, one gets:

$$\|\psi_2\|_{B^{-1}} \leq \sqrt{2} c_\kappa (\|\eta_2\|_{\omega_u} + \|\tilde{\psi}_2\|_{\omega_p}) = O(\tau^{m_\sigma} + h^{3/2}). \tag{2.36}$$

Next, apply the inequalities of Lemma 2.1.1 to get $\|Dz_{1,t}\|_{B^{-1}} \leq 2 c_\kappa c_\nu \|z_{1,t}\|_A$. Further, recall (2.33) so that

$$\|Dz_{1,t}\|_{B^{-1}} \leq O(h^{3/2}) \tag{2.37}$$

and after substitution of (2.37) into (2.35), one obtains:

$$\|z_2^{n+1}\|_A^2 + \|r^{n+1}\|_Q^2 \leq \|z_2^0\|_A^2 + \|r^0\|_Q^2 + \frac{\tau}{2} \sum_{k=0}^{n} \left(\|\psi_2^{k+1}\|_{B^{-1}}^2 + c_\kappa c_\nu \|\psi_{1,t}^k\|_{A^{-1}}^2 \right). \tag{2.38}$$

Finally, since (2.33) and (2.36) are valid, from (2.38) one concludes that $\|z_2\|_A + \|r\|_Q = O(h^{3/2} + \tau^{m_\sigma})$. Since the operator Q is essentially a multiplication by a diagonal matrix, it follows $\|r\|_{\omega_p} = O(h^{3/2} + \tau^{m_\sigma})$. Furthermore, using (2.33) one gets $\|z\|_A \leq \|z_1\|_A + \|z_2\|_A = O(h^{3/2} + \tau^{m_\sigma})$. So, convergence of the pressure in the discrete L_2-norm and convergence of the displacement in A-norm are proven. $\qquad \square$

2.2.3 Error estimate when the interface is a grid node in ω_u

The results from the previous subsection are valid for an interface position, independently of its location with respect to the grid points. A better estimate can be obtained in the particular case when the interface coincides with a node of the grid ω_u, i.e., $\xi = x_{i_{int}-0.5}$ and θ (defined in (2.12)), is zero.

Proposition 2.2.3. *Assume that the solution $u(x,t)$ and $p(x,t)$ of the problem (2.11) is sufficiently smooth for $t > 0$ in each of the subintervals $(0, \xi)$ and $(\xi, 1)$ and u^0 and p^0 are $O(h^2)$ approximations of $u(x,0)$ and $p(x,0)$, respectively and assume that $\xi = x_{i_{int}-0.5}$. Then the finite difference scheme (2.23) is convergent and the following a priori error estimate holds true:*

$$\|p^n - p(t_n)\|_{\omega_p} + \|u^n - u(t_n)\|_A \leq C(h^2 + \tau^{m_\sigma}), \tag{2.39}$$

with a constant C independent of h and τ, $m_\sigma = 1$ if $\sigma > 0.5$. Here $m_\sigma = 2$ if $\sigma = 0.5$.

Proof. Consider the local truncation error of the first equation of the system. Since (2.26) is valid and since in the case when $\theta = 0$, $\eta_{1,i} = O(h^2)$ for all i, one has $\|\psi_1\|_{A^{-1}} \leq \|\eta_1\|_{\omega_p} = O(h^2)$. Thus, if one splits $z = z_1 + z_2$, where $Az_1 = \psi_1$, then one has

$$\|z_1\|_A \leq C\|\psi_1\|_{A^{-1}} = O(h^2).$$

By taking into account the equation $Az_{1,t} = \psi_{1,t}$, one gets in a similar manner the estimate $\|z_{1,t}\|_A \leq C\|\psi_{1,t}\|_{A^{-1}} = O(h^2)$.

Now, the local truncation error ψ_2 is considered. As before, $\psi_{2,i}$ is split into two parts according to the formula (2.27) with $\tilde{\psi}_2 = O(h^2 + \tau^{m_\sigma})$. A better convergence rate can be obtained largely due to the fact that for $x = x_i \in \omega_p$

$$(D\eta_2)_i = \begin{cases} O(h^2 + \tau^{m_\sigma}) & \text{for } i \neq n-1, n \\ \frac{\eta_{2,n}}{h} + O(h + \tau^{m_\sigma}) & \text{for } i = n-1, \\ -\frac{\eta_{2,n}}{h} + O(h + \tau^{m_\sigma}) & \text{for } i = n, \end{cases}$$

where $\eta_{2,n} = O(h + \tau^{m_\sigma})$. This indicates that the local truncation error near the interface is essentially $O(1)$, but due to its particular form one can still prove second order convergence.

One proceeds in several steps. First, the problem (2.34) is decoupled. Since $A = -GND$, from the first equation one has $Dz_2 = N^{-1}r$. After substitution Dz_2 into the second equation of (2.34) one obtains a problem for the pressure error r only:

$$(Q + N^{-1})r_t + Br^\sigma = \psi_2 - Dz_{1,t}. \tag{2.40}$$

Note that $Q + N^{-1}$ is an operator with a diagonal matrix.

In order to get an optimal order error estimate, the local truncation error near the interface is split. Thus, one splits $\psi_2 = \psi_2^* + \psi_2^{**}$, where

$$\psi_{2,i}^* = \begin{cases} \eta_{2,n}/h, & \text{for } i = n-1, \\ -\eta_{2,n}/h, & \text{for } i = n, \\ 0, & \text{for } i \neq n-1, n \end{cases} \quad \text{and} \quad \psi_{2,i}^{**} = O(h^2 + \tau^{m_\sigma}) \ \forall i. \tag{2.41}$$

Based on this splitting, the error for the pressure is presented in the form $r = r_1 + r_2$, where r_1 and r_2 are solutions of the following problems, respectively

$$(Q + N^{-1})r_{1,t} + Br_1^\sigma = \psi_2^{**} - Dz_{1,t}, \tag{2.42}$$

$$(Q + N^{-1})r_{2,t} + Br_2^\sigma = \psi_2^*. \tag{2.43}$$

For $\sigma \geq 0.5$ the solution of the problem (2.42) can be estimated as (see, e.g. [54])

$$\|r_1^{n+1}\|_{\omega_p} \leq \|r_1^0\|_{\omega_p} + \sum_{n'=1}^{n} \tau\|\psi_2^{**n'} - Dz_1^{n'}\|_{\omega_p} \leq \|r_1^0\|_{\omega_p} + \tau \sum_{n'=1}^{n} \left(\|\psi_2^{**n'}\|_{\omega_p} + \|Dz_{1,t}^{n'}\|_{\omega_p}\right).$$

To estimate $Dz_{1,t}$, one uses Lemma 2.1.1 and the fact $\|z_{1,t}\|_A = O(h^2)$. Then combining all these one gets

$$\|r_1^{n+1}\|_{\omega_p} = O(h^2 + \tau^{m_\sigma}). \tag{2.44}$$

Consider now the problem (2.43). In view of (2.41), one can write down $\psi_2^* = (\eta_2^*)_x$, where the grid function η_2^* is defined on $\overline{\omega}_u$ as

$$\eta_{2,i}^* = \begin{cases} 0 & = \ 0, & i = 0, \ldots, n-2, \\ h\psi_{2,n-1}^* & = \ \eta_{2,n}, & i = n-1, \\ h(\psi_{2,n-1}^* + \psi_{2,n}^*) & = \ 0, & i = n, \ldots, N-1. \end{cases}$$

Using the identity $r_2^\sigma = r_2 + \sigma\tau r_{2,t}$ and applying the operator B^{-1} to (2.43), one can rewrite this problem as

$$\left(B^{-1}(Q + N^{-1}) + \sigma\tau E\right) r_{2,t} + r_2 = B^{-1}\psi_2^*. \tag{2.45}$$

Operators B^{-1} and N^{-1} are positive definite, Q is non negative, hence $B^{-1}(Q + N^{-1})$ is positive definite, and for $\sigma \geq 0.5$ the following inequality holds

$$B^{-1}(Q + N^{-1}) + \sigma\tau E \geq \frac{\tau}{2}E.$$

In this case one can write an estimate (see, e.g. [54]) for the solution of the problem (2.45):

$$\|r_2^{n+1}\|_{\omega_p} \leq \|B^{-1}\psi_2^{*0}\|_{\omega_p} + \|B^{-1}\psi_2^{*n}\|_{\omega_p} + \sum_{n'=1}^{n} \tau \|B^{-1}\psi_{2,\bar{t}}^{*n'}\|_{\omega_p}. \tag{2.46}$$

Here $\|B^{-1}\psi_2^{*n}\|_{\omega_p}$ can be estimated as (see [54])

$$\|B^{-1}\psi_2^{*n}\|_{\omega_p} \leq c(1, |\eta_2^*|)_{\overline{\omega}_u} = ch|\eta_{2,n}| = O(h^2), \tag{2.47}$$

where c is a constant independent on discretization parameters.

It follows from (2.46), that $\|r_2^{n+1}\|_{\omega_p} = O(h^2 + \tau^{m_\sigma})$. Using this and (2.44) one gets an estimate for the pressure error:

$$\|r\|_{\omega_p} \leq \|r_1\|_{\omega_p} + \|r_2\|_{\omega_p} = O(h^2 + \tau^{m_\sigma}).$$

To complete the proof, it remains to bound $\|z_2\|_A$. Multiplying the first equation of (2.34) by z_2, one obtains:

$$\|z_2\|_A^2 = -(Gr, z_2)_{\omega_u}.$$

Taking into account that $(Gr, z_2)_{\omega_u} = -(r, Dz_2)_{\omega_p}$ and then applying ϵ-inequality and Lemma 2.1.1 one gets

$$\|z_2\|_A^2 \leq \epsilon\|r\|_{\omega_p}^2 + \frac{1}{4\epsilon}\|Dz_2\|_{\omega_p}^2 \leq \epsilon\|r\|_{\omega_p}^2 + \frac{c_\nu^2}{4\epsilon}\|z_2\|_A^2, \quad \epsilon > 0.$$

Choosing ϵ properly one can kick back the term $\|r\|_{\omega_p}^2$ so that $\|z_2\|_A = O(h^2 + \tau^{m_\sigma})$. This yields

$$\|z\|_A \leq \|z_1\|_A + \|z_2\|_A = O(h^2 + \tau^{m_\sigma})$$

and concludes the proof. $\qquad\qquad\qquad\qquad\qquad\qquad\qquad\qquad\qquad\qquad\quad\square$

2.3   Modified finite volume approximations

Two modifications of the scheme, which will allow us to achieve better approximation for both "fluxes" $S(x,t)$ and $V(x,t)$, are derived below. Recall that $S(x,t)$ in the scheme (2.19) is approximated by S_i at the grid points $\overline{\omega}_p$ and $V(x,t)$ by V_i, at the grid points $\overline{\omega}_u$, where

$$\begin{aligned} S \in H_{\omega_p}: \quad S = NDu \quad \text{for} \quad u \in H_{\omega_u}, \\ V \in H_{\omega_u}: \quad V = -KGp \quad \text{for} \quad p \in H_{\omega_p}. \end{aligned} \tag{2.48}$$

2.3.1   Finite difference scheme with an improved approximation of the stress

Suppose now that interface position coincides with one of the points from ω_p, i.e., $\xi = x_{i_{int}}$, $1 \le i_{int} \le N-1$, $x_{i_{int}} \in \omega_p$.

Consider the approximation of the flux $S(x,t)$ using harmonic averaging of the coefficient ν at the interface point $x_{i_{int}}$:

$$S_{i_{int}} = \nu_{i_{int}}^H \frac{u_{i_{int}+1} - u_{i_{int}}}{h}, \text{ where } \nu_{i_{int}}^H = \frac{2\nu_1\nu_2}{\nu_1 + \nu_2}.$$

Now one expands $u_{i_{int}}$ and $u_{i_{int}+1}$ around $x_{i_{int}}$:

$$u_{i_{int}} = u(\xi - 0, t) - \frac{h}{2}\left(\partial_x u\right)^- + \frac{h^2}{8}\left(\partial_{xx} u\right)^- - \frac{h^3}{48}\left(\partial_{xxx} u\right)^- + O(h^4), \quad (2.49)$$

$$u_{i_{int}+1} = u(\xi + 0, t) + \frac{h}{2}\left(\partial_x u\right)^+ + \frac{h^2}{8}\left(\partial_{xx} u\right)^+ + \frac{h^3}{48}\left(\partial_{xxx} u\right)^+ + O(h^4), \quad (2.50)$$

where the notations $\left(\partial_x u\right)^- = \partial_x u(\xi - 0, t)$, $\left(\partial_{xx} u\right)^+ = \partial_{xx} u(\xi + 0, t)$, etc. are used.

Now, expansions (2.49) and (2.50) are substituted into the expressions for S_n and the interface condition $u(\xi - 0, t) = u(\xi + 0, t)$ is used:

$$\begin{aligned} S_{i_{int}} &= \frac{1}{\nu_1 + \nu_2}\left(\nu_2\nu_1\left(\partial_x u\right)^- + \nu_1\nu_2\left(\partial_x u\right)^+\right) \\ &\quad + \frac{h}{4(\nu_1 + \nu_2)}\left(\nu_1\left(\partial_x\left(\nu_2\partial_x u\right)\right)^+ - \nu_2\left(\partial_x\left(\nu_1\partial_x u\right)\right)^-\right) + O(h^2). \end{aligned} \tag{2.51}$$

Next, the stress continuity condition $\nu_1\left(\partial_x u\right)^- = \nu_2\left(\partial_x u\right)^+ = S$ is used, which allows to rewrite (2.51) as

$$S_{i_{int}} = S(x_{i_{int}}, t) + \frac{h}{4(\nu_1 + \nu_2)}\left(\nu_1(\partial_x S)^+ - \nu_2(\partial_x S)^-\right) + O(h^2),$$

from which one gets the following approximation for $S(x_{i_{int}}, t)$:

$$\tilde{S}_{i_{int}} \equiv \nu_{i_{int}}^H u_{\overline{x}, i_{int}+1} - \frac{h}{4}\frac{\nu_1(\partial_x S)^+ - \nu_2(\partial_x S)^-}{\nu_1 + \nu_2} = S(x_{i_{int}}, t) + O(h^2). \quad (2.52)$$

Taking now the limits in the first equation of (2.11) from left and from right of the interface, one gets:

$$(\partial_x S)^- = (\partial_x p)^- , \quad (\partial_x S)^+ = (\partial_x p)^+$$

and the expression (2.52) can be rewritten in the form:

$$\tilde{S}_{i_{int}} = \nu_{i_{int}}^H u_{\overline{x},i_{int}+1} - \frac{h}{4(\nu_1 + \nu_2)} \left(\nu_1 (\partial_x p)^+ - \nu_2 (\partial_x p)^- \right). \tag{2.53}$$

Using the continuity of the fluid velocity $\kappa_1 (\partial_x p)^- = \kappa_2 (\partial_x p)^+ = -V$ and approximating derivatives $(\partial_x p)^-$ and $(\partial_x p)^+$ with finite differences $p_{\overline{x},i_{int}}$ and $p_{\overline{x},i_{int}+1}$, respectively, one obtains the following approximations of the flux:

$$
\begin{aligned}
\tilde{S}_{i_{int}}^1 &= \nu_{i_{int}}^H u_{\overline{x},i_{int}+1} - h \frac{\kappa_1}{4} \frac{\frac{\nu_1}{\kappa_2} - \frac{\nu_2}{\kappa_1}}{\nu_1 + \nu_2} p_{\overline{x},i_{int}}, \\
\tilde{S}_{i_{int}}^2 &= \nu_{i_{int}}^H u_{\overline{x},i_{int}+1} - h \frac{\kappa_2}{4} \frac{\frac{\nu_1}{\kappa_2} - \frac{\nu_2}{\kappa_1}}{\nu_1 + \nu_2} p_{\overline{x},i_{int}+1}.
\end{aligned}
\tag{2.54}
$$

Note that $\tilde{S}_{i_{int}}^1 = S(x_{i_{int}},t) + O(h^2)$ and $\tilde{S}_{i_{int}}^2 = S(x_{i_{int}},t) + O(h^2)$.

The above discussion results in the following modifications of the scheme (2.23):

$$Au^{n+1} + \tilde{K}Gp^{n+1} = 0, \; n = 0,1,\ldots,M-1,$$

$$(p^n + Du^n)_t + Bp^\sigma = f^\sigma, \; n = 0,1,\ldots,M-1, \tag{2.55}$$

$$Qp^0 + Du^0 = 1, \; n = 0,$$

where the operator $\tilde{K} : H_{\omega_u} \rightarrow H_{\omega_u}$ is defined as

$$
(\tilde{K}u)_i = \begin{cases}
u_i, & \text{for } i \neq i_{int}, i_{int}+1, \\
\left(1 + \frac{\kappa_1}{4} \frac{\frac{\nu_1}{\kappa_2} - \frac{\nu_2}{\kappa_1}}{\nu_1 + \nu_2} \right) u_i, & \text{for } i = i_{int}, \\
\left(1 - \frac{\kappa_2}{4} \frac{\frac{\nu_1}{\kappa_2} - \frac{\nu_2}{\kappa_1}}{\nu_1 + \nu_2} \right) u_i, & \text{for } i = i_{int}+1.
\end{cases}
\tag{2.56}
$$

Obviously, the difference between the modified scheme (2.55) and the scheme (2.23) is in the approximation of the flux $S(x,t)$ at the interface point $x_{i_{int}}$. As a consequence, the approximation of the first equation of the system (2.11) has changed in the two neighboring to the interface points, $x_{i_{int}-0.5}$ and $x_{i_{int}+0.5}$. The modified scheme provides a second order of approximation for both stress and velocity when the interface position coincides with point $x_{i_{int}}$.

Remark 2.3.1. *The modified scheme is derived supposing that the $O(h)$ re-minder term in (2.51) is dominating the error. One can easily see from (2.54)*

that the above modifications give no improvement in the case when the parameters of the media are such that $\nu_1 \kappa_1 = \nu_2 \kappa_2$ and they give negligibly small improvement when the following inequalities hold:

$$\left| \frac{1}{4} \frac{\nu_2 - \nu_1 \frac{\kappa_1}{\kappa_2}}{\nu_1 + \nu_2} \right| << 1, \qquad \left| \frac{1}{4} \frac{\nu_2 \frac{\kappa_2}{\kappa_1} - \nu_1}{\nu_1 + \nu_2} \right| << 1. \tag{2.57}$$

2.3.2 Finite difference scheme with improved approximation of the velocity

If the interface position coincides with one of the grid points of $\overline{\omega}_u$, i.e. $\xi = x_{i_{int}-0.5}$, where $1 \leq i_{int} \leq N - 1$ is some integer, another modification of the scheme (2.23) can be derived. Similarly to the formula (2.52), one can write down the expression which approximates the fluid velocity with the second order:

$$\tilde{V}_{i_{int}} \equiv -\kappa^H_{i_{int}} p_{\overline{x}, i_{int}} - \frac{h}{4} \frac{\kappa_1 \left(\frac{\partial V}{\partial x}\right)^+_{i_{int}} - \kappa_2 \left(\frac{\partial V}{\partial x}\right)^-_{i_{int}}}{\kappa_1 + \kappa_2} = V(x_{i_{int}}, t) + O(h^2). \tag{2.58}$$

Now, taking limits in the second equation of (2.11) from left and from right of the interface, one obtains

$$(\partial_x V)^-_{i_{int}} = (f - \partial_t(a_1 p + \partial_x u))^-_{i_{int}},$$
$$(\partial_x V)^+_{i_{int}} = (f - \partial_t(a_2 p + \partial_x u))^+_{i_{int}},$$

what allows one to rewrite expression (2.60) in the form

$$\tilde{V}_{i_{int}} = -\kappa^H_{i_{int}} p_{\overline{x}, i_{int}} - \frac{h}{4(\kappa_1 + \kappa_2)} (\kappa_1(f - \partial_t(a_2 p + \partial_x u))^+_{i_{int}} - \kappa_2(f - \partial_t(a_1 p + \partial_x u))^-_{i_{int}}). \tag{2.59}$$

Then, the interface condition $\nu_1 (\partial_x u)^- = \nu_2 (\partial_x u)^+$ is used, and $(\partial_x u)^-$ and $(\partial_x u)^+$ are approximated with finite difference derivatives $u_{x, i_{int}-1}$ and $u_{x, i_{int}}$, respectively. From the expression (2.59) one can obtain approximations for $V(x, t_n)$, and $V(x, t_{n+1})$. Then, for the scheme, the linear combination $\tilde{V}^\sigma = (1 - \sigma)\tilde{V}^n + \sigma \tilde{V}^{n+1}$ is used.

In order to obtain approximation for $V(x, t_n)$, the time derivative ∂_t in the expression (2.59) is replaced with a forward difference time derivative. This gives:

$$\tilde{V}^{n,1}_{i_{int}} = -\kappa^H_{i_{int}} p_{\overline{x}, i_{int}} - \frac{h}{4(\kappa_1 + \kappa_2)} (\kappa_1 f^+_{i_{int}} - \kappa_2 f^-_{i_{int}} - \kappa_2(a_1 p_{i_{int}-1} + u_{x, i_{int}-1})_t$$
$$+ \kappa_1(a_2 p_{i_{int}-1} + \frac{\nu_1}{\nu_2} u_{x, i_{int}-1})_t),$$

$$\tilde{V}^{n,2}_{i_{int}} = -\kappa^H_{i_{int}} p_{\overline{x}, i_{int}} - \frac{h}{4(\kappa_1 + \kappa_2)} (\kappa_1 f^+_{i_{int}} - \kappa_2 f^-_{i_{int}} - \kappa_2(a_1 p_{i_{int}} + \frac{\nu_2}{\nu_1} u_{x, i_{int}})_t$$
$$+ \kappa_1 (a_2 p_{i_{int}} + u_{x, i_{int}})_t).$$

$$\tag{2.60}$$

To obtain approximation for $V(x, t_{n+1})$, one replaces ∂_t in the expression (2.59) with a backward difference time derivative and use the identity $(\,\hat{\cdot}\,)_{\overline{t}} \equiv (\,.\,)_t$. This gives:

$$\hat{\tilde{V}}^1_{i_{int}} \equiv \tilde{v}^{n+1,1}_{i_{int}} = -\kappa^H_{i_{int}} \hat{p}_{\overline{x}, i_{int}} - \frac{h}{4(\kappa_1 + \kappa_2)}(\kappa_1 \hat{f}^+_{i_{int}} - \kappa_2 \hat{f}^-_{i_{int}} - \kappa_2(a_1 p_{i_{int}-1} + u_{x, i_{int}-1})_t$$

$$+ \kappa_1(a_2 p_{i_{int}-1} + \frac{\nu_1}{\nu_2} u_{x, i_{int}-1})_t),$$

$$\hat{\tilde{V}}^2_{i_{int}} \equiv \tilde{v}^{n+1,2}_{i_{int}} = -\kappa^H_{i_{int}} \hat{p}_{\overline{x}, i_{int}} - \frac{h}{4(\kappa_1 + \kappa_2)}(\kappa_1 \hat{f}^+_{i_{int}} - \kappa_2 \hat{f}^-_{i_{int}} - \kappa_2(a_1 p_{i_{int}} + \frac{\nu_2}{\nu_1} u_{x, i_{int}})_t$$

$$+ \kappa_1(a_2 p_{i_{int}} + u_{x, i_{int}})_t). \tag{2.61}$$

According to these modified expressions for V, the equations of the (2.23) are changed just at the points $i = i_{int} - 1$ and $i = i_{int}$ so that the operator form of the modified scheme is now

$$Au^{n+1} + Gp^{n+1} = 0, \ n = 0, 1, \ldots, M-1,$$

$$\left(\tilde{Q}p^n + \tilde{N}Du^n\right)_t + Bp^\sigma = \tilde{f}^\sigma, \ n = 0, 1, \ldots, M-1, \tag{2.62}$$

$$Qp^0 + Du^0 = 1, \ n = 0.$$

The operators A, G, B and D were introduced above, $\tilde{Q} : H_{\omega_p} \to H_{\omega_p}$ and $\tilde{N} : H_{\omega_p} \to H_{\omega_p}$ are defined as

$$(\tilde{Q}p)_i = \begin{cases} a_1 p_i, & \text{for } i = 1, \ldots, i_{int} - 2, \\ \left(a_1 + \frac{1}{4}\frac{\kappa_1 a_2 - \kappa_2 a_1}{\kappa_1 + \kappa_2}\right) p_i, & \text{for } i = i_{int} - 1, \\ \left(a_2 - \frac{1}{4}\frac{\kappa_1 a_2 - \kappa_2 a_1}{\kappa_1 + \kappa_2}\right) p_i, & \text{for } i = i_{int}, \\ a_2 p_i, & \text{for } i = i_{int} + 1, \ldots, N-1, \end{cases} \tag{2.63}$$

$$(\tilde{N}q)_i = \begin{cases} q_i, & \text{for } i \neq i_{int} - 1, i_{int}, \\ \left(1 + \frac{\nu_1}{4}\frac{\frac{\kappa_1}{\nu_2} - \frac{\kappa_2}{\nu_1}}{\kappa_1 + \kappa_2}\right) q_i, & \text{for } i = i_{int} - 1, \\ \left(1 + \frac{\nu_2}{4}\frac{\frac{\kappa_2}{\nu_1} - \frac{\kappa_1}{\nu_2}}{\kappa_1 + \kappa_2}\right) q_i, & \text{for } i = i_{int}, \end{cases} \tag{2.64}$$

and the modified right hand side $\tilde{f}$ is

$$\tilde{f}_i = \begin{cases} f_i, & \text{for } i \neq i_{int} - 1, i_{int}, \\ f_i + \frac{1}{4}\frac{\kappa_1 f^+_{i_{int}} - \kappa_2 f^-_{i_{int}}}{\kappa_1 + \kappa_2}, & \text{for } i = i_{int} - 1, \\ f_i - \frac{1}{4}\frac{\kappa_1 f^+_{i_{int}} - \kappa_2 f^-_{i_{int}}}{\kappa_1 + \kappa_2}, & \text{for } i = i_{int}. \end{cases} \tag{2.65}$$

Remark 2.3.2. *One can easily see from (2.63), (2.64), (2.65), that the above modifications give no improvement in the case when the parameters of the media are such that*

$$\kappa_1 a_2 = \kappa_2 a_1, \quad \kappa_1 \nu_1 = \kappa_2 \nu_2, \quad \kappa_1 f^+_{i_{int}} = \kappa_2 f^-_{i_{int}},$$

and they give negligibly small improvement when the following inequalities hold:

$$\left| \frac{1}{4} \frac{\kappa_1 a_2 - \kappa_2 a_1}{\kappa_1 + \kappa_2} \right| << 1, \qquad \left| \frac{\nu_1}{4} \frac{\frac{\kappa_1}{\nu_2} - \frac{\kappa_2}{\nu_1}}{\kappa_1 + \kappa_2} \right| << 1,$$

$$\left| \frac{\nu_2}{4} \frac{\frac{\kappa_2}{\nu_1} - \frac{\kappa_1}{\nu_2}}{\kappa_1 + \kappa_2} \right| << 1, \qquad \left| \frac{1}{4} \frac{\kappa_1 f^+_{i_{int}} - \kappa_2 f^-_{i_{int}}}{\kappa_1 + \kappa_2} \right| << 1.$$

2.4   Numerical experiments

In this section, results of the several groups of numerical experiments are presented. In the first group, convergence of all unknowns of the system, i.e., u, p, S, V, produced by the scheme (2.19) with respect to the exact solution of the continuous problem is shown. In these experiments, the exact solution is known. Then, in the next group of experiments, problems with unknown exact solution are considered. Here, convergence of the unknowns on the sequence of the refined grids is analyzed, and distributions of some of the physical quantities are presented in the figures. In the last group, results of the comparison of the scheme (2.19) and the modified scheme (2.55) are presented. In all of the experiments, a system of linear algebraic equations had to be solved. For this, the block three-diagonal matrix algorithm (see, e.g. [54]) was implemented.

2.4.1   Example 1: convergence tests

In these tests, the numerical solution is compared to the known exact solution and the relative error in discrete L_2 - or discrete maximum norm (C-norm) are calculated according to the following formulae:

$$\|\epsilon_w\|_{L_2} = \frac{\sum\limits_{x_i \in \omega_{\bar{w}}} h |w^{ex}(x_i, t_n) - w^{app}_i|}{\max\limits_{\omega_{\bar{w}}} |w^{ex}(x_i, t_n)|},$$

$$\|\epsilon_w\|_c = \frac{\max\limits_{x_i \in \omega_{\bar{w}}} |w^{ex}(x_i, t_n) - w^{app}_i|}{\max\limits_{x_i \in \omega_{\bar{w}}} |w^{ex}(x_i, t_n)|},$$

where w^{ex} and w^{app} stand for the exact and numerical solutions, respectively and $w = \{u, p, V, S\}$. In these experiments, weight parameter $\sigma = 0.5$ so that the scheme has second order accuracy in time.

Example 1-a.

Here, the following values of the parameters are used:

$$\nu_1 = 1, \ \nu_2 = \frac{\tan{(1/12)} \tan{(10\pi/3)}}{8\pi} \approx 0.0058, \ \kappa_1 = 1,$$

$$\kappa_2 = \frac{1}{8\pi \tan{(1/12)} \tan{(10\pi/3)}} \approx 0.275, \ a_1 = 0, \ a_2 = 0, \ \text{and} \ f(x,t) = 0.$$

The position of the interface is at $\xi = 1/6$. Then an exact solution of the problem (2.11) with a different initial conditions is

$$p(x,t) = \begin{cases} \cos{(10\pi/3)} \sin(x/2)e^{-0.25t}, & x \le 1/6, \\ \sin{1/12} \cos(4\pi(1-x))e^{-0.25t}, & x > \frac{1}{6}, \end{cases}$$

$$u(x,t) = \begin{cases} -2\cos{(10\pi/3)} \cos(x/2)e^{-0.25t}, & x \le \frac{1}{6}, \\ -\dfrac{2\cos{(1/12)}}{\tan{(10\pi/3)}} \sin{(1/12)} \sin(4\pi(1-x))e^{-0.25t}, & x > 1/6. \end{cases}$$

This solution satisfies interface conditions from (2.11). The initial conditions are calculated from the above formulae at $t = 0$. Analytical expressions for the fluid velocity and for the stress of the solid are calculated from the Darcy law $V(x,t) = -\kappa \frac{\partial p(x,t)}{\partial x}$ and the stress-strain relationship $S(x,t) = \nu \frac{\partial u(x,t)}{\partial x}$, respectively. The resulting formulae are:

$$V(x,t) = \begin{cases} \cos{(10\pi/3)} \cos(x/2)e^{-0.25t}, & x \le 1/6, \\ \dfrac{\cos{(1/12)}}{8\pi \tan{(10\pi/3)}} \sin{1/12} \sin(4\pi(1-x))e^{-0.25t}, & x > 1/6, \end{cases}$$

$$S(x,t) = \begin{cases} \cos{10\pi/3} \sin(x/2)e^{-0.25t}, & x \le 1/6, \\ \sin{(1/12)} \cos(4\pi(1-x))e^{-0.25t}, & x > 1/6. \end{cases}$$

Convergence results are summarized in Tables 2.1 - 2.4. Note that the mesh size h is decreased in a way, preserving a constant value for the parameter θ in the expression $\xi = x_{n-0.5} + \theta h$. The convergence results are given for two time moments – $t = 0.1$ and $t = 1.0$.

The rate of convergence for the unknown q ($q = u, p, V, S$) is presented in each table in the last line and is calculated according to the formula

$$r_q = \frac{\ln{(\|\epsilon_{q,1}\|/\|\epsilon_{q,2}\|)}}{\ln(h_1/h_2)}, \tag{2.66}$$

where $\epsilon_{q,1}$ are $\epsilon_{q,2}$ are errors, calculated at the grids with the steps $h_1 = 1/640$ and $h_2 = 1/2560$ respectively.

Our first observation is that there is no substantial change in the errors at the monitored time moments $t = 0.1$ and $t = 1.0$. The existing theoretical error estimates for this problem (see, e.g. [34] for the case of continuous coefficients), predict some increase of the error in time. The computations show that the theoretical estimates are overestimating the error in this case.

Our second observation is that the displacement, the pressure, and the stress

$h = \tau$	$\|\epsilon_u\|_{L_2}$	r_u	$\|\epsilon_p\|_{L_2}$	r_p	$\|\epsilon_V\|_{L_2}$	r_V	$\|\epsilon_S\|_{L_2}$	r_S
1/10	0.222E-02	-	0.155E+00	-	0.130E+00	-	0.739E-01	-
1/40	0.508E-03	4.4	0.243E-01	6.4	0.153E-01	8.5	0.106E-01	7.0
1/160	0.368E-04	13.8	0.105E-02	23.1	0.789E-03	19.4	0.488E-03	21.7
1/640	0.222E-05	16.6	0.634E-04	16.6	0.639E-04	12.3	0.298E-04	16.4
1/2560	0.137E-06	16.2	0.393E-05	16.1	0.657E-05	9.7	0.185E-05	16.1
rate	-	2.0	-	2.0	-	1.6	-	2.0

Table 2.1: Example 1-a: convergence in L_2-norm at the time $t = 0.1$.

$h = \tau$	$\|\epsilon_u\|_{L_2}$	r_u	$\|\epsilon_p\|_{L_2}$	r_p	$\|\epsilon_V\|_{L_2}$	r_V	$\|\epsilon_S\|_{L_2}$	r_S
1/10	0.276E-01	-	0.559E-01	-	0.737E-01	-	0.273E-01	-
1/40	0.178E-02	15.5	0.248E-02	22.5	0.399E-02	18.5	0.156E-02	17.5
1/160	0.107E-03	16.6	0.157E-03	15.8	0.248E-03	16.1	0.973E-04	16.0
1/640	0.662E-05	16.1	0.977E-05	16.1	0.159E-04	15.6	0.607E-05	16.0
1/2560	0.413E-06	16.1	0.610E-06	16.0	0.110E-05	14.5	0.379E-06	16.0
rate	-	2.0	-	2.0	-	1.9	-	2.0

Table 2.2: Example 1-a: convergence in L_2-norm at the time $t = 1$.

$h = \tau$	$\|\epsilon_u\|_c$	r_u	$\|\epsilon_p\|_c$	r_p	$\|\epsilon_V\|_c$	r_V	$\|\epsilon_S\|_c$	r_S
1/10	0.518E-02	-	0.226E+00	-	0.322E+00	-	0.196E+00	-
1/40	0.306E-02	16.9	0.304E-01	7.4	0.833E-01	3.9	0.273E-01	7.2
1/160	0.337E-03	9.1	0.139E-02	21.9	0.470E-02	17.7	0.114E-02	23.9
1/640	0.224E-04	15.0	0.841E-04	16.5	0.107E-02	4.4	0.712E-04	16.0
1/2560	0.142E-05	15.8	0.522E-05	16.1	0.262E-03	4.1	0.442E-05	16.1
rate	-	2.0	-	2.0	-	1.0	-	2.0

Table 2.3: Example 1-a: convergence in maximum norm at the time $t = 0.1$.

converge with second order in time and in space both in L_2- and in maximum norms. The fluid velocity converges with second order in L_2-norm and with first order in maximum norm. On very coarse grids velocity converges with higher than first order in maximum norm, a possible reason is that these grids are far from the asymptotic regime. It is known that the space or time truncation error terms could dominate and thus could govern the error, depending on the set of space and time discretization parameters used. The Tables 2.3 and 2.4 also

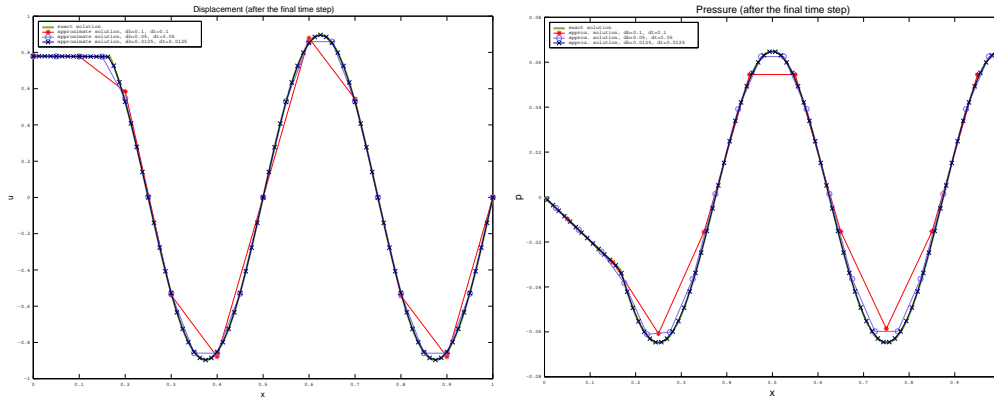| $h = \tau$	$\|\epsilon_u\|_c$	r_u	$\|\epsilon_p\|_c$	r_p	$\|\epsilon_V\|_c$	r_V	$\|\epsilon_S\|_c$	r_S
1/10	0.645E-01	-	0.963E-01	-	0.145E+00	-	0.581E-01	-
1/40	0.620E-02	10.7	0.481E-02	20.0	0.619E-02	23.4	0.277E-02	21.0
1/160	0.382E-03	16.2	0.284E-03	16.9	0.387E-03	16.0	0.151E-03	18.3
1/640	0.238E-04	16.1	0.174E-04	16.3	0.832E-04	4.7	0.913E-05	16.5
1/2560	0.148E-05	16.1	0.108E-05	16.1	0.210E-04	4.0	0.566E-06	16.1
rate	-	2.0	-	2.0	-	1.0	-	2.0

Table 2.4: Example 1-a: convergence in maximum norm at the time $t = 1$.

Figure 2.3: Example 1-a: Convergence of displacement (left), pressure (right).

illustrate such a behavior: on the coarse grids the time discretization governs the error for the velocity, while on the finer grids the space discretization error dominates.

Example 1-b.

In this example, compressible fluid (a_1 and a_2 are nonzero) is considered. The following values for the coefficients are used:

$$\nu_1 = 1, \ \nu_2 = \frac{\tan(2/3)\tan(10/3)}{10} \approx 0.0153, \ \kappa_1 = 1, \ \kappa_2 = \frac{1}{10\tan(2/3)\tan(10/3)} \approx 0.6547,$$

$$a_1 = 0.01, \ a_2 = \frac{10.1}{\tan(2/3)\tan(10/3)} \approx 66.1227, \ f(x,t) = 0.$$

Position of the interface is $\xi = 2/3$. Exact solution is

$$p(x,t) = \begin{cases} \cos(10/3)\sin(x)e^{-\frac{100}{101}t}, & x \le 2/3, \\[2mm] \sin(2/3)\cos(10(1-x))e^{-\frac{100}{101}t}, & x > 2/3, \end{cases}$$

$$u(x,t) = \begin{cases} -\cos(10/3)\cos(x)e^{-\frac{100}{101}t}, & x \le 2/3, \\[2mm] -\dfrac{\sin(2/3)\sin(10(1-x))}{10\tan(2/3)\tan(10/3)}e^{-\frac{100}{101}t}, & x > 2/3. \end{cases}$$
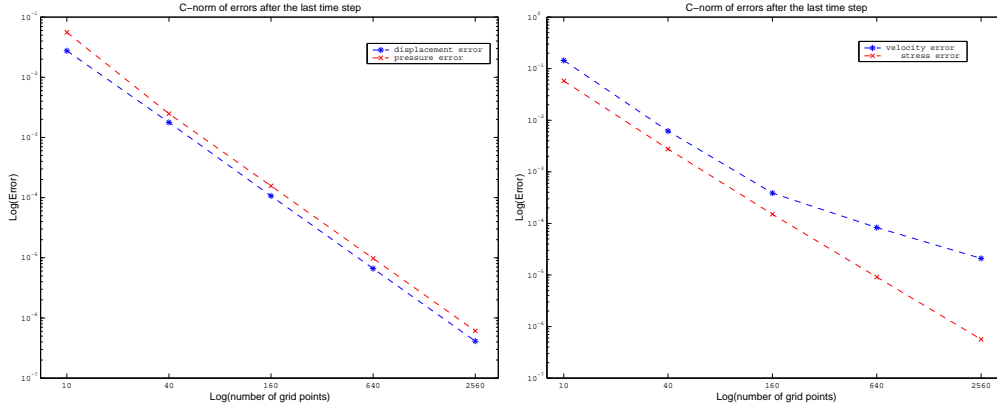
Figure 2.4: Example 1-a: Errors for pressure and displacement (left), velocity and stress (right).

$h = \tau$	$\|\epsilon_u\|_c$	ratio	$\|\epsilon_p\|_c$	ratio	$\|\epsilon_v\|_c$	ratio	$\|\epsilon_s\|_c$	ratio
1/10	0.631E-01	-	0.621E-01	-	0.301E-01	-	0.422E-01	-
1/40	0.471E-02	13.4	0.423E-02	14.7	0.183E-02	16.4	0.231E-02	18.3
1/160	0.300E-03	15.7	0.265E-03	16.0	0.107E-03	17.1	0.149E-03	15.5
1/640	0.188E-04	16.0	0.165E-04	16.0	0.206E-04	5.2	0.937E-05	15.9
1/2560	0.118E-05	16.0	0.103E-05	16.0	0.477E-05	4.3	0.586E-06	13.7
rate	-	2.0	-	2.0	-	1.1	-	1.9

Table 2.5: Example 1-b: convergence in maximum norm at the time $t = 1$.

Convergence results for Example 1-b are summarized in Tables 2.5 and 2.6. The convergence orders for the compressible case are the same as for the incompressible one, as it is illustrated in Figure 2.6. Analytical and numerical solutions, calculated on the meshes of different thickness for the displacement and pressure, are plotted in Figure 2.5.

Example 1-c.

In this test incompressible fluid is considered, but the ratio between coefficients κ_1 and κ_2 is large (about four orders of magnitude). The values for the coeffi-

$h = \tau$	$\|\epsilon_u\|_{L_2}$	r_u	$\|\epsilon_p\|_{L_2}$	r_p	$\|\epsilon_v\|_{L_2}$	r_V	$\|\epsilon_s\|_{L_2}$	r_S
1/10	0.277E-01	-	0.219E-01	-	0.967E-02	-	0.206E-01	-
1/40	0.183E-02	12.4	0.169E-02	13.0	0.530E-03	18.2	0.152E-02	13.6
1/160	0.117E-03	15.6	0.108E-03	15.6	0.324E-04	16.4	0.974E-04	15.6
1/640	0.733E-05	16.0	0.681E-05	15.9	0.217E-05	14.9	0.613E-05	15.9
1/2560	0.459E-06	16.0	0.426E-06	16.0	0.171E-06	12.7	0.384E-06	16.0
rate	-	2.0	-	2.0	-	18.3	-	2.0

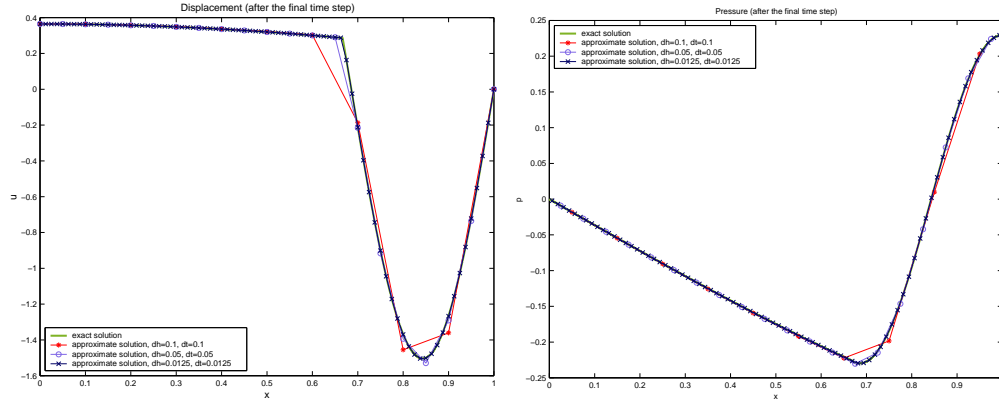Table 2.6: Example 1-b: convergence in L_2 norm at the time $t = 1$.

Figure 2.5: Example 1-b: Convergence of displacement (left), pressure (right).
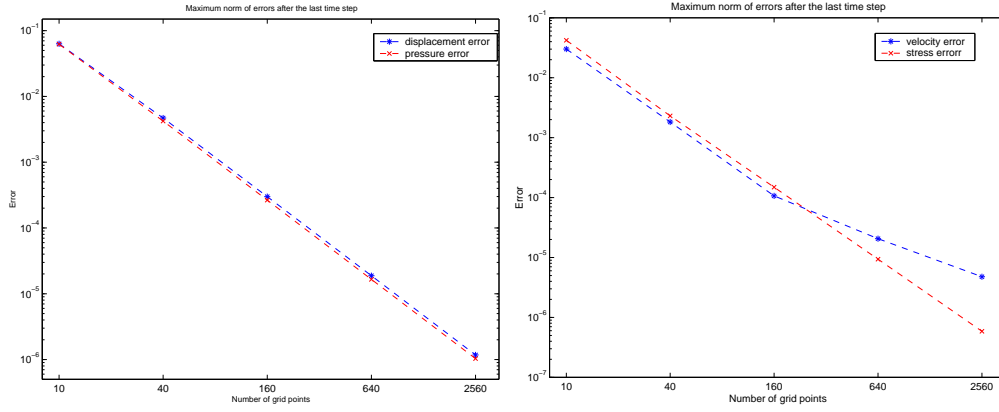

Figure 2.6: Example 1-b: Errors in maximum norm for pressure and displacement (left), velocity and stress (right).

cients are the following:

$$\nu_1 = 1, \ \nu_2 = (1/100)\tan(8/15)\tan(80/3) \approx 0.1601,$$

$$\kappa_1 = 1, \ \kappa_2 = \frac{1}{\tan(8/15)\tan(80/3)} \approx 6.2479 \cdot 10^{-4}, \ a_1 = 0, \ a_2 = 0, \ f(x,t) = 0.$$

Position of the interface is $\xi = 2/3$. The exact solution is given by

$$p(x,t) = \begin{cases} \cos(10/3)\sin(4x/5)e^{-\frac{16}{25}t}, & x \le 2/3, \\[2mm] \sin(8/15)\cos(80(1-x))e^{-\frac{16}{25}t}, & x > 2/3, \end{cases}$$

$$u(x,t) = \begin{cases} -(5/4)\cos(10/3)\cos(4x/5)e^{-\frac{16}{25}t}, & x \le 2/3, \\[2mm] -\dfrac{5\cos(8/15)}{4\tan(80/3)}\sin(80(1-x))e^{-\frac{16}{25}t}, & x > 2/3. \end{cases}$$

$h = \tau$	$\|\epsilon_u\|_c$	r_u	$\|\epsilon_p\|_c$	r_p	$\|\epsilon_v\|_c$	r_V	$\|\epsilon_s\|_c$	r_S
1/10	0.155E+01	-	0.138E+01	-	0.189E+01	-	0.114E+01	-
1/40	0.185E+00	8.4	0.380E-01	3.6	0.867E+00	2.2	0.401E-01	28.4
1/160	0.138E-01	13.4	0.413E-02	9.2	0.165E+00	5.25	0.401E-02	10.0
1/640	0.811E-03	17.0	0.226E-03	18.3	0.379E-01	4.4	0.224E-03	17.9
1/2560	0.496E-04	16.4	0.135E-04	16.7	0.928E-02	4.1	0.136E-04	16.5
rate	-	2.8	-	2.0	-	1.0	-	2.8

Table 2.7: Example 1-c: convergence in maximum norm at the time $t = 1$.

$h = \tau$	$\|\epsilon_u\|_{L_2}$	r_u	$\|\epsilon_p\|_{L_2}$	r_p	$\|\epsilon_v\|_{L_2}$	r_V	$\|\epsilon_s\|_{L_2}$	r_S
1/10	0.843E+00	-	0.542E+00	-	0.754E+00	-	0.521E+00	-
1/40	0.757E-01	11.1	0.823E-02	65.9	0.204E+00	4.9	0.819E-02	6.4
1/160	0.480E-02	15.8	0.123E-02	6.7	0.186E-01	11.0	0.124E-02	6.6
1/640	0.296E-03	16.2	0.773E-04	15.9	0.209E-02	8.9	0.774E-04	16.0
1/2560	0.184E-04	16.1	0.481E-05	16.1	0.254E-03	8.2	0.481E-05	16.1
rate	-	2.0	-	2.0	-	1.5	-	2.0

Table 2.8: Example 1-c: convergence in L_2 norm at the time $t = 1$.

Convergence results are summarized in Tables 2.7 and 2.8. It is seen that convergence order does not depend on the jumps of coefficients (see also Figure 2.8). At the same time, the numerical solution on very coarse grids can give a bad approximation to the exact solution. This can be observed on Figure 2.7, where analytical and numerical solutions are plotted.

2.4.2   Example 2: convergence when exact solution is unknown

Consider the case when pore fluid is incompressible. If some load through the porous slab is applied on the top, then, initially whole load is taken by the pore
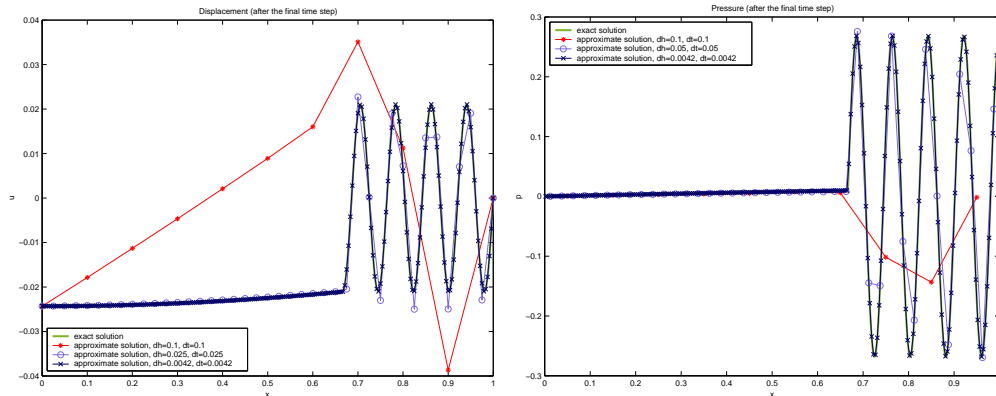

Figure 2.7: Example 1-c: Convergence of displacement (left), pressure (right).
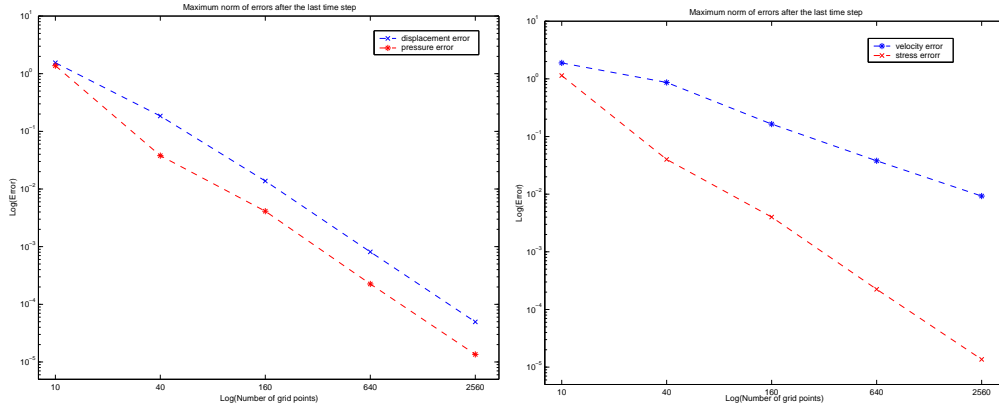
Figure 2.8: Example 1-c: Errors in maximum norm for displacement and pressure (left), velocity and stress (right).

fluid and there is negligibly little compression of the soil sample immediately after placing the load. This means the following initial conditions:

$$p(x,0) = s_0, \ u(x,0) = 0.$$

During the consolidation process the fluid pressure is dissipating and simultaneously the effective stress of the solid is increasing. There is no known analytical solution in this case and the solutions can be only qualitatively compared with the results of other authors. Note that all parameters in the tests below are non-dimensional and all results are also plotted non-dimensionally.

Example 2-a.
In this test, the material properties of the layers are the following:

$$\kappa_1 = 1.0, \ \kappa_2 = 10.0, \ \nu_1 = 1.0, \ \nu_2 = 0.1.$$

These values of the parameters mean that upper layer is ten times less permeable, and ten times stiffer. Figure 2.9 shows pore pressure and stress of the solid distributions at different moments of time. Remind that in this set of numerical experiments exact solution of the problem is unknown and it cannot be compared to the numerical results, but behavior of the numerical solution can be analyzed during the grid thickening. Figure 2.10 shows displacement calculated on the grids of different thickness at the fixed time $t = 0.05$ and the rate of the settlement of the soil surface in time.

Example 2-b.
In this test, the location of layers from Example 2-a is changed. Now, the upper layer is ten times more permeable and ten times less stiff. The values of the
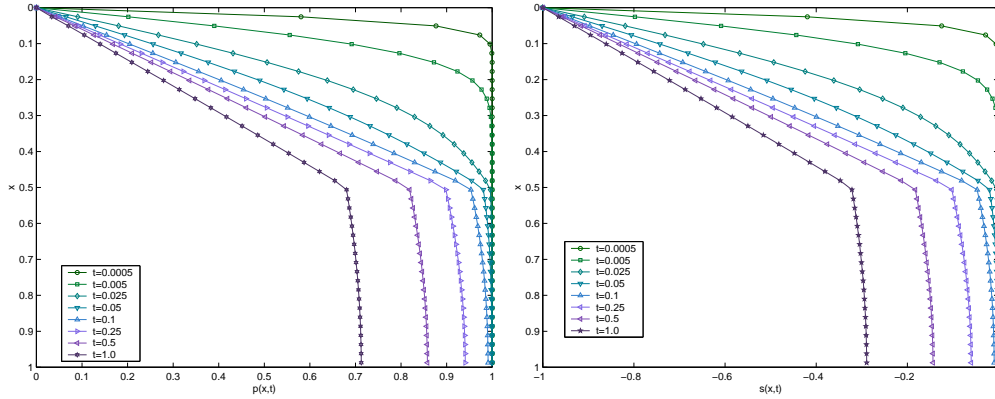
Figure 2.9: Example 2-a: Pore pressure (left), stress of the solid (right) distributions in time.
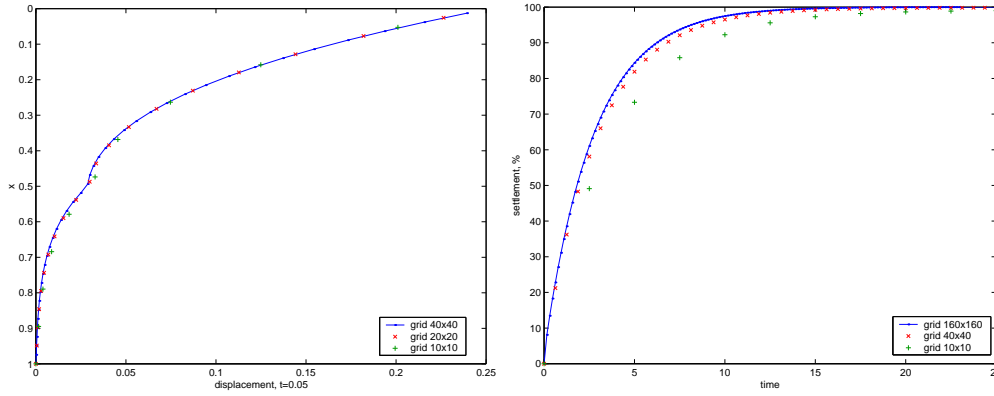

Figure 2.10: Example 2-a: Displacement in the profile (left), rate of settlement of the soil surface (right).

parameters are:

$$\kappa_1 = 1.0, \ \kappa_2 = 0.1, \ \nu_1 = 1.0, \ \nu_2 = 10.0.$$

Some results of this experiment are plotted in the Figure 2.11. Distributions of pore pressure and rate of settlement obtained in the previous two numerical experiments were compared to results published in [52] and a very good qualitative agreement was observed.

2.4.3   Example 3: comparison of the improved and the standard schemes

In this group of experiments, the stress values calculated with the schemes (2.19) and (2.55) are compared. The aim is to illustrate the accuracy of the modified scheme for different sets of the parameters. Solid lines in these figures represent the exact solution obtained on a very fine mesh by the scheme (2.19). Note that
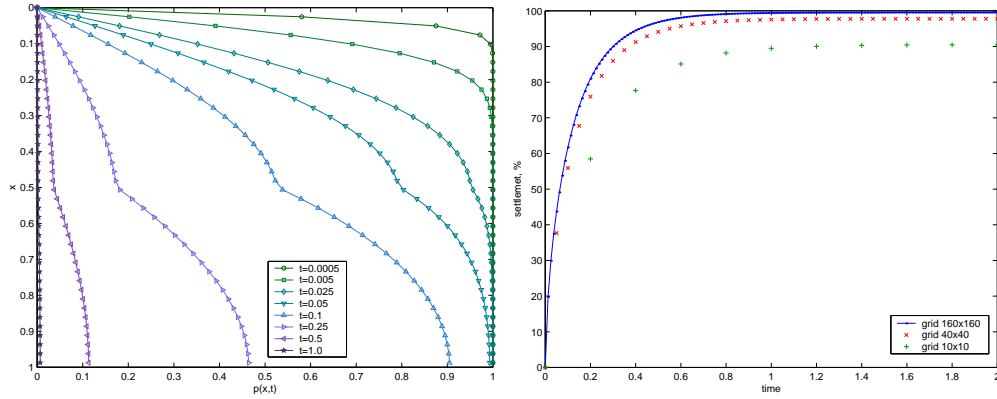
Figure 2.11: Example 2-b: Pressure distribution in time (left), rate of settlement of the soil surface (right).

on such grids both schemes, the basic and the modified one, give very similar results which are not distinguishable on these pictures. The advantage of the modified scheme becomes more evident on coarser grids.

Example 3-a. In this experiment, the following input parameters are chosen:

$$\xi = \frac{2}{3}, \ \nu_1 = 1.0, \ \nu_2 = 0.01, \ \kappa_1 = 1.0, \ \kappa_2 = 0.1, \ a = 0, \ t = 1.0.$$

Figure 2.12 shows that the modified scheme gives very good approximation to the solution even on relatively coarse grids, which is not the case for the standard (not modified) scheme.

Example 3-b. Input data for this test is as follows:

$$\xi = \frac{2}{7}, \ \nu_1 = 1.0, \ \nu_2 = 50.0, \ \kappa_1 = 1.0, \ \kappa_2 = 0.5, \ a = 0.$$

Comparison results at the time $t = 0.05$ are shown on Fig. 2.12. One can see that coarse grid solutions calculated with both schemes differ from the fine grid solution, however the modified scheme provides a better approximation.

Example 3-c.
In this Example, the situation when input parameters are such that performed modifications give almost no improvement, is presented. The values of the parameters are:

$$\xi = \frac{2}{3}, \ \nu_1 = 1.0, \ \nu_2 = 0.1, \ \kappa_1 = 1.0, \ \kappa_2 = 9.0, \ a = 0, \ t = 0.1.$$

The reason for this is that we are in the case discussed in Remark 2.3.1. One can see on Fig. 2.13 that both schemes produce almost same results.
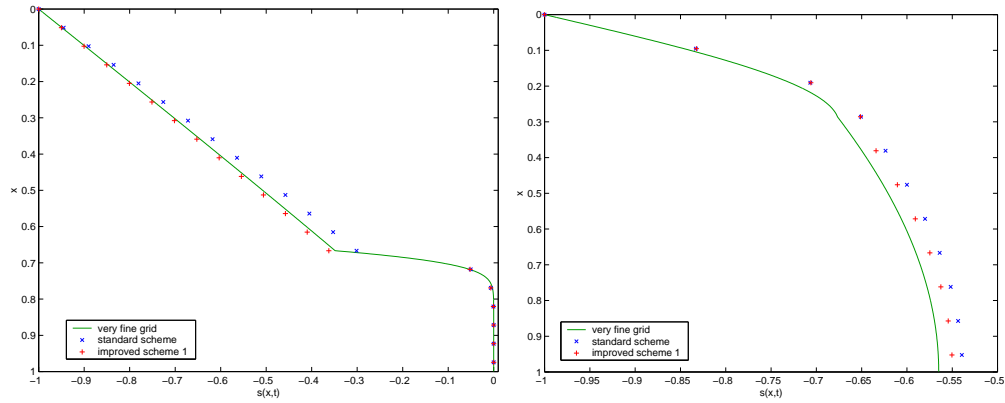
Figure 2.12: Stress values produced by standard and improved schemes, for the Example 3-a (left), Example 3-b (right).
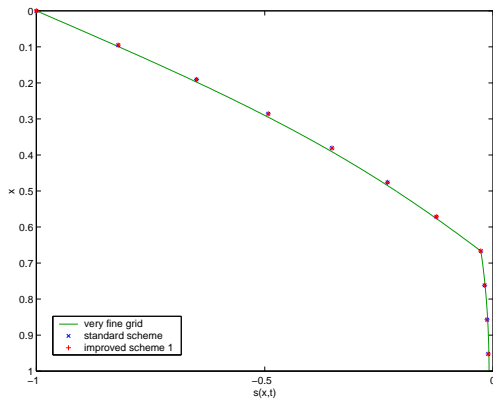

Figure 2.13: Example 3-c: stress values, produced by standard and improved schemes.

Chapter 3

Biot model in three dimensions. Finite volume discretization

In this chapter, we derive a finite volume discretization for the three-dimensional Biot poroelasticity system in multilayered domains. For stability reasons, the discretization is done on staggered grids. The discretization involves the construction of special interpolating polynomials in the dual volumes. This technique produces a difference scheme, which accounts for the possible discontinuities in the coefficients of the problem and provides accurate computation of the primary as well as of flux unknowns. Numerical experiments, which establish convergence of the proposed discretization, are presented in the end of the chapter.

3.1 Continuous system

Let us consider a parallelepiped domain Ω with boundary Γ. For simplicity suppose that Ω is a cube $(0, L) \times (0, L) \times (0, L)$. In the domain Ω, consider the Biot model

$$- \nabla \cdot \mathbf{S} + \nabla p = 0,$$
$$\frac{\partial}{\partial t} \left(\phi \beta p + \nabla \cdot \mathbf{u} \right) + \nabla \cdot \mathbf{V} = f(\mathbf{x}, t), \tag{3.1}$$

where

$$\mathbf{S} = (S^{ij})_{i,j=1,2,3} = \mu \left(\nabla \mathbf{u} + (\nabla \mathbf{u})^T \right) + \lambda \nabla \cdot \mathbf{u} \, \mathbf{I} \tag{3.2}$$

$$\mathbf{V} = (V^i)_{i=1,2,3} = -\frac{\kappa}{\nu} \nabla p \tag{3.3}$$

Suppose that the porous medium in the domain Ω consists of two horizontal layers, what induces that coefficients of the system are discontinuous across some interface $z = \xi$. We assume that these coefficients are piecewise constant:

$$\lambda(\mathbf{x}) = \left\{ \begin{array}{ll} \lambda_1 & z < \xi, \\ \lambda_2 & z > \xi, \end{array} \right. \qquad \mu(\mathbf{x}) = \left\{ \begin{array}{ll} \mu_1 & z < \xi, \\ \mu_2 & z > \xi, \end{array} \right.$$

$$\kappa(\mathbf{x}) = \left\{ \begin{array}{ll} \kappa_1 & z < \xi, \\ \kappa_2 & z > \xi, \end{array} \right. \qquad \phi(\mathbf{x}) = \left\{ \begin{array}{ll} \phi_1 & z < \xi, \\ \phi_2 & z > \xi. \end{array} \right.$$

Larger number of interfaces can also be considered, but we restrict here to just one interface only for simplicity of the presentation.

Recalling interface conditions, which where introduced in the Chapter 1, we write:

$$[\mathbf{u}] = 0, \ [p] = 0, \ [\mathbf{S} \cdot \mathbf{n}] = 0, \ [\mathbf{V} \cdot \mathbf{n}] = 0, \tag{3.4}$$

what is continuity of the displacement, of the fluid pressure, of the normal component of the stress tensor of the porous skeleton, and of the normal fluid flux. In the formulae above $\mathbf{n}$ stands for the unit normal to the interface, and $[\, q\,] = q|_{z=\xi+0} - q|_{z=\xi-0}, \, q = \{\mathbf{u}, p, \mathbf{S}, \mathbf{V}\}$.

Certain initial and boundary conditions must supplement the system (3.1) so that the system has a unique solution. However, we postpone their specification to the section, where certain numerical experiments are presented, and where these conditions will be specified for each experiment.

The model (3.1), (3.4) can be rewritten as a system of PDEs with respect to the unknown displacement components u, v, w and the fluid pressure p. A non-dimensional version of this system can be written as following

$$- \left((\lambda + 2\mu)u_x + \lambda\left(v_y + w_z\right)\right)_x - \left(\mu\left(u_y + v_x\right)\right)_y - \left(\mu\left(u_z + w_x\right)\right)_z + p_x = 0,$$

$$- \left(\mu\left(v_x + u_y\right)\right)_x - \left((\lambda + 2\mu)v_y + \lambda\left(w_z + u_x\right)\right)_y - \left(\mu\left(v_z + w_y\right)\right)_z + p_y = 0,$$

$$- \left(\mu\left(w_x + u_z\right)\right)_x - \left(\mu\left(w_y + v_z\right)\right)_y - \left((\lambda + 2\mu)w_z + \lambda\left(u_x + v_y\right)\right)_z + p_z = 0,$$

$$(ap + u_x + v_y + w_z)_t - (\kappa p_x)_x - (\kappa p_y)_y - (\kappa p_z)_z = f(\mathbf{x}, t), \quad (\mathbf{x}, t) \in \Omega \times (0; T],$$
$$\tag{3.5}$$

$$[u] = 0, \quad [v] = 0, \quad [w] = 0, \quad [p] = 0,$$

$$[\mu\left(w_x + u_z\right)] = 0, \quad [\mu\left(w_y + v_z\right)] = 0,$$

$$[(\lambda + 2\mu)w_z + \lambda\left(u_x + v_y\right)] = 0, \quad [\kappa p_z] = 0, \quad (\mathbf{x}, t) \in \Omega \cap (z = \xi) \times (0, T].$$
$$\tag{3.6}$$

where scaling has been taken with respect to the characteristic length of the porous medium L, and some reference values λ_0, μ_0, κ_0, η_0, a_0 in the following formulae:

$$x := \frac{x}{L}, \ y := \frac{y}{L}, \ z := \frac{z}{L}, \ t := \frac{(\lambda_0 + 2\mu_0)\kappa_0 t}{L^2 \eta_0}, \ u := \frac{u}{L}, \ v := \frac{v}{L}, \ w := \frac{w}{L},$$

$$p := \frac{p}{\lambda_0 + 2\mu_0}, \lambda := \frac{\lambda}{\lambda_0 + 2\mu_0}, \ \mu := \frac{\mu}{\lambda_0 + 2\mu_0}, \ \kappa := \frac{\kappa/\eta}{\kappa_0/\eta_0}, \ f := \frac{L^2 f \eta_0}{(\lambda_0 + 2\mu_0)\kappa_0},$$

and $a = \phi\beta(\lambda_0 + 2\mu_0)$ is a new non-dimensional parameter.

3.2 Finite volume discretization

3.2.1 Staggered grids and grid notations

To overcome stability difficulties, which often arise when the discretization of the Biot model is done on the collocate grids, the use of staggered grids was proposed in [66]. Pressure points of this grid are located on the physical boundary and the displacement points are defined at the respective cell faces. In the three-dimensional case, a staggered grid is composed of the four following types of grid points:

$$\omega^u = \omega^u_{h_x, h_y, h_z} = \{(x_{i+0.5}, y_j, z_k) = ((i+0.5)h_x, jh_y, kh_z), \ i = 0, .., N_1 - 1,$$
$$j = 0, .., N_2, \ k = 0, .., N_3\},$$

$$\omega^v = \omega^v_{h_x, h_y, h_z} = \{(x_i, y_{j+0.5}, z_k) = (ih_x, (j+0.5)h_y, kh_z), \ i = 0, .., N_1,$$
$$j = 0, .., N_2 - 1, \ k = 0, .., N_3\},$$

$$\omega^w = \omega^w_{h_x, h_y, h_z} = \{(x_i, y_j, z_{k+0.5}) = (ih_x, jh_y, (k+0.5)h_z), \ i = 0, .., N_1,$$
$$j = 0, .., N_2, \ k = 0, .., N_3 - 1\},$$

$$\omega^p = \omega^p_{h_x, h_y, h_z} = \{(x_i, y_j, z_k) = (ih_x, jh_y, kh_z), \ i = 0, .., N_1, \ j = 0, .., N_2, \ k = 0, .., N_3\},$$
$$(3.7)$$

where $h_x = 1/N_1$, $h_y = 1/N_2$, $h_z = 1/N_3$ are the grid step sizes. Respective location of the grid points is depicted in the Figure 3.1.

For the time discretization we introduce a grid in time with a step-size τ
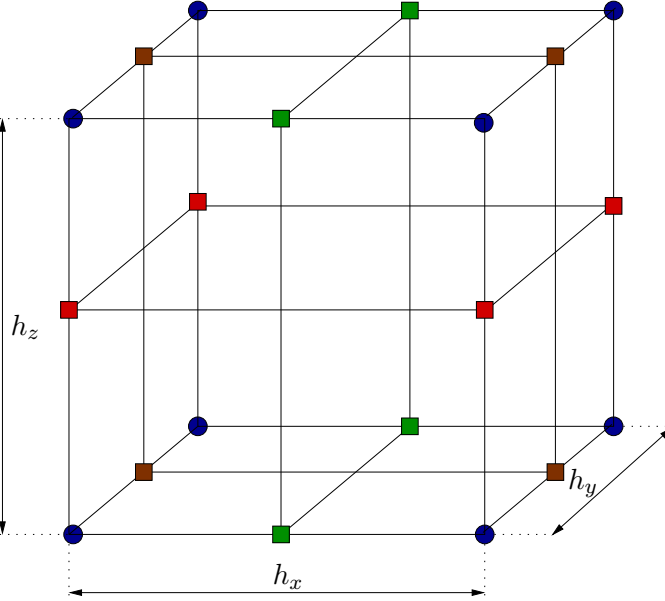
$$\omega^t = \{t_n : \ t_n = n\tau, \ n = 0, 1, \ldots, M\}.$$

We introduce also the following grid functions:

$$u = u^n_{i+0.5, j, k} = u_{i+0.5, j, k} = u(x_{i+0.5}, y_j, z_k, t_n),$$
$$v = v^n_{i, j+0.5, k} = v_{i, j+0.5, k} = v(x_i, y_{j+0.5}, z_k, t_n),$$
$$w = w^n_{i, j, k+0.5} = w_{i, j, k+0.5} = w(x_i, y_j, z_{k+0.5}, t_n),$$
$$p = p^n_{i, j, k} = p_{i, j, k} = p(x_i, y_j, z_k, t_n),$$

which are defined on the grids $\omega^u \times \omega^t$, $\omega^v \times \omega^t$, $\omega^w \times \omega^t$ and $\omega^p \times \omega^t$, respectively. Components of the discrete fluid flux and discrete stress tensor are also defined in the appropriate grid points:

$$V^1 = V^{1,n}_{i+0.5, j, k} = V^1_{i+0.5, j, k} = V^1(x_{i+0.5}, y_j, z_k, t_n),$$
$$V^2 = V^{2,n}_{i, j+0.5, k} = V^2_{i, j+0.5, k} = V^2(x_i, y_{j+0.5}, z_k, t_n),$$
$$V^3 = V^{3,n}_{i, j, k+0.5} = V^3_{i, j, k+0.5} = V^3(x_i, y_j, z_{k+0.5}, t_n),$$

Figure 3.1: Staggered grid in three dimensions.

$$S^{11} = S^{11,n}_{i,j,k} = S^{11}_{i,j,k} = S^{11}(x_i, y_j, z_k, t_n),$$

$$S^{22} = S^{22,n}_{i,j,k} = S^{22}_{i,j,k} = S^{22}(x_i, y_j, z_k, t_n),$$

$$S^{33} = S^{33,n}_{i,j,k} = S^{33}_{i,j,k} = S^{33}(x_i, y_j, z_k, t_n),$$

$$S^{12} = S^{12,n}_{i+0.5,j+0.5,k} = S^{12}_{i+0.5,j+0.5,k} = S^{12}(x_{i+0.5}, y_{j+0.5}, z_k, t_n),$$

$$S^{13} = S^{13,n}_{i+0.5,j,k+0.5} = S^{13}_{i+0.5,j,k+0.5} = S^{13}(x_{i+0.5}, y_j, z_{k+0.5}, t_n),$$

$$S^{23} = S^{23,n}_{i,j+0.5,k+0.5} = S^{23}_{i,j+0.5,k+0.5} = S^{23}(x_i, y_{j+0.5}, z_{k+0.5}, t_n).$$

We shall use the standard notations for the finite differences on a uniform mesh (see, e.g., [54]):

$$p_x := p_{x,i,j,k} = (p_{i+1,j,k} - p_{i,j,k})/h_x,$$

$$p_{\bar{x}} := p_{\bar{x},i,j,k} = (p_{i,j,k} - p_{i-1,j,k})/h_x,$$

$$u_x := u_{x,i+0.5,j,k} = (u_{i+1.5,j,k} - u_{i+0.5,j,k})/h_x,$$

$$u_{\bar{x}} := u_{\bar{x},i+0.5,j,k} = (u_{i+0.5,j,k} - u_{i-0.5,j,k})/h_x,$$

$$u_{xy} := u_{xy,i+0.5,j,k} = (u_{i+1.5,j+1,k} - u_{i+1.5,j,k} - u_{i+0.5,j+1,k} + u_{i+0.5,j,k})/h_x h_y.$$

The finite differences p_y, $p_{\bar{y}}$, p_z, $p_{\bar{z}}$, u_y, $u_{\bar{y}}$, u_z, $u_{\bar{z}}$, v_x, $v_{\bar{x}}$, etc. are defined in a similar way. We introduce also a finite difference in time

$$p_t = \frac{p^{n+1} - p^n}{\tau},$$

and further, we will also use the notation

$$p^\sigma := \sigma p^{n+1} + (1 - \sigma)p^n. \tag{3.8}$$

Weighted discretization in time, applied to the second equation of (3.1), results in the following semi-discrete equation:

$$(ap + \nabla \cdot u)_t - \nabla \cdot V^\sigma = f^\sigma, \tag{3.9}$$

where σ is the so-called weight parameter. This discretization corresponds to the Crank-Nicolson discretization, if $\sigma = 0.5$, and to the fully implicit discretization, if $\sigma = 1$, etc.

3.2.2 Integral form of the governing equations

Following the finite volume method, we integrate the first equation of (3.1), and equation (3.9) over the corresponding set of the control volumes

$$\mathbf{V}^u = \mathbf{V}^u_{ijk} = (x_i, x_{i+1}) \times (y_{j-0.5}, y_{j+0.5}) \times (z_{k-0.5}, z_{k+0.5}),$$

$$\mathbf{V}^v = \mathbf{V}^v_{ijk} = (x_{i-0.5}, x_{i+0.5}) \times (y_j, y_{j+1}) \times (z_{k-0.5}, z_{k+0.5}),$$

$$\mathbf{V}^w = \mathbf{V}^w_{ijk} = (x_{i-0.5}, x_{i+0.5}) \times (y_{j-0.5}, y_{j+0.5}) \times (z_k, z_{k+1}),$$

$$\mathbf{V}^p = \mathbf{V}^p_{ijk} = (x_{i-0.5}, x_{i+0.5}) \times (y_{j-0.5}, y_{j+0.5}) \times (z_{k-0.5}, z_{k+0.5}).$$

Applying then the divergence theorem to the integrated equations, and taking into account interface conditions (3.4), we transform the volume integrals into surface integrals, and obtain the following system of integral equations:

$$-\int_{\partial \mathbf{V}^u} \mathbf{S}^1 \cdot \mathbf{n}^u dS + \int_{\partial \mathbf{V}^u_x} p \cdot n^u_x dS = 0, \tag{3.10}$$

$$-\int_{\partial \mathbf{V}^v} \mathbf{S}^2 \cdot \mathbf{n}^v dS + \int_{\partial \mathbf{V}^v_y} p \cdot n^v_y dS = 0, \tag{3.11}$$

$$-\int_{\partial \mathbf{V}^w} \mathbf{S}^3 \cdot \mathbf{n}^w dS + \int_{\partial \mathbf{V}^w_z} p \cdot n^w_z dS = 0, \tag{3.12}$$

$$\left(\int_{\mathbf{V}^p} apdV + \int_{\partial \mathbf{V}^p} \mathbf{u} \cdot \mathbf{n}^p dS - \tau\sigma \int_{\partial \mathbf{V}^p} \mathbf{V} \cdot \mathbf{n}^p dS\right)^{n+1} =$$

$$\tau \int_{\mathbf{V}^p} f^\sigma dV + \left(\int_{\mathbf{V}^p} apdV + \int_{\partial \mathbf{V}^p} \mathbf{u} \cdot \mathbf{n}^p dS - \tau(1 - \sigma) \int_{\partial \mathbf{V}^p} \mathbf{V} \cdot \mathbf{n}^p dS\right)^n, \tag{3.13}$$

where $\mathbf{S}^1 = (S^{11}, S^{12}, S^{13})$, $\mathbf{S}^2 = (S^{12}, S^{22}, S^{23})$, $\mathbf{S}^3 = (S^{13}, S^{23}, S^{33})$ are components of the stress tensor; $\mathbf{n}^u = (n_x^u, n_y^u, n_z^u)$, $\mathbf{n}^v = (n_x^v, n_y^v, n_z^v)$, $\mathbf{n}^w = (n_x^w, n_y^w, n_z^w)$, $\mathbf{n}^p = (n_x^p, n_y^p, n_z^p)$ are unit outward normal vectors to the volume boundaries $\partial \mathbf{V^u}$, $\partial \mathbf{V^v}$, $\partial \mathbf{V^w}$ and $\partial \mathbf{V^p}$, respectively. Control volumes' faces $\partial \mathbf{V_x^u}$, $\partial \mathbf{V_y^v}$ and $\partial \mathbf{V_z^w}$ are defined by the formulae $\partial \mathbf{V}_x^u = \partial \mathbf{V}^u \cap (\{x = x_i\} \cup \{x = x_{i+1}\})$, $\partial \mathbf{V}_y^v = \partial \mathbf{V}^v \cap (\{y = y_j\} \cup \{y = y_{j+1}\})$, $\partial \mathbf{V}_z^w = \partial \mathbf{V}^w \cap (\{z = z_k\} \cup \{z = z_{k+1}\})$.

Next, we approximate the integrals over the volumes' faces in (3.10) - (3.13) by the midpoint rule, and divide each equation over $h_x h_y h_z$, what results in the following system of discrete equations

$$-\frac{S_{i+1,j,k}^{11} - S_{i,j,k}^{11}}{h_x} - \frac{S_{i+0.5,j+0.5,k}^{12} - S_{i+0.5,j-0.5,k}^{12}}{h_y} - \frac{S_{i+0.5,j,k+0.5}^{13} - S_{i+0.5,j,k-0.5}^{13}}{h_z}$$
$$+ \frac{p_{i+1,j,k} - p_{i,j,k}}{h_x} = 0,$$

$$-\frac{S_{i+0.5,j+0.5,k}^{12} - S_{i-0.5,j+0.5,k}^{12}}{h_x} - \frac{S_{i,j+1,k}^{22} - S_{i,j,k}^{22}}{h_y} - \frac{S_{i,j+0.5,k+0.5}^{23} - S_{i,j+0.5,k-0.5}^{23}}{h_z}$$
$$+ \frac{p_{i,j+1,k} - p_{i,j,k}}{h_y} = 0,$$

$$-\frac{S_{i+0.5,j,k+0.5}^{13} - S_{i-0.5,j,k+0.5}^{13}}{h_x} - \frac{S_{i,j+0.5,k+0.5}^{23} - S_{i,j-0.5,k+0.5}^{23}}{h_y} - \frac{S_{i,j,k+1}^{33} - S_{i,j,k}^{33}}{h_z}$$
$$+ \frac{p_{i,j,k+1} - p_{i,j,k}}{h_z} = 0,$$

$$\left(\langle a \rangle p_{i,j,k} + \frac{u_{i+0.5,j,k} - u_{i-0.5,j,k}}{h_x} + \frac{v_{i,j+0.5,k} - v_{i,j-0.5,k}}{h_y} + \frac{w_{i,j,k+0.5} - w_{i,j,k-0.5}}{h_z} \right)_t$$
$$+ \frac{V_{i+0.5,j,k}^{1,\sigma} - V_{i-0.5,j,k}^{1,\sigma}}{h_x} + \frac{V_{i,j+0.5,k}^{2,\sigma} - V_{i,j-0.5,k}^{2,\sigma}}{h_y} + \frac{V_{i,j,k+0.5}^{3,\sigma} - V_{i,j,k-0.5}^{3,\sigma}}{h_z} = \langle f \rangle^\sigma,$$
$$(3.14)$$

where

$$\langle a \rangle = \frac{1}{h_x h_y h_z} \int\limits_{\mathbf{V^p}} a(\mathbf{x}) dV, \quad \langle f \rangle = \frac{1}{h_x h_y h_z} \int\limits_{\mathbf{V^p}} f(\mathbf{x}, t) dV. \qquad (3.15)$$

3.2.3 Polynomial approximation on the dual grid

Next, we approximate the fluxes of the problem (i.e. the stress tensor and the fluid velocity vector), and transform the system (3.14) into a system with respect to the primary variables (i.e. p, u, v, w) only. For this purpose, we construct interpolating polynomials $P(\mathbf{x})$, $U(\mathbf{x})$, $V(\mathbf{x})$, $W(\mathbf{x})$ for $p(\mathbf{x})$, $u(\mathbf{x})$, $v(\mathbf{x})$, $w(\mathbf{x})$, respectively, in the appropriately chosen sets of control volumes. The derivatives of $p(\mathbf{x})$, $u(\mathbf{x})$, $v(\mathbf{x})$ and $w(\mathbf{x})$ in the respective expressions for fluxes are approximated by the derivatives of the interpolating polynomials.

Let us suppose, that index k_{int}, $0 \leq k_{int} < N_3$ is such that interface position is represented in the following way

$$\xi = z_{k_{int}} + \theta h_z = k_{int} h_z + \theta h_z, \qquad (3.16)$$

where parameter $0 \leq \theta < 1$. This representation will be used below, during the derivation of the polynomials.

First, we construct polynomials $P(\mathbf{x})$ for the pressure unknown in each volume

$$\mathbf{V}_{i,j,k}^{P(\mathbf{x})} = \mathbf{V}^{P(\mathbf{x})} = (x_i, x_{i+1}) \times (y_j, y_{j+1}) \times (z_k, z_{k+1})$$

of the domain Ω. Note that the volume $\mathbf{V}^{P(\mathbf{x})}$ is different from the volume $\mathbf{V}_{i,j,k}^p$, which was defined above. The approximations of the fluid flux components are calculated in the respective grid points according to the following formulae:

$$V_{i+0.5,j,k}^1 = -\kappa \frac{\partial P}{\partial x}(\mathbf{x}_{i+0.5,j,k}),$$

$$V_{i,j+0.5,k}^2 = -\kappa \frac{\partial P}{\partial y}(\mathbf{x}_{i,j+0.5,k}), \qquad (3.17)$$

$$V_{i,j,k+0.5}^3 = -\kappa \frac{\partial P}{\partial z}(\mathbf{x}_{i,j,k+0.5}).$$

We prescribe polynomials $P(\mathbf{x})$ to be piecewise-trilinear in each volume, which is intersected by the interface $z = \xi$, and trilinear in the rest of the volumes. In fact, these are the highest order polynomials, which belong to the kernel of the diffusion operator. The interface intersects the volume $\mathbf{V}_{i,j,k}^{P(\mathbf{x})}$ in the case when index k is such that $z_k < \xi < z_{k+1}$, what is equivalent to $k = k_{int}$ (see representation (3.16)). The expression for such polynomial can be written as following:

$$P(x,y,z) =$$
$$\begin{cases} a_1^p(x-x_i)(y-y_j)(z-z_{k_{int}}) + b_1^p(x-x_i)(y-y_j) + c_1^p(x-x_i)(z-z_{k_{int}}) \\ \quad + d_1^p(y-y_j)(z-z_{k_{int}}) + e_1^p(x-x_i) + f_1^p(y-y_j) + g_1^p(z-z_{k_{int}}) + p_{i,j,k_{int}}, \\ \hfill z_{k_{int}} < z \leq \xi, \\[6pt] a_2^p(x-x_i)(y-y_j)(z-z_{k_{int}}) + b_2^p(x-x_i)(y-y_j) + c_2^p(x-x_i)(z-z_{k_{int}}) \\ \quad + d_2^p(y-y_j)(z-z_{k_{int}}) + e_2^p(x-x_i) + f_2^p(y-y_j) + g_2^p(z-z_{k_{int}}) + p_{i,j,k_{int}+1}, \\ \hfill \xi < z < z_{k_{int}+1}. \end{cases}$$
$$(3.18)$$

Unknown coefficients a_1^p, a_2^p, b_1^p, b_2^p, c_1^p, c_2^p, d_1^p, d_2^p, e_1^p, e_2^p, f_1^p, f_2^p, g_1^p, g_2^p of the polynomial can be found from the following conditions, which should be fulfilled:

1. Interpolation at the vertices of the volume:

$$P(x_i, y_j, z_{k_{int}}) = p_{i,j,k_{int}},\ P(x_{i+1}, y_j, z_{k_{int}}) = p_{i+1,j,k_{int}},\ P(x_i, y_{j+1}, z_{k_{int}}) = p_{i,j+1,k_{int}},$$

$P(x_i, y_j, z_{k_{int}+1}) = p_{i,j,k_{int}+1}$, $P(x_{i+1}, y_{j+1}, z_{k_{int}}) = p_{i+1,j+1,k_{int}}$, $P(x_i, y_{j+1}, z_{k_{int}+1}) = p_{i,j+1,k_{int}+1}$, $P(x_{i+1}, y_j, z_{k_{int}+1}) = p_{i+1,j,k_{int}+1}$, $P(x_{i+1}, y_{j+1}, z_{k_{int}+1}) = p_{i+1,j+1,k_{int}+1}$.

2. Continuity of the polynomial across the interface:

$$[P] = 0 \quad \text{for any} \quad \mathbf{x} \in \mathbf{V}_{i,j,k_{int}}^{P(\mathbf{x})} \cap \{z = \xi\},$$

3. Continuity of the normal fluid flux $\kappa \frac{\partial p}{\partial x}$, calculated on the polynomial $P(\mathbf{x})$, across the interface:

$$\left[\kappa \frac{\partial P}{\partial z}\right] = 0 \quad \text{for any} \quad \mathbf{x} \in \mathbf{V}_{i,j,k_{int}}^{P(\mathbf{x})} \cap \{z = \xi\}.$$

Solving the system defined by the conditions 1. - 3. above with respect to the unknown coefficients, we obtain the following expressions:

$$a_1^p = \frac{\kappa_2}{(1-\theta)\kappa_1 + \theta\kappa_2} p_{xyz,i,j,k_{int}}, \ b_1^p = p_{xy,i,j,k_{int}}, \ c_1^p = \frac{\kappa_2}{(1-\theta)\kappa_1 + \theta\kappa_2} p_{xz,i,j,k_{int}},$$

$$d_1^p = \frac{\kappa_2}{(1-\theta)\kappa_1 + \theta\kappa_2} p_{yz,i,j,k_{int}}, \ e_1^p = p_{x,i,j,k_{int}}, \ f_1^p = p_{y,i,j,k_{int}},$$

$$g_1^p = \frac{\kappa_2}{(1-\theta)\kappa_1 + \theta\kappa_2} p_{z,i,j,k_{int}};$$

$$a_2^p = \frac{\kappa_1}{(1-\theta)\kappa_1 + \theta\kappa_2} p_{xyz,i,j,k_{int}}, \quad b_2^p = p_{xy,i,j,k_{int}+1}, \quad c_2^p = \frac{\kappa_1}{(1-\theta)\kappa_1 + \theta\kappa_2} p_{xz,i,j+1,k_{int}},$$

$$d_2^p = \frac{\kappa_1}{(1-\theta)\kappa_1 + \theta\kappa_2} p_{yz,i+1,j,k_{int}}, \ e_2^p = p_{x,i,j+1,k_{int}+1}, \ f_2^p = p_{y,i+1,j,k_{int}+1},$$

$$g_2^p = \frac{\kappa_1}{(1-\theta)\kappa_1 + \theta\kappa_2} p_{z,i+1,j+1,k_{int}},$$

where p_x, p_{xy}, etc. are the notations introduced in the subsection 3.2.1.

Next, we substitute these coefficients into the expression (3.18), and calculate approximate components of the fluid velocity vector according to the formulae (3.17).

If the volume $\mathbf{V}_{i,j,k}^{P(\mathbf{x})}$ is not intersected by the interface, the interpolating polynomial $P(x, y, z)$ is built just as an interpolation of the values in the nodes of the volume. Resulting expressions for the fluid velocity components can be written in the following way:

$$\begin{aligned} V_{i+0.5,j,k}^1 &= -\langle \kappa \rangle_{i+0.5,j,k}^1 p_{\bar{x},i+1,j,k}, \\ V_{i,j+0.5,k}^2 &= -\langle \kappa \rangle_{i,j+0.5,k}^2 p_{\bar{y},i,j+1,k}, \\ V_{i,j,k+0.5}^3 &= -\langle \kappa \rangle_{i,j,k+0.5}^3 p_{\bar{z},i,j,k+1}, \end{aligned} \qquad (3.19)$$

where

$$\langle \kappa \rangle^1_{i+0.5,j,k} = \begin{cases} \kappa_1, & k \le k_{int}, \\ \kappa_2, & k > k_{int}, \end{cases} \qquad \langle \kappa \rangle^2_{i,j+0.5,k} = \begin{cases} \kappa_1, & k \le k_{int}, \\ \kappa_2, & k > k_{int}, \end{cases}$$

$$\langle \kappa \rangle^3_{i,j,k+0.5} = \begin{cases} \kappa_1, & k < k_{int}, \\ \dfrac{\kappa_1 \kappa_2}{(1-\theta)\kappa_1 + \theta\kappa_2}, & k = k_{int}, \\ \kappa_2, & k > k_{int}, \end{cases}$$

Note that this approximations of the fluid flux in each direction is identical to the approximation of the flux in [54], where one dimensional diffusion equation with discontinuous coefficients is considered. In fact, our discretization can be derived as a tensor product of one-dimensional ones, but the approach we present here is more general.

Next, we derive approximations of the stress tensor components, needed for the equations (3.14). For this purpose, we construct interpolating polynomials $U(\mathbf{x})$, $V(\mathbf{x})$, $W(\mathbf{x})$ for each component of the displacement vector respectively. Then, the approximations of the stress tensor components are calculated in the appropriate grid points as following:

$$
\begin{aligned}
S^{11}_{i,j,k} &= \left((\lambda + 2\mu)\frac{\partial U}{\partial x} + \lambda \left(\frac{\partial V}{\partial y} + \frac{\partial W}{\partial z} \right) \right) (x_i, y_j, z_k), \\
S^{22}_{i,j,k} &= \left((\lambda + 2\mu)\frac{\partial V}{\partial y} + \lambda \left(\frac{\partial U}{\partial x} + \frac{\partial W}{\partial z} \right) \right) (x_i, y_j, z_k), \\
S^{33}_{i,j,k} &= \left((\lambda + 2\mu)\frac{\partial W}{\partial z} + \lambda \left(\frac{\partial U}{\partial x} + \frac{\partial V}{\partial y} \right) \right) (x_i, y_j, z_k), \\
S^{12}_{i+0.5,j+0.5,k} &= \mu \left(\frac{\partial U}{\partial y} + \frac{\partial V}{\partial x} \right) (x_{i+0.5}, y_{j+0.5}, z_k), \\
S^{13}_{i+0.5,j,k+0.5} &= \mu \left(\frac{\partial U}{\partial z} + \frac{\partial W}{\partial x} \right) (x_{i+0.5}, y_j, z_{k+0.5}), \\
S^{23}_{i,j+0.5,k+0.5} &= \mu \left(\frac{\partial V}{\partial z} + \frac{\partial W}{\partial y} \right) (x_i, y_{j+0.5}, z_{k+0.5}).
\end{aligned}
\tag{3.20}
$$

Let us consider now the following cubic volumes, built on the nodes of the grids ω^u, ω^v, ω^w respectively

$$
\begin{aligned}
\mathbf{V}^{U(\mathbf{x})}_{ijk} &= \mathbf{V}^{U(\mathbf{x})} = (x_{i-0.5}, x_{i+0.5}) \times (y_j, y_{j+1}) \times (z_k, z_{k+1}), \\
\mathbf{V}^{V(\mathbf{x})}_{ijk} &= \mathbf{V}^{V(\mathbf{x})} = (x_i, x_{i+1}) \times (y_{j-0.5}, y_{j+0.5}) \times (z_k, z_{k+1}), \\
\mathbf{V}^{W(\mathbf{x})}_{ijk} &= \mathbf{V}^{W(\mathbf{x})} = (x_i, x_{i+1}) \times (y_j, y_{j+1}) \times (z_{k-0.5}, z_{k+0.5}).
\end{aligned}
\tag{3.21}
$$

The volumes $\mathbf{V}^{U(\mathbf{x})}_{i,j,k}$, $\mathbf{V}^{V(\mathbf{x})}_{i,j,k}$ are intersected by the interface $z = \xi$, when index $k = k_{int}$, while the volume $\mathbf{V}^{W(\mathbf{x})}_{ijk}$ is intersected, when $k = k_{int}$ and parameter

$\theta < 0.5$, or when $k = k_{int} + 1$ and $\theta > 0.5$.

Next, we subdivide each of the volumes $\mathbf{V}_{i,j,k}^{U(\mathbf{x})}$, $\mathbf{V}_{i,j,k}^{V(\mathbf{x})}$, $\mathbf{V}_{i,j,k}^{W(\mathbf{x})}$ into four subdomains: two pentahedrons and two tetrahedrons (see Fig. 3.2 for the subdivision of the volume $\mathbf{V}^{U(\mathbf{x})}$). Then, we build interpolating polynomials $U(x, y, z)$,
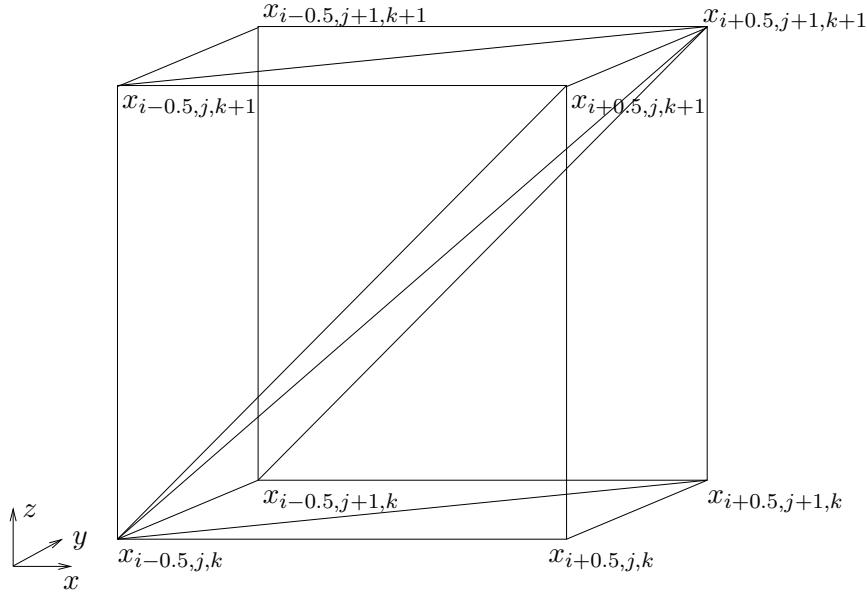
PSfrag replacements

Figure 3.2: Subdivision of the volume $\mathbf{V}^{U(\mathbf{x})}$.

$V(x, y, z)$ and $W(x, y, z)$ in the respective subvolumes. As one can see from the formulae (3.20), the approximations of the stress tensor components S^{11}, S^{22}, S^{33} should be calculated in the points $\{\ \mathbf{x}_{i,j,k} \cap \Omega\ \}$, component S^{12} in the points $\{\ \mathbf{x}_{i+0.5,j+0.5,k} \cap \Omega\ \}$, component S^{13} in the points $\{\ \mathbf{x}_{i+0.5,j,k+0.5} \cap \Omega\ \}$, and component S^{23} in the points $\{\ \mathbf{x}_{i,j+0.5,k+0.5} \cap \Omega\ \}$. Hence, it is sufficient to build the polynomials $U(x, y, z)$, $V(x, y, z)$, and $W(x, y, z)$ in the sets of pentahedrons from the subdivisions.

We choose these polynomials to be piecewise-linear ones, extended with one special piecewise-bilinear term in all pentahedrons, intersected by the interface, and linear ones, extended with one bilinear term otherwise. Note that these are the highest order polynomials, which belong to the kernel of the linear elasticity operator. There are two types of the pentahedrons for each displacement component: $\mathbf{V}_{i,j,k}^{U(\mathbf{x}),1}, \mathbf{V}_{i,j,k}^{U(\mathbf{x}),2} \subset \mathbf{V}_{i,j,k}^{U(\mathbf{x})}$, $\mathbf{V}_{i,j,k}^{V(\mathbf{x}),1}, \mathbf{V}_{i,j,k}^{V(\mathbf{x}),2} \subset \mathbf{V}_{i,j,k}^{V(\mathbf{x})}$,

$\mathbf{V}_{i,j,k}^{W(\mathbf{x}),1}, \mathbf{V}_{i,j,k}^{W(\mathbf{x}),2} \subset \mathbf{V}_{i,j,k}^{U(\mathbf{x})}$. These pentahedrons have the following vertices:

$$\mathbf{V}_{i,j,k}^{U(\mathbf{x}),1} : \{\mathbf{x}_{i-0.5,j,k},\ \mathbf{x}_{i+0.5,j,k},\ \mathbf{x}_{i+0.5,j+1,k},\ \mathbf{x}_{i+0.5,j,k+1},\ \mathbf{x}_{i+0.5,j+1,k+1}\},$$

$$\mathbf{V}_{i,j,k}^{U(\mathbf{x}),2} : \{\mathbf{x}_{i-0.5,j,k},\ \mathbf{x}_{i-0.5,j+1,k},\ \mathbf{x}_{i-0.5,j,k+1},\ \mathbf{x}_{i-0.5,j+1,k+1},\ \mathbf{x}_{i+0.5,j+1,k+1}\},$$

$$\mathbf{V}_{i,j,k}^{V(\mathbf{x}),1} : \{\mathbf{x}_{i,j-0.5,k},\ \mathbf{x}_{i,j+0.5,k},\ \mathbf{x}_{i,j+0.5,k+1},\ \mathbf{x}_{i+1,j+0.5,k},\ \mathbf{x}_{i+1,j+0.5,k+1}\},$$

$$\mathbf{V}_{i,j,k}^{V(\mathbf{x}),2} : \{\mathbf{x}_{i,j-0.5,k},\ \mathbf{x}_{i,j-0.5,k+1},\ \mathbf{x}_{i+1,j-0.5,k},\ \mathbf{x}_{i+1,j-0.5,k+1},\ \mathbf{x}_{i+1,j+0.5,k+1}\},$$

$$\mathbf{V}_{i,j,k}^{W(\mathbf{x}),1} : \{\mathbf{x}_{i,j,k-0.5},\ \mathbf{x}_{i,j,k+0.5},\ \mathbf{x}_{i+1,j,k+0.5},\ \mathbf{x}_{i,j+1,k+0.5},\ \mathbf{x}_{i+1,j+1,k+0.5}\},$$

$$\mathbf{V}_{i,j,k}^{W(\mathbf{x}),2} : \{\mathbf{x}_{i,j,k-0.5},\ \mathbf{x}_{i+1,j,k-0.5},\ \mathbf{x}_{i,j+1,k-0.5},\ \mathbf{x}_{i+1,j+1,k-0.5},\ \mathbf{x}_{i+1,j+1,k+0.5}\}.$$

In the pentahedrons, intersected by the interface (it happens if and only if the corresponding cubic volume is intersected), polynomials should fulfill the continuity conditions on the interface.

Let us consider three such neighboring pentahedrons $\mathbf{V}_{i,j,k_{int}}^{U(\mathbf{x}),1}$, $\mathbf{V}_{i,j,k_{int}}^{V(\mathbf{x}),1}$, and $\mathbf{V}_{i,j,k_{int}}^{W(\mathbf{x}),1}$ in the case when the parameter θ satisfies $\theta < 0.5$. In this case, interface ξ is located between coordinates $z_{k_{int}}$ and $z_{k_{int}+0.5}$ and, hence these three pentahedrons are intersected by the interface. The general representation of the polynomials in these tetrahedrons can be written as follows:

$$U(x,y,z) = \begin{cases} a_1^u(y-y_j)(z-z_{k_{int}}) + b_1^u(x-x_{i-0.5}) + c_1^u(y-y_j) \\ +d_1^u(z-z_{k_{int}}) + u_{i-0.5,j,k_{int}}, & \mathbf{x} \in \mathbf{V}_{i,j,k_{int}}^{U(\mathbf{x}),1} \cap (z < \xi), \\ a_2^u(y-y_j)(z-z_{k_{int}+1}) + b_2^u(x-x_{i+0.5}) + c_2^u(y-y_j) \\ +d_2^u(z-z_{k_{int}+1}) + u_{i+0.5,j,k_{int}+1}, & \mathbf{x} \in \mathbf{V}_{i,j,k_{int}}^{U(\mathbf{x}),1} \cap (z > \xi), \end{cases}$$
(3.22)

$$V(x,y,z) = \begin{cases} a_1^v(x-x_i)(z-z_{k_{int}}) + b_1^v(x-x_i) + c_1^v(y-y_{j-0.5}) \\ +d_1^v(z-z_{k_{int}}) + v_{i,j-0.5,k_{int}}, & \mathbf{x} \in \mathbf{V}_{i,j,k_{int}}^{V(\mathbf{x}),1} \cap (z < \xi), \\ a_2^v(x-x_i)(z-z_{k_{int}+1}) + b_2^v(x-x_i) + c_2^v(y-y_{j+0.5}) \\ +d_2^v(z-z_{k_{int}+1}) + v_{i,j+0.5,k_{int}+1}, & \mathbf{x} \in \mathbf{V}_{i,j,k_{int}}^{V(\mathbf{x}),1} \cap (z > \xi), \end{cases}$$
(3.23)

$$W(x,y,z) = \begin{cases} a_1^w(x-x_i)(y-y_j) + b_1^w(x-x_i) + c_1^w(y-y_j) \\ +d_1^w(z-z_{k_{int}-0.5}) + w_{i,j,k_{int}-0.5}, & \mathbf{x} \in \mathbf{V}_{i,j,k_{int}}^{V(\mathbf{x}),1} \cap (z < \xi), \\ a_2^w(x-x_i)(y-y_j) + b_2^w(x-x_i) + c_2^w(y-y_j) \\ +d_2^w(z-z_{k_{int}+0.5}) + w_{i,j,k_{int}+0.5}, & \mathbf{x} \in \mathbf{V}_{i,j,k_{int}}^{V(\mathbf{x}),1} \cap (z > \xi). \end{cases}$$
(3.24)

Unknown coefficients of the polynomials (3.22), (3.23), (3.24) can be determined from the following conditions:

1. Interpolation at the vertices of the pentahedrons:

$$U(x_{i-0.5}, y_j, z_{k_{int}}) = u_{i-0.5,j,k_{int}}, \qquad U(x_{i+0.5}, y_j, z_{k_{int}}) = u_{i+0.5,j,k_{int}},$$

$$U(x_{i+0.5}, y_{j+1}, z_{k_{int}}) = u_{i+0.5,j+1,k_{int}}, \quad U(x_{i+0.5}, y_j, z_{k_{int}+1}) = u_{i+0.5,j,k_{int}+1},$$

$$U(x_{i+0.5}, y_{j+1}, z_{k_{int}+1}) = u_{i+0.5,j+1,k_{int}+1},$$

$$V(x_i, y_{j-0.5}, z_{k_{int}}) = v_{i,j-0.5,k_{int}}, \qquad V(x_i, y_{j+0.5}, z_{k_{int}}) = v_{i,j+0.5,k_{int}},$$

$$V(x_{i+1}, y_{j+0.5}, z_{k_{int}}) = v_{i+1,j+0.5,k_{int}}, \quad V(x_i, y_{j+0.5}, z_{k_{int}+1}) = v_{i,j+0.5,k_{int}+1},$$

$$V(x_{i+1}, y_{j+0.5}, z_{k_{int}+1}) = v_{i+1j+0.5k_{int}+1},$$

$$W(x_i, y_j, z_{k_{int}-0.5}) = w_{i,j,k_{int}-0.5}, \qquad W(x_i, y_j, z_{k_{int}+05}) = w_{i,j,k_{int}+0.5},$$

$$W(x_{i+1}, y_j, z_{k_{int}+0.5}) = w_{i+1,j,k_{int}+0.5}, \quad W(x_i, y_{j+1}, z_{k_{int}+0.5}) = w_{i,j+1,k_{int}+0.5},$$

$$W(x_{i+1}, y_{j+1}, z_{k_{int}+0.5}) = w_{i+1,j+1,k_{int}+0.5}.$$

2. Continuity of all displacement components across the interface:

$$[U] = 0, \quad \text{for any} \quad \mathbf{x} \in \mathbf{V}_{i,j,k_{int}}^{U(\mathbf{x}),1} \cap \{z = \xi\},$$

$$[V] = 0, \quad \text{for any} \quad \mathbf{x} \in \mathbf{V}_{i,j,k_{int}}^{V(\mathbf{x}),1} \cap \{z = \xi\},$$

$$[W] = 0, \quad \text{for any} \quad \mathbf{x} \in \mathbf{V}_{i,j,k_{int}}^{W(\mathbf{x}),1} \cap \{z = \xi\}.$$

3. Continuity of the normal components of the stress tensor across the interface:

$$\left[\mu \left(\frac{\partial U}{\partial z} + \frac{\partial W}{\partial x} \right) \right] = 0, \quad \text{for any} \quad \mathbf{x} \in \mathbf{V}_{i,j,k_{int}}^{U(\mathbf{x}),1} \cap \mathbf{V}_{i,j,k_{int}}^{W(\mathbf{x}),1} \cap \{z = \xi\},$$

$$\left[\mu \left(\frac{\partial V}{\partial z} + \frac{\partial W}{\partial y} \right) \right] = 0, \quad \text{for any} \quad \mathbf{x} \in \mathbf{V}_{i,j,k_{int}}^{V(\mathbf{x}),1} \cap \mathbf{V}_{i,j,k_{int}}^{W(\mathbf{x}),1} \cap \{z = \xi\},$$

$$\left[(\lambda + 2\mu) \frac{\partial W}{\partial z} + \lambda \left(\frac{\partial U}{\partial x} + \frac{\partial V}{\partial y} \right) \right] = 0,$$

$$\text{for any} \quad \mathbf{x} \in \mathbf{V}_{i,j,k_{int}}^{U(\mathbf{x}),1} \cap \mathbf{V}_{i,j,k_{int}}^{V(\mathbf{x}),1} \cap \mathbf{V}_{i,j,k_{int}}^{W(\mathbf{x}),1} \cap \{z = \xi\}.$$

Conditions 1. - 3. result in the following expressions for coefficients of the polynomials (3.22), (3.23), (3.24):

$$a_1^u = \frac{(\theta - 1)(\mu_1 - \mu_2)w_{xy,i,j,k_{int}+0.5} + \mu_2 u_{yz,i+0.5,j,k_{int}}}{(1 - \theta)\mu_1 + \theta\mu_2}, \quad b_1^u = u_{x,i-0.5,j,k_{int}},$$

$$d_1^u = \frac{\mu_2 u_{z,i+0.5,j,k_{int}} + (\theta - 1)(\mu_1 - \mu_2)w_{x,i,j,k_{int}+0.5}}{(1 - \theta)\mu_1 + \theta\mu_2}, \quad c_1^u = u_{y,i+0.5,j,k_{int}},$$

$$a_2^u = \frac{\theta(\mu_1 - \mu_2)w_{xy,i,j,k_{int}+0.5} + \mu_1 u_{yz,i+0.5,j,k_{int}}}{(1 - \theta)\mu_1 + \theta\mu_2}, \quad b_2^u = u_{x,i-0.5,j,k_{int}},$$

$$d_2^u = \frac{\mu_1 u_{z,i+0.5,j,k_{int}} + \theta(\mu_1 - \mu_2)w_{x,i,j,k_{int}+0.5}}{(1-\theta)\mu_1 + \theta\mu_2}, \quad c_2^u = u_{y,i+0.5,j,k_{int}+1},$$

$$a_1^v = \frac{(\theta-1)(\mu_1-\mu_2)w_{xy,ijk_{int}+0.5} + \mu_2 v_{xz,i,j+0.5,k_{int}}}{(1-\theta)\mu_1 + \theta\mu_2}, \quad b_1^v = v_{x,i,j+0.5,k_{int}},$$

$$d_1^v = \frac{\mu_2 v_{z,ij+0.5k_{int}} + (\theta-1)(\mu_1-\mu_2)w_{y,i,j,k_{int}+0.5}}{(1-\theta)\mu_1 + \theta\mu_2}, \quad c_1^v = v_{y,i,j-0.5,k_{int}},$$

$$a_2^v = \frac{\theta(\mu_1-\mu_2)w_{xy,ijk_{int}+0.5} + \mu_2 v_{xz,ij+0.5k_{int}}}{(1-\theta)\mu_1 + \theta\mu_2}, \quad b_2^v = v_{x,i,j+0.5,k_{int}+1},$$

$$d_2^v = \frac{\mu_1 v_{z,ij+0.5k_{int}} + \theta(\mu_1-\mu_2)w_{y,ijk_{int}+0.5}}{(1-\theta)\mu_1 + \theta\mu_2}, \quad c_2^v = v_{y,i,j-0.5,k_{int}},$$

$$a_1^w = w_{xy,i,j,k_{int}+0.5}, \quad b_1^w = w_{x,i,j,k_{int}+0.5}, \quad c_1^w = w_{y,i,j,k_{int}+0.5},$$

$$d_1^w = \frac{(\lambda_2 + 2\mu_2)w_{z,i,j,k_{int}-0.5} + (\theta-0.5)(\lambda_1-\lambda_2)(u_{x,i-0.5,j,k_{int}} + v_{y,i,j-0.5,k_{int}})}{(0.5-\theta)(\lambda_1+2\mu_1) + (0.5+\theta)(\lambda_2+2\mu_2)},$$

$$a_2^w = w_{xy,i,j,k_{int}+0.5}, \quad b_2^w = w_{x,i,j,k_{int}+0.5}, \quad c_2^w = w_{y,i,j,k_{int}+0.5},$$

$$d_2^w = \frac{(\lambda_1 + 2\mu_1)w_{z,i,j,k_{int}-0.5} + (\theta+0.5)(\lambda_1-\lambda_2)(u_{x,i-0.5,j,k_{int}} + v_{y,i,j-0.5,k_{int}})}{(0.5-\theta)(\lambda_1+2\mu_1) + (0.5+\theta)(\lambda_2+2\mu_2)}.$$

Then, after the substitution of these coefficients into the expressions for the polynomials 3.22, 3.23, 3.24, one calculates approximate stress tensor components, using the formulae (3.20).

If the interface lies between the coordinates $z_{k_{int}+0.5}$ and $z_{k_{int}+1}$, a triple of the pentahedrons $\mathbf{V}_{ijk_{int}}^{U(\mathbf{x}),2}$, $\mathbf{V}_{ijk_{int}}^{V(\mathbf{x}),2}$ and $\mathbf{V}_{ijk_{int}+1}^{W(\mathbf{x}),2}$ (all of them being intersected by the interface), is considered. The general representation of the polynomials, built in these pentahedrons, is the following:

$$U(x,y,z) = \begin{cases} a_1^u(y-y_j)(z-z_{k_{int}}) + b_1^u(x-x_{i+0.5}) + c_1^u(y-y_j) \\ +d_1^u(z-z_{k_{int}}) + u_{i+0.5jk_{int}}, \quad \mathbf{x} \in \mathbf{V}_{ijk_{int}}^{U(\mathbf{x}),2} \cap (z < \xi), \\ a_2^u(y-y_j)(z-z_{k_{int}+1}) + b_2^u(x-x_{i+0.5}) + c_2^u(y-y_j) \\ +d_2^u(z-z_{k_{int}+1}) + u_{i+0.5jk_{int}+1}, \quad \mathbf{x} \in \mathbf{V}_{ijk_{int}}^{U(\mathbf{x}),2} \cap (z > \xi), \end{cases}$$
$$(3.25)$$

$$V(x,y,z) = \begin{cases} a_1^v(x-x_i)(z-z_{k_{int}}) + b_1^v(x-x_i) + c_1^v(y-y_{j+0.5}) \\ +d_1^v(z-z_{k_{int}}) + v_{ij+0.5k_{int}}, \quad \mathbf{x} \in \mathbf{V}_{ijk_{int}}^{V(\mathbf{x}),2} \cap (z < \xi), \\ a_2^v(x-x_i)(z-z_{k_{int}+1}) + b_2^v(x-x_i) + c_2^v(y-y_{j+0.5}) \\ +d_2^v(z-z_{k_{int}+1}) + v_{ij+0.5k_{int}+1}, \quad \mathbf{x} \in \mathbf{V}_{ijk_{int}}^{V(\mathbf{x}),2} \cap (z > \xi), \end{cases}$$
$$(3.26)$$

$$W(x,y,z) = \begin{cases} a_1^w(x-x_i)(y-y_j) + b_1^w(x-x_i) + c_1^w(y-y_j) \\ +d_1^w(z-z_{k_{int}+0.5}) + w_{ijk_{int}+0.5}, \quad \mathbf{x} \in \mathbf{V}_{ijk_{int}}^{W(\mathbf{x}),2} \cap (z < \xi), \\ a_2^w(x-x_i)(y-y_j) + b_2^w(x-x_i) + c_2^w(y-y_j) \\ +d_2^w(z-z_{k_{int}+1.5}) + w_{ijk_{int}+1.5}, \quad \mathbf{x} \in \mathbf{V}_{ijk_{int}}^{W(\mathbf{x}),2} \cap (z > \xi). \end{cases}$$
$$(3.27)$$

Similar to the case described above, polynomials should satisfy the following conditions:

1. Interpolation at the grid points:

$$U(x_{i-0.5}, y_j, z_{k_{int}+1}) = u_{i-0.5jk_{int}+1}, \quad U(x_{i+0.5}, y_j, z_{k_{int}}) = u_{i+0.5jk_{int}},$$
$$U(x_{i+0.5}, y_j, z_{k_{int}+1}) = u_{i+0.5jk_{int}+1}, \quad U(x_{i+0.5}, y_{j+1}, z_{k_{int}}) = u_{i+0.5j+1k_{int}},$$
$$U(x_{i+0.5}, y_{j+1}, z_{k_{int}+1}) = u_{i+0.5j+1k_{int}+1},$$
$$V(x_i, y_{j-0.5}, z_{k_{int}+1}) = v_{ij-0.5k_{int}+1}, \quad V(x_i, y_{j+0.5}, z_{k_{int}}) = v_{ij+0.5k_{int}},$$
$$V(x_i, y_{j+0.5}, z_{k_{int}+1}) = v_{ij+0.5k_{int}+1}, \quad V(x_{i+1}, y_{j+0.5}, z_{k_{int}+1}) = v_{i+1j+0.5k_{int}+1},$$
$$V(x_{i+1}, y_{j+0.5}, z_{k_{int}}) = v_{i+1j+0.5k_{int}},$$
$$W(x_i, y_j, z_{k_{int}+0.5}) = w_{ijk_{int}+0.5}, \qquad W(x_{i+1}, y_j, z_{k_{int}+05}) = w_{i+1jk_{int}+0.5},$$
$$W(x_i, y_{j+1}, z_{k_{int}+0.5}) = w_{ij+1k_{int}+0.5}, \quad W(x_i, y_j, z_{k_{int}+1.5}) = w_{ijk_{int}+1.5},$$
$$W(x_{i+1}, y_{j+1}, z_{k_{int}+0.5}) = w_{i+1j+1k_{int}+0.5}.$$

2. Continuity of all displacement components across the interface:

$$[U] = 0, \quad \text{for any} \quad \mathbf{x} \in \mathbf{V}_{ijk_{int}}^{U(\mathbf{x}),2} \cap \{z = \xi\};$$
$$[V] = 0, \quad \text{for any} \quad \mathbf{x} \in \mathbf{V}_{ijk_{int}}^{V(\mathbf{x}),2} \cap \{z = \xi\};$$
$$[W] = 0, \quad \text{for any} \quad \mathbf{x} \in \mathbf{V}_{ijk_{int}+1}^{W(\mathbf{x}),2} \cap \{z = \xi\}.$$

3. Continuity of the normal components of the stress tensor across the interface:

$$\left[\mu\left(\frac{\partial U}{\partial z} + \frac{\partial W}{\partial x}\right)\right] = 0, \quad \text{for any} \quad \mathbf{x} \in \mathbf{V}_{ijk_{int}}^{U(\mathbf{x}),2} \cap \mathbf{V}_{ijk_{int}+1}^{W(\mathbf{x}),2} \cap \{z = \xi\},$$
$$\left[\mu\left(\frac{\partial V}{\partial z} + \frac{\partial W}{\partial y}\right)\right] = 0, \quad \text{for any} \quad \mathbf{x} \in \mathbf{V}_{ijk_{int}}^{V(\mathbf{x}),2} \cap \mathbf{V}_{ijk_{int}+1}^{W(\mathbf{x}),2} \cap \{z = \xi\},$$
$$\left[(\lambda + 2\mu)\frac{\partial W}{\partial z} + \lambda\left(\frac{\partial U}{\partial x} + \frac{\partial V}{\partial y}\right)\right] = 0,$$
$$\text{for any} \quad \mathbf{x} \in \mathbf{V}_{ijk_{int}}^{U(\mathbf{x}),2} \cap \mathbf{V}_{ijk_{int}}^{V(\mathbf{x}),2} \cap \mathbf{V}_{ijk_{int}+1}^{W(\mathbf{x}),2} \cap \{z = \xi\}.$$

These conditions result in the following expressions for the coefficients of the polynomials (3.25), (3.26), (3.27):

$$a_1^u = \frac{(\theta - 1)(\mu_1 - \mu_2)w_{xy,ijk_{int}+0.5} + \mu_2 u_{yz,i+0.5jk_{int}}}{(1 - \theta)\mu_1 + \theta\mu_2}, \quad b_1^u = u_{x,i-0.5jk_{int}+1},$$

$$d_1^u = \frac{\mu_2 u_{z,i+0.5jk_{int}} + (\theta - 1)(\mu_1 - \mu_2)w_{x,ijk_{int}+0.5}}{(1 - \theta)\mu_1 + \theta\mu_2}, \quad c_1^u = u_{y,i+0.5jk_{int}},$$

$$a_2^u = \frac{\theta(\mu_1 - \mu_2)w_{xy,ijk_{int}+0.5} + \mu_1 u_{yz,i+0.5jk_{int}}}{(1 - \theta)\mu_1 + \theta\mu_2}, \quad b_2^u = u_{x,i-0.5jk_{int}+1},$$

$$d_2^u = \frac{\mu_1 u_{z,i+0.5jk_{int}} + \theta(\mu_1 - \mu_2)w_{x,ijk_{int}+0.5}}{(1-\theta)\mu_1 + \theta\mu_2}, \quad c_2^u = u_{y,i+0.5jk_{int}+1},$$

$$a_1^v = \frac{(\theta-1)(\mu_1 - \mu_2)w_{xy,ijk_{int}+0.5} + \mu_2 v_{xz,ij+0.5k_{int}}}{(1-\theta)\mu_1 + \theta\mu_2}, \quad b_1^v = v_{x,ij+0.5k_{int}},$$

$$d_1^v = \frac{\mu_2 v_{z,ij+0.5k_{int}} + (\theta-1)(\mu_1 - \mu_2)w_{y,ijk_{int}+0.5}}{(1-\theta)\mu_1 + \theta\mu_2}, \quad c_1^v = v_{y,ij-0.5k_{int}+1},$$

$$a_2^v = \frac{\theta(\mu_1 - \mu_2)w_{xy,ijk_{int}+0.5} + \mu_2 v_{xz,ij+0.5k_{int}}}{(1-\theta)\mu_1 + \theta\mu_2}, \quad b_2^v = v_{x,ij+0.5k_{int}+1},$$

$$d_2^v = \frac{\mu_1 v_{z,ij+0.5k_{int}} + \theta(\mu_1 - \mu_2)w_{y,ijk_{int}+0.5}}{(1-\theta)\mu_1 + \theta\mu_2}, \quad c_2^v = v_{y,ij-0.5k_{int}+1},$$

$$a_1^w = w_{xy,ijk_{int}+0.5}, \quad b_1^w = w_{x,ijk_{int}+0.5}, \quad c_1^w = w_{y,ijk_{int}+0.5},$$

$$d_1^w = \frac{(\lambda_2 + 2\mu_2)w_{z,ijk_{int}+0.5} + (\theta-1.5)(\lambda_1 - \lambda_2)(u_{x,i-0.5jk_{int}+1} + v_{y,ij-0.5k_{int}+1})}{(1.5-\theta)(\lambda_1 + 2\mu_1) + (\theta-0.5)(\lambda_2 + 2\mu_2)},$$

$$a_2^w = w_{xy,ijk_{int}+0.5}, \quad b_2^w = w_{x,ijk_{int}+0.5}, \quad c_2^w = w_{y,ijk_{int}+0.5},$$

$$d_2^w = \frac{(\lambda_1 + 2\mu_1)w_{z,ijk_{int}+0.5} + (\theta-0.5)(\lambda_1 - \lambda_2)(u_{x,i-0.5jk_{int}+1} + v_{y,ij-0.5k_{int}+1})}{(0.5-\theta)(\lambda_1 + 2\mu_1) + (0.5+\theta)(\lambda_2 + 2\mu_2)}.$$

In the case when pentahedrons are not intersected by the interface, the polynomials are derived only as interpolation of the values in the vertices. In the volumes adjacent to the boundary Γ, the proper boundary conditions are taken into account as well.

Summarizing all the cases mentioned above, approximations for the stress tensor components can be written in the following way:

$$S_{i+0.5,j+0.5,k}^{12} = \langle\mu\rangle_{i+0.5,j+0.5,k}^{uv}(u_{y,i+0.5,j,k} + v_{x,i,j+0.5,k}),$$

$$S_{i+0.5,j,k+0.5}^{13} = \langle\mu\rangle_{i+0.5,j,k+0.5}^{uw}(u_{z,i+0.5,j,k} + w_{x,i,j,k+0.5}),$$

$$S_{i,j+0.5,k+0.5}^{23} = \langle\mu\rangle_{i,j+0.5,k+0.5}^{vw}(v_{z,i,j+0.5,k} + w_{y,i,j,k+0.5}),$$

$$S_{i,j,k}^{11} = \left(\langle\lambda\rangle_{i,j,k}^{u} + 2\mu_1\right)u_{x,i-0.5,j,k} + \langle\lambda\rangle_{ijk}^{v}v_{y,i,j-0.5,k} + \langle\lambda\rangle_{i,j,k}^{w}w_{z,i,j,k-0.5},$$

$$S_{i,j,k}^{22} = \left(\langle\lambda\rangle_{i,j,k}^{v} + 2\mu_1\right)v_{y,i,j-0.5,k} + \langle\lambda\rangle_{i,j,k}^{u}u_{x,i-0.5,j,k} + \langle\lambda\rangle_{i,j,k}^{w}w_{z,i,j,k-0.5},$$

$$S_{i,j,k}^{33} = \langle\lambda + 2\mu\rangle_{ijk}^{w}w_{z,i,j,k-0.5} + \langle\lambda\rangle_{i,j,k}^{uv}\left(u_{x,i-0.5,j,k} + v_{y,i,j-0.5,k}\right),$$

$$(3.28)$$

where

$$\langle\mu\rangle^{uv}_{i+0.5,j+0.5,k} = \left\{ \begin{array}{ll} \mu_1, & k \le k_{int}, \\ \mu_2, & k > k_{int}, \end{array} \right.$$

$$\langle\mu\rangle^{uw}_{i+0.5,j,k+0.5} = \langle\mu\rangle^{vw}_{i,j+0.5,k+0.5} = \left\{ \begin{array}{ll} \mu_1, & k < k_{int}, \\ \dfrac{\mu_1\mu_2}{(1-\theta)\mu_1 + \theta\mu_2}, & k = k_{int}, \\ \mu_2, & k > k_{int} + 1, \end{array} \right.$$

$$\langle\lambda\rangle^u_{i,j,k} = \langle\lambda\rangle^v_{i,j,k}$$
$$= \left\{ \begin{array}{ll} \lambda_1, & k < k_{int} \text{ or } k = k_{int}, \ \theta > 0.5, \\ \lambda_1\dfrac{(0.5-\theta)(\lambda_2+2\mu_1)+(0.5+\theta)(\lambda_2+2\mu_2)}{(0.5-\theta)(\lambda_1+2\mu_1)+(0.5+\theta)(\lambda_2+2\mu_2)}, & k = k_{int}, \ \theta < 0.5, \\ \lambda_2\dfrac{(\theta-0.5)(\lambda_1+2\mu_2)+(1.5-\theta)(\lambda_1+2\mu_1)}{(1.5-\theta)(\lambda_1+2\mu_1)+(\theta-0.5)(\lambda_2+2\mu_2)}, & k = k_{int}+1, \ \theta > 0.5, \\ \lambda_2, & k > k_{int}+1, \text{ or } k = k_{int}+1, \ \theta < 0.5, \end{array} \right.$$

$$\langle\lambda\rangle^w_{i,j,k} = \left\{ \begin{array}{ll} \lambda_1, & k < k_{int}, \text{ or } k = k_{int}, \ \theta > 0.5, \\ \lambda_1\dfrac{\lambda_2+2\mu_2}{(0.5-\theta)(\lambda_1+2\mu_1)+(0.5+\theta)(\lambda_2+2\mu_2)}, & k = k_{int}, \ \theta < 0.5, \\ \lambda_2\dfrac{\lambda_1+2\mu_1}{(1.5-\theta)(\lambda_1+2\mu_1)+(\theta-0.5)(\lambda_2+2\mu_2)}, & k = k_{int}+1, \ \theta > 0.5, \\ \lambda_2, & k > k_{int}+1, \text{ or } k = k_{int}+1, \ \theta < 0.5, \end{array} \right.$$

$$\langle\lambda\rangle^{uv}_{i,j,k} = \left\{ \begin{array}{ll} \lambda_1, & k < k_{int}, \text{ or } k = k_{int}, \ \theta > 0.5, \\ \dfrac{(0.5-\theta)(\lambda_1+2\mu_1)\lambda_2+(0.5+\theta)(\lambda_2+2\mu_2)\lambda_1}{(0.5-\theta)(\lambda_1+2\mu_1)+(0.5+\theta)(\lambda_2+2\mu_2)}, & k = k_{int}, \ \theta < 0.5, \\ \dfrac{(1.5-\theta)(\lambda_1+2\mu_1)\lambda_2+(\theta-0.5)(\lambda_2+2\mu_2)\lambda_1}{(1.5-\theta)(\lambda_1+2\mu_1)+(\theta-0.5)(\lambda_2+2\mu_2)}, & k = k_{int}+1, \ \theta > 0.5, \\ \lambda_2, & k > k_{int}+1, \text{ or } k = k_{int}+1, \ \theta < 0.5, \end{array} \right.$$

$$\langle\lambda+2\mu\rangle^w_{i,j,k} = \left\{ \begin{array}{ll} \lambda_1+2\mu_1, & k < k_{int}, \text{ or } k = k_{int}, \ \theta > 0.5, \\ \dfrac{(\lambda_1+2\mu_1)(\lambda_2+2\mu_2)}{(0.5-\theta)(\lambda_1+2\mu_1)+(0.5+\theta)(\lambda_2+2\mu_2)}, & k = k_{int}, \ \theta < 0.5, \\ \dfrac{(\lambda_1+2\mu_1)(\lambda_2+2\mu_2)}{(1.5-\theta)(\lambda_1+2\mu_1)+(\theta-0.5)(\lambda_2+2\mu_2)}, & k = k_{int}+1, \ \theta > 0.5, \\ \lambda_2+2\mu_2, & k > k_{int}+1, \text{ or } k = k_{int}+1, \ \theta < 0.5, \end{array} \right.$$

$$\langle\lambda+2\mu\rangle^u_{i,j,k} = \langle\lambda\rangle^u_{i,j,k} + 2\mu_{i,j,k}, \quad \langle\lambda+2\mu\rangle^v_{i,j,k} = \langle\lambda\rangle^v_{i,j,k} + 2\mu_{i,j,k},$$

Now, we substitute derived approximating expressions for the stress tensor components (3.28) and fluid velocity components (3.19) into the equations (3.14), and obtain a discrete system of equations for the unknown grid functions u, v, w, p:

$$-(\langle\lambda+2\mu\rangle^u_{i,j,k}u_{\bar{x},i+0.5,j,k} + \langle\lambda\rangle^v_{i,j,k}v_{\bar{y},i,j+0.5,k} + \langle\lambda\rangle^w_{i,j,k}w_{\bar{z},i,j,k+0.5})_x$$
$$-(\mu_{i+0.5,j-0.5,k}(u_{\bar{y},i+0.5,j,k} + v_{\bar{x},i+1,j-0.5,k}))_y$$
$$-(\langle\mu\rangle^{uw}_{i+0.5,j,k-0.5}(u_{\bar{z},i+0.5,j,k} + w_{\bar{x},i+1,j,k-0.5}))_z + p_{\bar{x},i,j,k} = 0, \quad (3.29)$$

$$- (\langle\lambda + 2\mu\rangle^v_{i,j,k} v_{\bar{y},i,j+0.5,k} + \langle\lambda\rangle^u_{i,j,k} u_{\bar{x},i+0.5,j,k} + \langle\lambda\rangle^w_{i,j,k} w_{\bar{z},i,j,k+0.5})_y$$
$$- (\mu_{i-0.5,j+0.5,k}(v_{\bar{x},i+1,j+0.5,k} + u_{\bar{y},i-0.5,j+1,k}))_x$$
$$- (\langle\mu\rangle^{vw}_{i,j+0.5,k-0.5}(v_{\bar{z},i,j+0.5,k} + w_{\bar{y},i,j+1,k-0.5}))_z + p_{\bar{y},i,j,k} = 0, \quad (3.30)$$

$$- (\langle\lambda + 2\mu\rangle^w_{i,j,k} w_{\bar{z},i,j,k+0.5} + \langle\lambda\rangle^{uv}_{i,j,k}(u_{\bar{x},i+0.5,j,k} + v_{\bar{y},i,j+0.5,k}))_z$$
$$- (\langle\mu\rangle^{uw}_{i-0.5,j,k+0.5}(w_{\bar{x},i,j,k+0.5} + u_{\bar{z},i-0.5,j,k+1}))_x$$
$$- (\langle\mu\rangle^{vw}_{i,j-0.5,k+0.5}(w_{\bar{y},i,j,k+0.5} + v_{\bar{z},i,j-0.5,k+1}))_y + p_{\bar{z},i,j,k} = 0, \quad (3.31)$$

$$(\langle a\rangle_{i,j,k} p_{i,j,k} + u_{x,i-0.5,j,k} + v_{y,i,j-0.5,k} + w_{z,i,j,k-0.5})_t$$
$$- (\langle\kappa\rangle^1_{i-0.5,j,k} p^\sigma_{\bar{x}})_x - (\langle\kappa\rangle^2_{i,j-0.5,k} p^\sigma_{\bar{y}})_y - (\langle\kappa\rangle^3_{i-0.5,j,k} p^\sigma_{\bar{z}})_z = \langle f\rangle^\sigma_{i,j,k}, \quad (3.32)$$

where $\langle a\rangle$ and $\langle f\rangle$ are calculated according to the formulae (3.15).

Note that finite volume methods are known for their property to preserve fluxes of the problem, and to produce the so-called conservative discretizations. The derived finite difference scheme (3.29) - (3.32) is hence conservative due to the derivation. Still, the matrix of the obtained system can be non-symmetric due to the specific averagings of the coefficients in the stresses S^{11}, S^{22} and S^{33}, what can produce, e.g., different coefficients in front of the mixed derivative $w_{\bar{z}x}$ (in the first equation) and in front of $u_{\bar{x}z}$ (in the third equation).

Up to our knowledge, no such scheme was derived earlier. In the case of constant coefficients, the scheme is identical with the finite difference scheme from [66], where the Biot model in the homogeneous porous medium is considered.

3.3 Numerical experiments: convergence tests

Here we present a set of numerical experiments, which are based on the discrete model (3.29) - (3.32). First, we show that the derived method is exact for the piecewise-continuous polynomials of certain order. Second, we study the convergence for both the basic unknowns of the problem (displacement components and pressure) and the fluxes of the problem (components of the stress tensor and of the fluid velocity) with respect to an exact solution of a continuous problem. In the experiments in this Chapter, altering directions line Gauss-Seidel method was used to solve the linear system, produced by the discretization.

Example A.

In this example we show that our method is exact if the solution of the problem (3.5) and (3.6) is represented by certain polynomials. In particular, these polynomials should be piecewise-linear, extended with one special piecewise-bilinear

term for each displacement component and piecewise-trilinear for pressure. For example, the following polynomials are of this kind:

$$
U^{ex}(x,y,z) = \begin{cases} yz + x + y + z + 1, & 0 < z < \xi, \\ \dfrac{2\mu_1 - \mu_2}{\mu_2}yz + x + \dfrac{2\mu_2\xi + \mu_2 - 2\mu_1\xi}{\mu_2}y + 2z + 1 - \xi, & \xi < z < 1, \end{cases}
$$

$$
V^{ex}(x,y,z) = \begin{cases} xz + x + \dfrac{3\lambda_2 + 4\mu_2 - 2\lambda_1 - 2\mu_1}{\lambda_1 - \lambda_2}y + z + 1, & 0 < z < \xi, \\ \dfrac{2\mu_1 - \mu_2}{\mu_2}xz + \dfrac{2\xi\mu_2 - 2\xi\mu_1 + \mu_2}{\mu_2}x \\ \quad + \dfrac{3\lambda_2 + 4\mu_2 - 2\lambda_1 - 2\mu_1}{\lambda_1 - \lambda_2}y + 2z + 1 - \xi, & \xi < z < 1, \end{cases}
$$

$$
W^{ex}(x,y,z) = \begin{cases} xy + \dfrac{\mu_1 - 2\mu_2}{\mu_2 - \mu_1}x + \dfrac{\mu_1 - 2\mu_2}{\mu_2 - \mu_1}y + z + 1, & 0 < z < \xi, \\ xy + \dfrac{\mu_1 - 2\mu_2}{\mu_2 - \mu_1}x + \dfrac{\mu_1 - 2\mu_2}{\mu_2 - \mu_1}y + 2z + 1 - \xi, & \xi < z < 1, \end{cases}
$$

$$
P^{ex}(x,y,z) = \begin{cases} \kappa_2 xy(z - \xi), & 0 < z < \xi, \\ \kappa_1 xy(z - \xi), & \xi < z < 1. \end{cases}
$$

Initial conditions are prescribed from the exact solution and values for the boundary conditions are calculated from the exact solution and look as following:

$$
p(\mathbf{x}, t) = P^{ex}(\mathbf{x}, t),\ \mathbf{x} \in \Gamma,
$$
$$
\frac{\partial u}{\partial x} = \frac{\partial U^{ex}}{\partial x},\ v = V^{ex},\ w = W^{ex},\ \text{at } x = 0, 1,
$$
$$
u = U^{ex},\ \frac{\partial v}{\partial y} = \frac{\partial V^{ex}}{\partial y},\ w = W^{ex},\ \text{at } y = 0, 1,
$$
$$
u = U^{ex},\ v = V^{ex},\ \frac{\partial w}{\partial z} = \frac{\partial W^{ex}}{\partial z},\ \text{at } z = 0, 1.
$$

After the discretization (3.29) - (3.32) is performed, we vary coefficients λ_1, λ_2, μ_1, μ_2, κ_1, κ_2 and solve obtained linear system with an iterative solver. Results of the experiments show that the solver converges always after the first iteration and reproduces the exact solution in the grid points.

Example B.

In this example, we choose exact solution of the continuous problem (3.5) - (3.6) as following:

$$
u^{ex}(x,y,z,t) = \begin{cases} \dfrac{1}{\mu_1}\cos(\pi x)y\sin(z - \xi)e^{-t}, & 0 < z < \xi, \\ \dfrac{1}{\mu_2}\cos(\pi x)y\sin(z - \xi)e^{-t}, & \xi < z < 1, \end{cases}
$$

$$
v^{ex}(x,y,z,t) = \begin{cases} \dfrac{1}{\mu_1}x\cos(\pi y)\sin(z - \xi)e^{-t}, & 0 < z < \xi, \\ \dfrac{1}{\mu_2}x\cos(\pi y)\sin(z - \xi)e^{-t}, & \xi < z < 1, \end{cases}
$$

$$w^{ex}(x,y,z,t) = \begin{cases} \dfrac{1}{\lambda_1 + 2\mu_1} xy \sin(z-\xi)e^{-t}, & 0 < z < \xi, \\ \dfrac{1}{\lambda_2 + 2\mu_2} xy \sin(z-\xi)e^{-t}, & \xi < z < 1, \end{cases}$$

$$p^{ex}(x,y,z,t) = \begin{cases} \dfrac{1}{\kappa_1} xy(z-\xi)\sin(z)e^{-t}, & 0 < z < \xi, \\ \dfrac{1}{\kappa_2} xy(z-\xi)\sin(z)e^{-t}, & \xi < z < 1. \end{cases}$$

Exact solutions for the stress tensor and the fluid velocity vector are calculated, using the solutions u^{ex}, v^{ex}, w^{ex}, p^{ex}, according to the formulae (3.2), (3.3) respectively.

The boundary conditions and initial conditions are calculated in the same way, as described in Example A. The right hand sides of the equations are calculated by means of substitution of the exact solution into the system.

The following values of the parameters are chosen in this experiment: $T = 0.001$, $\xi = 0.5001$, and $a = 0$ (fluid is incompressible). We assign the time discretization parameter $\sigma = 1$, which corresponds to the fully-implicit discretization in time.

Within our numerical experiments, we compare numerical solutions calculated on the different grids to the known analytical solutions and calculate relative discrete maximum norm (C-norm) of the errors of the solution. The experiments are performed consequently on the grids with $N_1 = N_2 = N_3 = 8$, 16, 32, 64. The ratio between the norms of the errors of the unknowns on the two consequent grids is calculated as

$$r_q = \frac{\|\epsilon_q^{prev}\|_c}{\|\epsilon_q\|_c},$$

where $q = \{u, v, w, p, S^{11}, S^{22}, S^{33}, S^{12}, S^{13}, S^{23}, V^1, V^2, V^3\}$, $\|\epsilon_q\|_c$ is the maximum norm of the error of unknown q, calculated on the current grid and $\|\epsilon_q^{prev}\|_c$ is the maximum norm of the error of unknown q, calculated on the previous (coarser) grid from the sequence of grids mentioned above.

The rate of convergence for each unknown is presented in the experiments as well and it is calculated according to the formula

$$rate = \frac{\ln \dfrac{\|\epsilon_{q,1}\|_c}{\|\epsilon_{q,2}\|_c}}{\ln \dfrac{h_1}{h_2}}, \tag{3.33}$$

where $\epsilon_{q,1}$ are $\epsilon_{q,2}$ are errors of the unknown q, calculated on the grids with the steps $h_1 = 1/32$ and $h_2 = 1/64$, respectively.

In the experiments, we use only one step in time, i.e., $\tau = T$. Since the time interval T is rather small, this means that the time step τ is rather small. Usually, solution of the poroelasticity problem with the small time step is more difficult

grid	$\|\epsilon_u\|_c$	r_u	$\|\epsilon_v\|_c$	r_v	$\|\epsilon_w\|_c$	r_w	$\|\epsilon_p\|_c$	r_p
8^3	$0.1336E-02$	$-$	$0.1336E-02$	$-$	$0.2259E-02$	$-$	$0.4182E-02$	$-$
16^3	$0.3639E-03$	3.7	$0.3639E-03$	3.7	$0.6016E-03$	3.8	$0.1074E-02$	3.9
32^3	$0.9205E-04$	4.0	$0.9205E-04$	4.0	$0.1525E-03$	3.9	$0.2805E-03$	3.8
64^3	$0.2317E-04$	4.0	$0.2317E-04$	4.0	$0.3847E-04$	4.0	$0.6944E-04$	4.0
rate	$-$	2.0	$-$	2.0	$-$	2.0	$-$	2.0

Table 3.1: Example B - 1: Convergence of u, v, w, p in the maximum norm.

grid	$\|\epsilon_{S^{11}}\|_c$	$r_{S^{11}}$	$\|\epsilon_{S^{22}}\|_c$	$r_{S^{22}}$	$\|\epsilon_{S^{33}}\|_c$	$r_{S^{33}}$
8^3	$0.1482E-01$	$-$	$0.1482E-01$	$-$	$0.1877E-01$	$-$
16^3	$0.5440E-02$	2.7	$0.5440E-02$	2.7	$0.4870E-02$	3.9
32^3	$0.1606E-02$	3.4	$0.1606E-02$	3.4	$0.1235E-02$	3.9
64^3	$0.4306E-03$	3.7	$0.4306E-03$	3.7	$0.3080E-03$	4.0
rate	$-$	1.9	$-$	1.9	$-$	2.0

Table 3.2: Example B - 1: Convergence of the stress tensor components in the maximum norm.

numerically, and often it results in artificial oscillations of the pressure at the first time steps of the process. On the other hand, the small time step guarantees that during the refinement of the mesh in space, there is no dominance of the error part, depending on the time step τ.

Example B - 1

In this example, coefficients λ, μ and κ experience jumps of six orders of magnitude: $\lambda_1 = 1$, $\mu_1 = 1$, $\kappa_1 = 1$, $\lambda_2 = 10^6$, $\mu_2 = 10^6$, $\kappa_2 = 10^6$.

Convergence results for this set of parameters are summarized in Tables 3.1 - 3.4. One can see from the tables that the second order of convergence is observed for primary unknowns (u, v, w and p) as well as for the fluxes of the problem (stress tensor and fluid velocity components).

Example B - 2

grid	$\|\epsilon_{S^{12}}\|_c$	$r_{S^{12}}$	$\|\epsilon_{S^{13}}\|_c$	$r_{S^{13}}$	$\|\epsilon_{S^{23}}\|_c$	$r_{S^{23}}$
8^3	$0.1367E-01$	$-$	$0.1947E-01$	$-$	$0.1947E-01$	$-$
16^3	$0.4573E-02$	3.0	$0.5041E-02$	3.9	$0.5041E-02$	3.9
32^3	$0.1367E-02$	3.3	$0.1280E-02$	3.9	$0.1280E-02$	3.9
64^3	$0.3711E-03$	3.7	$0.3198E-03$	4.0	$0.3198E-03$	4.0
rate	$-$	1.9	$-$	2.0	$-$	2.0

Table 3.3: Example B - 1: Convergence of the stress tensor components in the maximum norm.

grid	$\|\epsilon_{V^1}\|_c$	r_{V^1}	$\|\epsilon_{V^2}\|_c$	r_{V^2}	$\|\epsilon_{V^3}\|_c$	r_{V^3}
8^3	$0.1867E+00$	–	$0.1867E+00$	–	$0.2818E+00$	–
16^3	$0.4256E-01$	4.4	$0.4256E-01$	4.4	$0.4992E-01$	5.6
32^3	$0.1159E-01$	3.7	$0.1159E-01$	3.7	$0.1169E-01$	4.2
64^3	$0.3802E-02$	3.0	$0.3802E-02$	3.0	$0.3236E-02$	3.6
rate	–	1.6	–	1.6	–	1.8

Table 3.4: Example B - 1: Convergence of the fluid velocity components in the maximum norm.

In this example, we change the location of the layers from Example B - 1, what corresponds to $\lambda_1 = 10^6$, $\mu_1 = 10^6$, $\kappa_1 = 10^6$, $\lambda_2 = 1$, $\mu_2 = 1$, $\kappa_2 = 1$. The respective convergence results are summarized in Tables 3.5 - 3.8. As in Example B - 1, the second order of convergence is observed for all unknowns.

grid	$\|\epsilon_u\|_c$	r_u	$\|\epsilon_v\|_c$	r_v	$\|\epsilon_w\|_c$	r_w	$\|\epsilon_p\|_c$	r_p
8^3	$0.1337E-02$	–	$0.1337E-02$	–	$0.2321E-02$	–	$0.3858E-02$	–
16^3	$0.3637E-03$	3.7	$0.3637E-03$	3.7	$0.6153E-03$	3.8	$0.9877E-03$	3.9
32^3	$0.9189E-04$	4.0	$0.9189E-04$	4.0	$0.1563E-03$	3.9	$0.2583E-03$	3.8
64^3	$0.2308E-04$	4.0	$0.2308E-04$	4.0	$0.3942E-04$	4.0	$0.6412E-04$	4.0
rate	–	2.0	–	2.0	–	2.0	–	2.0

Table 3.5: Example B - 2: Convergence of u, v, w, p in the maximum norm.

grid	$\|\epsilon_{S^{11}}\|_c$	$r_{S^{11}}$	$\|\epsilon_{S^{22}}\|_c$	$r_{S^{22}}$	$\|\epsilon_{S^{33}}\|_c$	$r_{S^{23}}$
8^3	$0.1463E-01$	–	$0.1463E-01$	–	$0.1857E-01$	–
16^3	$0.5401E-02$	2.7	$0.5401E-02$	2.7	$0.4828E-02$	3.8
32^3	$0.1598E-02$	3.4	$0.1598E-02$	3.4	$0.1224E-02$	3.9
64^3	$0.4300E-03$	3.7	$0.4300E-03$	3.7	$0.3056E-03$	4.0
rate	–	1.9	–	1.9	–	2.0

Table 3.6: Example B - 2: Convergence of the stress tensor components in the maximum norm.

grid	$\|\epsilon_{S^{12}}\|_c$	$r_{S^{12}}$	$\|\epsilon_{S^{13}}\|_c$	$r_{S^{13}}$	$\|\epsilon_{S^{23}}\|_c$	$r_{S^{23}}$
8^3	$0.1256E - 01$	–	$0.1679E - 01$	–	$0.1679E - 01$	–
16^3	$0.4713E - 02$	2.7	$0.4708E - 02$	3.6	$0.4708E - 02$	3.6
32^3	$0.1405E - 02$	3.4	$0.1233E - 02$	3.8	$0.1233E - 02$	3.8
64^3	$0.3811E - 03$	3.7	$0.3133E - 03$	3.9	$0.3133E - 03$	3.9
rate	–	1.9	–	2.0	–	2.0

Table 3.7: Example B - 2: Convergence of the stress tensor components in the maximum norm.

grid	$\|\epsilon_{V^1}\|_c$	r_{V^1}	$\|\epsilon_{V^2}\|_c$	r_{V^2}	$\|\epsilon_{V^3}\|_c$	r_{V^3}
8^3	$0.2021E + 00$	–	$0.2021E + 00$	–	$0.1743E + 00$	–
16^3	$0.4510E - 01$	4.5	$0.4510E - 01$	4.5	$0.4066E - 01$	4.3
32^3	$0.1207E - 01$	3.7	$0.1207E - 01$	3.7	$0.1074E - 01$	3.8
64^3	$0.3849E - 02$	3.1	$0.3849E - 02$	3.1	$0.3144E - 02$	3.4
rate	–	1.6	–	1.6	–	1.8

Table 3.8: Example B - 2: Convergence of the fluid velocity components in the maximum norm.

Chapter 4

Multigrid solver for the three dimensional Biot system

In this chapter, a multigrid solver for the three-dimensional discretized Biot model is developed in order to solve efficiently the produced linear system. The crucial point is to derive problem-dependent restriction and prolongation operators. The developed multigrid solver is tested on a number of model problems. Numerical experiments showed that, due to the proper problem-dependent prolongation and (or) restriction, the multigrid solver is robust with respect to the possible jumps of the coefficients. Finally, real poroelastic process in the two-layered porous medium is modelled by the Biot system with discontinuous coefficients. The respective system is then discretized and solved by means of the multigrid method.

4.1   Multigrid method

Multigrid methodology allows one to construct efficient linear solvers for large class of problems, including discretized elliptic PDEs and systems of PDEs.

Multigrid method is based on two principles: smoothing of the error and coarse grid correction. First principle exploits the fact that many basic iterative methods, being applied to a discrete elliptic problem, although possessing poor convergence, have a strong smoothing effect on the error of the solution. Due to this property, within the multigrid algorithm, such iterative methods are called smoothers. The second principle states that a smooth error of the solution can be well (and naturally less expansive) approximated on the coarser grid. The proper combination of these two principles gives a good foundation for development of efficient multilevel linear solvers.

Although the multigrid strategy is very general, here we focus on it as a strategy to solve the discrete elliptic problems. Below, we present a brief sketch of the method.

Let us consider the discrete elliptic problem

$$L_h u_h = f_h, \tag{4.1}$$

which is associated with a grid ω_h, h being a grid step size.

Then, let us double the step size, and consider a grid ω_{2h}. We will call this grid coarse with respect to the grid ω_h, which is, in its turn called fine with respect to ω_{2h}. Now, we can introduce the so-called two-grid cycle, which will be used as a basis for the definition the multigrid algorithm. The two-grid cycle reads:

1. Perform n_1 steps using the pre-smoothing operator S_h on the fine grid, using some initial guess $u^{(0)}$:

$$u_h^{(1)} = S_h^{n_1}(u^{(0)}, L_h, f_h),$$

2. Calculate the residual $r_h = f_h - L_h u_h^{(1)}$ and transfer it to the coarse grid, using restriction operator $R_{h,2h}$:

$$r_{2h} = R_{h,2h} r_h,$$

3. Solve the coarse grid defect equation $L_{2h} e_{2h} = r_{2h}$ exactly

$$e_{2h} = L_{2h}^{-1} r_{2h},$$

4. Interpolate calculated correction to the fine grid using prolongation operator $P_{2h,h}$:

$$e_h = P_{2h,h} e_{2h}$$

5. Correct the current fine grid approximation, obtained at the step 1., $u_h^{(2)} = u^{(1)} + e_h$ and perform n_2 post-smoothing steps on the fine grid:

$$u_h^{(3)} = S_h^{n_2}(u^{(2)}, L_h, f_h).$$

To move on from the two grid cycle to the multigrid, we consider a hierarchy of grids

$$\omega_h, \ \omega_{2h}, \ \omega_{4h}, \ ..., \ \omega_{h_0}, \tag{4.2}$$

which is obtained by means of doubling the grid steps successively, until the coarsest grid ω_{h_0} is approached.

If, instead of inverting L_{2h} at the step 3 of the two-grid cycle, the coarse grid equation is solved recursively by the two-grid algorithm, employing the grid ω_{4h},

and so on, proceeding with recursion until the coarsest grid is approached, we define a multigrid method.

As it can be seen from the definition, the multigrid method has a complex structure. The following components must be specified: smoothing procedure, coarsening procedure, restriction operator, coarse grid operator, and interpolation operator.

These components have to be carefully chosen and adjusted to each particular problem. Unfortunately, the choice of multigrid components is not obvious and there are no universal rules, which indicate it. Each problem one wants to solve with the multigrid should first be carefully analyzed.

4.1.1 Multigrid method for systems of PDEs

Originally, multigrid method was designed to solve the discrete scalar PDEs. However, in practical applications, a big variety of PDE systems often has to be solved, e.g. elasticity system, Stokes or Navier-Stokes system, etc. This motivates the development of certain extensions of the scalar multigrid, which would be able to handle the discretized systems of PDEs as well.

The straightforward application of the scalar multigrid methodology to solve the discretized systems of PDEs can handle efficiently only weakly coupled systems. In some multigrid literature, this approach is called variable-based multigrid (see, e.g. [[59, 23]]). However, when the coupling between the unknowns of the system is strong enough, this kind of approach becomes inefficient and more appropriate extension of the multigrid method is needed. The crucial property of the multigrid method for such systems is the following - the solver should distinguish the unknowns, which correspond to different physical unknowns of the initial system of PDEs. This can be done in the following way: the unknowns, which correspond to the same grid point, are grouped together and coefficient matrix is written in the point-block form. In some multigrid literature (see, e.g. [35],[23]), this approach is called point-block multigrid (or point-based multigrid). It implies the following:

1. The use of the collective relaxation as pre- and post-smoothing procedures. It means that all the unknowns, which correspond to one grid point, are relaxed simultaneously,

2. Block-wise interpolation and, probably, restriction.

This approach can handle efficiently strongly coupled systems.

4.1.2 Multigrid method for problems with discontinuous coefficients

Problems with discontinuous coefficients arise in many practical applications, since many natural as well as industrial materials have an inhomogeneous structure.

In general, the convergence of a standard multigrid solver deteriorates when the coefficients of the initial PDE experience large discontinuities across certain interfaces between subdomains with different physical properties. Moreover, the rate of convergence depends on the magnitude of the discontinuity and on its location with respect to the grid lines.

This implies that, in order to efficiently solve problems with discontinuous coefficients, a very careful adjustment of the multigrid components should be done. This includes the proper choice of the relaxation method, coarse grid operator, prolongation and restriction operators. Below, we explain in more details why these choices are important. First, the relaxation method used in pre- and post- smoothing steps should be applicable when the coefficients of the problem are discontinuous. Then, the coarse grid problem should represent the fine grid problem good enough. If the discretization of the problem is done in such a way that the fine grid lines are tied up to the interfaces of discontinuities, it can naturally happen that these interfaces do not lie on the coarse grid lines. In this case, the direct discretization L_{2h} on the coarse grid is not necessarily the good approximation of the fine grid discretization L_h. This might lead to the deterioration of the multigrid convergence or even to a divergence. The two basic approaches allow one to obtain a satisfactory coarse grid discretization. First, to build the discretization of the problem in such a way that it allows the discontinuities to be freely located with respect to the grid lines (both fine and coarse). In this case, the coarse grid operator L_{2h} is obtained in a natural way as a discretization of the problem on the coarse grid. Second approach is to use the so-called Galerkin coarse grid operator, which is defined as

$$L_{2h} = R_{h,2h} L_h P_{2h,h},$$

where $R_{h,2h}$ and $P_{2h,h}$ are restriction and prolongation operators, respectively. In this context, in order to preserve the symmetry of the coarse grid operator, the restriction operator is often chosen as the transpose of the prolongation.

The choice of prolongation and restriction operators is not so trivial and, probably, the most important. In problems with discontinuous coefficients, the difficulty arises from the fact that discontinuities of the coefficients result in the discontinuities of the same order of the partial derivatives of the solution. This implies that the use of prolongation operator, which is based on linear (bilinear, trilinear) interpolation is not reasonable, since it relies on the continuity of the

partial derivatives of the interpolant. It means that for non-smooth functions such interpolation is inexact near the interfaces of discontinuities, and can cause deterioration of the convergence or even divergence of the multigrid solver. The use of problem-dependent prolongation (and/or restriction) operator is a well known remedy, which helps to tackle the mentioned difficulties. For the origins of this approach see, e.g., [62], [1], [67], [41]. The problem-dependent interpolation can capture the jumps of the partial derivatives, and transfer them properly between the grids. The basic idea is to preserve continuity of the fluxes. This means explicit (or implicit) use of the interface continuity conditions of the differential problem. Finite volume methods are known for their property to preserve fluxes, and produce the so-called conservative discretizations in a natural way. Properly used information from the finite volume discretization allows to derive the inter-grid transfer operators, which can guarantee a robust behavior of the multigrid solver in the case of discontinuous coefficients.

4.1.3   Multigrid components for the discretized Biot system with discontinuous coefficients

The derived here multigrid solver is an extension of [32], [66], where only solution of Biot system with continuous coefficients is considered.

Let us consider the finite difference scheme (3.29) - (3.32), obtained as a discretization of the continuous Biot model (3.5) - (3.6) on the staggered grid (3.7). The discrete system (3.29) - (3.32) represents a large sparse system of linear algebraic equations. In order to derive a multigrid solver, which can efficiently handle this system, we should make the best use of the system's nature. Besides that, we want, as far as possible, to make the solver consistent with the discretization. One should keep in mind that this system was derived as a finite volume discretization of the system of PDEs (not a single PDE), which in turn has discontinuous coefficients. In fact, we do not really want to separate the two stages - discretization of the continuous problem and solution of the obtained discrete system, but make them very closely related.

We start from the construction of a grid hierarchy, based on the staggered at each level grids (3.7), starting from the finest level, where the discrete Biot system needs to be resolved, and then, at every next coarser level, by doubling the grid steps successively, approach the coarsest level:

$$\text{Level } 1: \quad \omega^1 = \{\omega^u_{h_x,h_y,h_z}, \omega^v_{h_x,h_y,h_z}, \omega^w_{h_x,h_y,h_z}, \omega^p_{h_x,h_y,h_z}\},$$

$$\text{Level } 2: \quad \omega^2 = \{\omega^u_{2h_x,2h_y,2h_z}, \omega^v_{2h_x,2h_y,2h_z}, \omega^w_{2h_x,2h_y,2h_z}, \omega^p_{2h_x,2h_y,2h_z}\},$$

$$\text{Level } 3: \quad \omega^3 = \{\omega^u_{4h_x,4h_y,4h_z}, \omega^v_{4h_x,4h_y,4h_z}, \omega^w_{4h_x,4h_y,4h_z}, \omega^p_{4h_x,4h_y,4h_z}\}, \quad (4.3)$$

$$...$$

$$\text{Level } m: \quad \omega^m = \{\omega^u_{h_x^0,h_y^0,h_z^0}, \omega^v_{h_x^0,h_y^0,h_z^0}, \omega^w_{h_x^0,h_y^0,h_z^0}, \omega^p_{h_x^0,h_y^0,h_z^0}\}.$$

Note that, since the grids ω^u, ω^v, ω^w, ω^p are staggered at each level, this kind of coarsening produces a non-nested grid sequence for each of the displacement component unknowns:

$$\omega^u_{h_x,h_y,h_z}, \omega^u_{2h_x,2h_y,2h_z}, \omega^u_{4h_x,4h_y,4h_z}, \; \cdots \; , \; \omega^u_{h^0_x,h^0_y,h^0_z},$$

$$\omega^v_{h_x,h_y,h_z}, \omega^v_{2h_x,2h_y,2h_z}, \omega^v_{4h_x,4h_y,4h_z}, \; \cdots \; , \; \omega^v_{h^0_x,h^0_y,h^0_z},$$

$$\omega^w_{h_x,h_y,h_z}, \omega^w_{2h_x,2h_y,2h_z}, \omega^w_{4h_x,4h_y,4h_z}, \; \cdots \; , \; \omega^w_{h^0_x,h^0_y,h^0_z},$$

and nested grid sequence for the pressure unknowns:

$$\omega^p_{h_x,h_y,h_z}, \omega^p_{2h_x,2h_y,2h_z}, \omega^p_{4h_x,4h_y,4h_z}, \; \cdots \; , \; \omega^p_{h^0_x,h^0_y,h^0_z}.$$

Now, having the grid hierarchy, and the system (3.29) - (3.32), written on the finest grid, we can proceed and think how to specify the other multigrid components so that they efficiently interplay and ensure robust behavior of the solver.

Let us define a relaxation operator for the pre- and post-smoothing procedures. As it was mentioned, when the systems of PDEs are solved by the multigrid method, smoothing by collective relaxation is preferable. In view of this, we use the altering line Gauss-Seidel relaxation. This smoother works in the following way: it updates together all the unknowns u, v, w, p grouped in lines in x -, y -, and z - directions consequently.

Let us proceed now and define the coarse grid operator. As it was mentioned above - there are two reasonable options, and one of them is to use the direct analogue of the fine grid operator on the coarse grid. Is it a reasonable choice for our problem? Let us remind some details about our finite volume discretization. We did not put any restriction on the location of the interface with respect to grid lines, but introduced a special parameter, which indicates this location. It means that on any coarser grid, we can easily specify the analogous discretization. Of course, the relative position of the interface with respect to grid lines can change, but it will be naturally taken into account by the finite volume discretization. This procedure will produce such a coarse grid operator, which can be considered a good representative of the fine grid operator on the coarse grid.

In order to perform the transfer of grid functions between the grids of the hierarchy, the proper restriction and prolongation operators must be defined. For this, let us consider two consequent grid levels from the multigrid hierarchy (4.2). The corresponding fine and coarse grids at these levels look as following:

$$\{\omega^u_f, \; \omega^v_f, \; \omega^w_f, \; \omega^p_f\} = \{\omega^u_{h^f_x,h^f_y,h^f_z}, \; \omega^v_{h^f_x,h^f_y,h^f_z}, \; \omega^w_{h^f_x,h^f_y,h^f_z}, \; \omega^p_{h^f_x,h^f_y,h^f_z}\},$$

$$\{\omega^u_c, \; \omega^v_c, \; \omega^w_c, \; \omega^p_c\} = \{\omega^u_{h^c_x,h^c_y,h^c_z}, \; \omega^v_{h^c_x,h^c_y,h^c_z}, \; \omega^w_{h^c_x,h^c_y,h^c_z}, \; \omega^p_{h^c_x,h^c_y,h^c_z}\},$$

where $h^c_x = 2h^f_x$, $h^c_y = 2h^f_y$, and $h^c_z = 2h^f_z$.

A restriction operator maps the grid functions defined on the fine grid, to the functions defined on the coarse grid. In multigrid algorithm, it is used to transfer residuals produced after the pre-smoothing step from a fine to a coarse grid. The pre-smoothing procedure, applied to the system (3.29) - (3.32), produces at each level four residuals: r_1^f, r_2^f, r_3^f, r_4^f – the grid functions, defined on the grids ω_f^u, ω_f^v, ω_f^w, ω_f^p, respectively. Each of these residuals needs to be transferred to the corresponding coarse grid ω_c^u, ω_c^v, ω_c^w, or ω_c^p. It means that four restriction operators - R_1, R_2, R_3, and R_4 - need to be defined.

The easiest choice for the restriction operator is the injection operator, which identifies certain values at a coarse grid points with the corresponding values at the fine grid points. This means that the residual is transferred directly between the coinciding fine and coarse points. Injection operator is fast and easy, however, it is not robust and moreover, it cannot be applied in the case of non-nested grids, what is the case here. Another possibility for the restriction operator is to use the so-called full weighting operator, which implies that the value of the function in the coarse point is calculated as a weighted average of the values of the grid functions in the neighboring fine points. The full weighting operator R^{FW} can be derived from the following condition:

$$\int_{\mathbf{V}(\mathbf{x})} r^c dV = \int_{\mathbf{V}(\mathbf{x})} R^{FW} r^f dV, \tag{4.4}$$

for $\mathbf{V}(\mathbf{x}) = \mathbf{V}(x,y,z) = (x - h_x, x + h_x) \times (y - h_y, y + h_y) \times (z - h_z, z + h_z) \cap \Omega$, where $\mathbf{x} = (x, y, z)$ is a coarse grid point, r^c is residual on the coarse grid, r^f is residual on the fine grid, and the midpoint rule is applied to approximate the integral from the right-hand side of the equation, and trapezoidal rule (or trapezoidal rule consequently with the midpoint rule in case of staggered grid) is used to approximate the integral from the left-hand side.

If we apply the formula (4.4) to the residual of the fourth equation with a consequent application of the approximate integration rules, we obtain the following 27 - point formula for the restriction operator R_4^{FW}

$$\begin{aligned}
r_4^c(x,y,z) &= R_4^{FW} r_4^f(x,y,z) \\
&= \frac{1}{64} \big(8r_4^f(x,y,z) + 4r_4^f(x - h_x^f, y, z) + 4r_4^f(x + h_x^f, y, z) \\
&+ 4r_4^f(x, y - h_y^f, z) + 4r_4^f(x, y + h_y^f, z) + 4r_4^f(x, y, z - h_z^f) + 4r_4^f(x, y, z + h_z^f) \\
&+ 2r_4^f(x - h_x^f, y - h_y^f, z) + 2r_4^f(x - h_x^f, y + h_y^f, z) + 2r_4^f(x + h_x^f, y - h_y^f, z) \\
&+ 2r_4^f(x + h_x^f, y + h_y^f, z) + 2r_4^f(x - h_x^f, y, z - h_z^f) + 2r_4^f(x - h_x^f, y, z + h_z^f) \\
&+ 2r_4^f(x + h_x^f, y, z - h_z^f) + 2r_4^f(x + h_x^f, y, z + h_z^f) + 2r_4^f(x, y - h_Y^f, z - h_z^f) \\
&+ 2r_4^f(x, y - h_y^f, z + h_z^f) + 2r_4^f(x, y + h_y^f, z - h_z^f) + 2r_4^f(x, y + h_y^f, z + h_z^f)
\end{aligned}$$

$$
\begin{aligned}
&+ r_4^f(x - h_x^f, y - h_y^f, z - h_z^f) + r_4^f(x - h_x^f, y - h_y^f, z + h_z^f) \\
&+ r_4^f(x - h_x^f, y + h_y^f, z - h_z^f) + r_4^f(x + h_x^f, y - h_y^f, z - h_z^f) \\
&+ r_4^f(x - h_x^f, y + h_y^f, z + h_z^f) + r_4^f(x + h_x^f, y + h_y^f, z - h_z^f) \\
&+ r_4^f(x + h_x^f, y - h_y^f, z + h_z^f) + r_4^f(x + h_x^f, y + h_y^f, z + h_z^f)),
\end{aligned}
\tag{4.5}
$$

where the point $(x, y, z) \in \omega_c^p$. One should remember that fine and coarse grids ω_f^p and ω_c^p are nested.

Next, we apply formula (4.4) to derive formulae for the restriction of the residuals of the first, second and third equations, which are defined on the grids ω_f^u, ω_f^v and ω_f^w, respectively. It is important to remember that the coarsening was done in such a way, that corresponding coarse grids are not nested with the respective fine ones. Application of the trapezoidal rule as well as middle-point rule to approximate the integral in the right-hand side of the formula (4.4), results in the 18 - point restriction operators R_1, R_2, and R_3. Below, we present the formula for the restriction operator R_1:

$$
\begin{aligned}
r_1^c(x, y, z) = R_1^{FW} r_1^f(x, y, z) = &\frac{1}{32}(4r_1^f(x - h_x^f/2, y, z) + 4r_1^f(x + h_x^f/2, y, z) \\
&+ 2r_1^f(x - h_x^f/2, y - h_y^f, z) + 2r_1^f(x - h_x^f/2, y + h_y^f, z) + 2r_1^f(x - h_x^f/2, y, z - h_z^f) \\
&+ 2r_1^f(x - h_x^f/2, y, z + h_z^f) + 2r_1^f(x + h_x^f/2, y - h_y^f, z) + 2r_1^f(x + h_x^f/2, y + h_y^f, z) \\
&+ 2r_1^f(x + h_x^f/2, y, z - h_z^f) + 2r_1^f(x + h_x^f/2, y, z + h_z^f) \\
&+ r_1^f(x - h_x^f/2, y - h_y^f, z - h_z^f) + r_1^f(x - h_x^f/2, y - h_y^f, z + h_z^f) \\
&+ r_1^f(x - h_x^f/2, y + h_y^f, z - h_z^f) + r_1^f(x - h_x^f/2, y + h_y^f, z + h_z^f) \\
&+ r_1^f(x + h_x^f/2, y - h_y^f, z - h_z^f) + r_1^f(x + h_x^f/2, y - h_y^f, z + h_z^f) \\
&+ r_1^f(x + h_x^f/2, y + h_y^f, z - h_z^f) + r_1^f(x + h_x^f/2, y + h_y^f, z + h_z^f)),
\end{aligned}
$$

$$\tag{4.6}$$

where $(x, y, z) \in \omega_c^u$. The respective location of the fine and coarse grid points, which take part in the restriction, is depicted in the Figure 4.1.

Note that formulae (4.5) and (4.6) should be modified near the boundaries, where the boundary conditions should be taken into account.

Formulae for the restriction of the residuals r_2 and r_3 are written in a similar way.

The prolongation (interpolation) operator maps the grid functions defined on a coarse grid to the functions defined on a fine grid. In multigrid algorithm, it is used to transfer correction to the solution from a coarse to a fine grid (note that, in the so-called full multigrid algorithm, it is used to transfer the approximations to the solution). In our problem, we have to transfer four corrections - ϵ_u^c, ϵ_v^c, ϵ_w^c and ϵ_p^c - from the coarse grids ω_c^u, ω_c^v, ω_c^w, ω_c^p to the respective fine grids ω_f^u, ω_f^v, ω_f^w, ω_f^p. It means that we have to derive four prolongation operators - P_u, P_v, P_w, P_p - one for each correction.

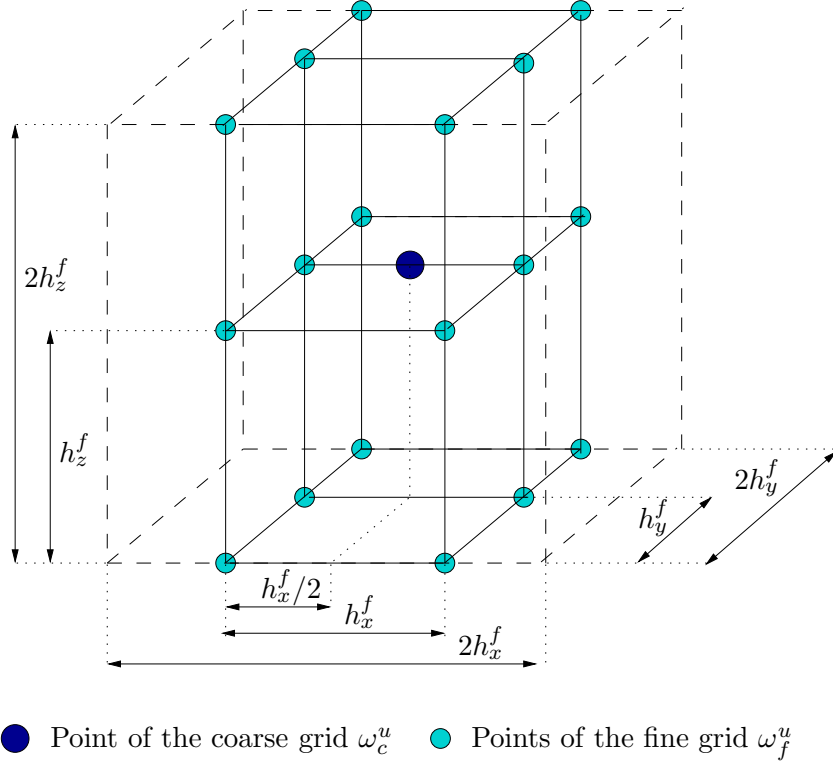Point of the coarse grid ω_c^u Points of the fine grid ω_f^u

Figure 4.1: Respective location of the coarse and a fine grid points indicating restriction into the point of the grid ω_c^u.

The most commonly used prolongation operator in three dimensions is based on the trilinear (bilinear in two-dimensional problems) interpolation.

The use of trilinear interpolation results in the following formulae for prolongation of the correction to the pressure unknown:

$$\epsilon_p^f(x,y,z) = P_p\epsilon_p^c = \begin{cases} \epsilon_p^c(x,y,z), & (x,y,z) \in \omega_f^{p,1}, \\[2mm] \dfrac{1}{2}(\epsilon_p^f(x - h_x^f, y, z) + \epsilon_p^f(x + h_x^f, y, z)), & (x,y,z) \in \omega_f^{p,2}, \\[2mm] \dfrac{1}{2}(\epsilon_p^f(x, y - h_y^f, z) + \epsilon_p^f(x, y + h_y^f, z)), & (x,y,z) \in \omega_f^{p,3}, \\[2mm] \dfrac{1}{2}(\epsilon_p^f(x, y, z - h_z^f) + \epsilon_p^f(x, y, z + h_z^f)), & (x,y,z) \in \omega_f^{p,4}, \end{cases}$$
$$(4.7)$$

where $\omega_f^{p,1}$, $\omega_f^{p,2}$, $\omega_f^{p,3}$, $\omega_f^{p,4}$ are the sub-grids of the fine grid ω_f^p. The subdivision of the grid ω_f^p into these sub-grids is schematically shown in the Figure 4.2.

The interpolation of the corrections e^u, e^v and e^w is done in a different way, since the coarse and fine grids, where they are defined, are not nested. Below,
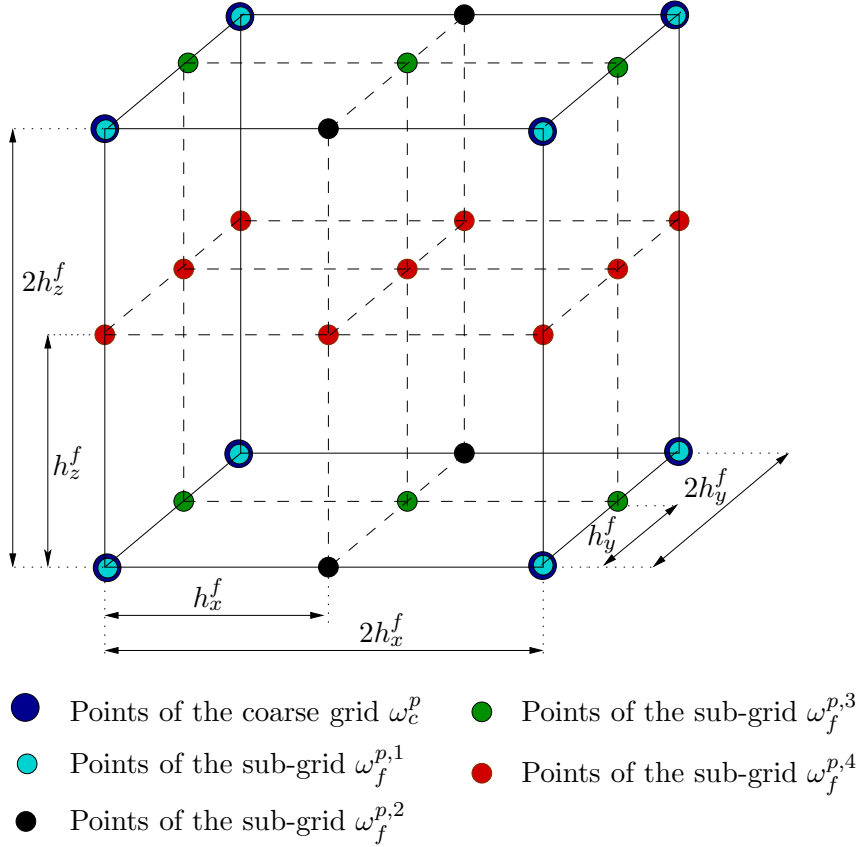
Figure 4.2: A fine and a coarse grids for the pressure unknown with symbols indicating the interpolation.

we present the interpolation of the correction e^u:

$$\epsilon_f^u(x,y,z) = P_c^f e_c^u$$

$$= \begin{cases} \dfrac{3}{4}\epsilon_u^c(x - h_x^c/4, y, z) + \dfrac{1}{4}\epsilon_u^c(x + 3h_x^c/4, y, z), & (x,y,z) \in \omega_f^{u,1}, \\[2mm] \dfrac{1}{4}\epsilon_u^c(x - h_x^c/4, y, z) + \dfrac{3}{4}\epsilon_u^c(x + 3h_x^c/4, y, z), & (x,y,z) \in \omega_f^{u,2}, \\[2mm] \dfrac{1}{2}(\epsilon_u^f(x, y - h_y^f, z) + \epsilon_u^f(x, y + h_y^f, z)), & (x,y,z) \in \omega_f^{u,3}, \\[2mm] \dfrac{1}{2}(\epsilon_u^f(x, y, z - h_z^f) + \epsilon_u^f(x, y, z + h_z^f)), & (x,y,z) \in \omega_f^{u,4}, \end{cases} \tag{4.8}$$

where $\omega_f^{u,1}, \omega_f^{u,2}, \omega_f^{u,3}, \omega_f^{u,4}$ are the sub-grids of the fine grid ω_f^u and the respective location of these points is depicted in the Figure 4.3.

However, trilinear interpolation implicitly relies on the fact that interpolants belong to the class C^1, which is not the case if the coefficients of the differential problem experience discontinuities. This means that the prolongation operator, based on liner (bilinear, trilinear) interpolation, is inaccurate across the interfaces of discontinuities, what can result in poor convergence or even divergence

Points of the coarse grid ω_c^u

Points of the sub-grid $\omega_f^{u,1}$

Points of the sub-grid $\omega_f^{u,2}$

Points of the sub-grid $\omega_f^{u,3}$
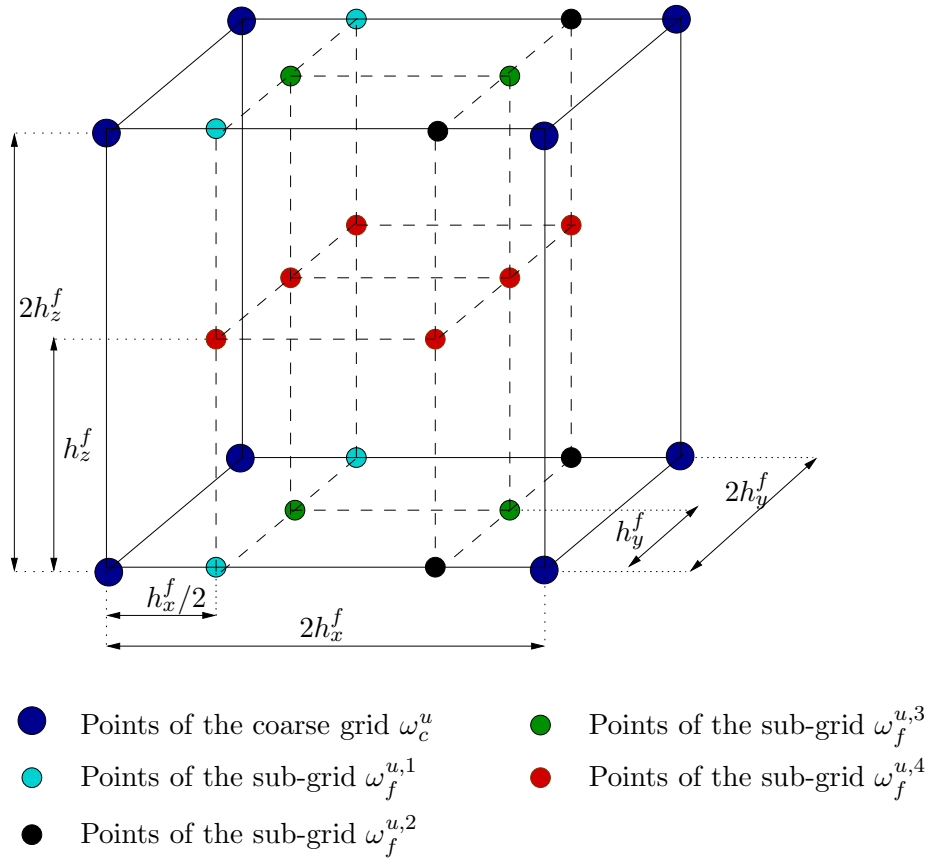
Points of the sub-grid $\omega_f^{u,4}$

Figure 4.3: A fine and a coarse grids for the first displacement component with symbols indicating the interpolation.

of the whole multigrid method. For the problems with discontinuous coefficients, we need some more appropriate interpolation, which can capture the jumps of the gradients of the interpolants across the interface. This motivates the use of the problem-dependent prolongation for the interpolation of the values across the interfaces of discontinuities. Often, restriction operator is taken as the properly scaled transpose to the prolongation operator. If the prolongation operator is problem-dependent, this procedure produces problem-dependent restriction operator as well. Sometimes, after the transposing and scaling, additional lumping of the stencil of the obtained restriction operator is performed, which is done in order to prevent the overgrowth of the stencil.

4.1.4 Problem-dependent restriction and prolongation

In this subsection, we derive the problem-dependent inter-grid transfer operators – prolongation and restriction – for the discrete Biot system (3.29) - (3.32). The following is important: to capture and properly transfer the jumps of the gradients of the corrections e^u, e^v, e^w, e^p across the interface $z = \xi$, taking

into account their interdependence within the solvable system. The proper use of the information from the finite volume discretization makes these operators consistent with the discretization.

At a certain stage of finite volume discretization, the interpolating polynomials for all basic unknowns of the system were derived in the corresponding sets of control volumes. One should remember that these polynomials were obtained in such a way that they

1. interpolate the values in the vertices of the volumes;

2. satisfy respective continuity conditions at the interface $z = \xi$.

Note that condition 2. provides fulfillment of the interface conditions as well as the proper interdependence of the interpolating polynomials $U(\mathbf{x})$, $V(\mathbf{x})$, $W(\mathbf{x})$ in the volumes, which are intersected by the interface $z = \xi$. This means that these polynomials, written on the coarse grid, can be used in the interpolation method. We can use this method as a basis for the problem-dependent prolongation operator. Such prolongation will possess all the necessary properties we required. It will properly interpolate the corrections and their gradients, performing the interpolation of each of the correction in a proper dependence with the others.

First, interpolation of the corrections e^u, e^v, and e^p in x-, and y-directions is done linearly (see formulae (4.7) and (4.8) for the interpolation of e^p and e^u respectively). Then, interpolation of these corrections in z-direction should be done. This interpolation means calculation of the corrections e^u in the points of the sub-grid $\omega_f^{u,4}$ (the points of $\omega_f^{u,4}$ are depicted in Figure 4.3), and calculation of the pressure corrections in the points of the sub-grid $\omega_f^{p,4}$ (the points of $\omega_f^{p,4}$ are depicted in Figure 4.2).

According to the location of the grid points, interpolation of the correction e^w is done in z-direction first. This interpolation is problem-dependent as well.

To derive the formulae for the interpolation, we write down the interpolating polynomials $U(\mathbf{x})$, $V(\mathbf{x})$, $W(\mathbf{x})$, and $P(\mathbf{x})$ on the coarse grid $\{\omega_c^u, \omega_v^c, \omega_w^c, \omega_p^c\}$ according to the formulae (3.22), (3.23), (3.24), and (3.18).

Let us start from the interpolation of the correction e^u. Suppose that we want to interpolate, for example, the value of e^u in the fine grid point (x, y, z), which is the point of the sub-grid $\omega_f^{u,4}$ (red circle in the Figure 4.4).

The structure of the interpolating polynomials implies consideration of the following sub-cases:

1. $z_{k_{int}^c} < z < z_{k_{int}^c+1}$, and $\theta^c \leq 1/2$,

2. $z_{k_{int}^c} < z < z_{k_{int}^c+1}$, and $\theta^c > 1/2$,

3. $z \leq z_{k_{int}^c}$, or $z \geq z_{k_{int}^c+1}$.

In case 1., polynomial $U(\mathbf{x})$ produces the following formula for the interpolation:

$$
e_u^f(x,y,z) = \frac{1}{2}\frac{\mu_1}{\langle\mu\rangle}e_u^f(x,y,z-h_z^f) + \left(1 - \frac{1}{2}\frac{\mu_1}{\langle\mu\rangle}\right)e_u^f(x,y,z+h_z^f)
$$

$$
-\frac{1}{2}h_z^c\theta^c\frac{\mu_1-\mu_2}{\langle\mu\rangle}e_{w,x}^c(x-3h_x^f/2,y,z)
$$

$$
= \frac{3}{8}\frac{\mu_1}{\langle\mu\rangle}e_u^c(x-h_x^f/2,y,z-h_z^f) + \frac{1}{8}\frac{\mu_1}{\langle\mu\rangle}e_u^c(x+3h_x^f/2,y,z-h_z^f)
$$

$$
+\frac{3}{4}\left(1-\frac{1}{2}\frac{\mu_1}{\langle\mu\rangle}\right)e_u^c(x-h_x^f/2,y,z+h_z^f) + \frac{1}{4}\left(1-\frac{1}{2}\frac{\mu_1}{\langle\mu\rangle}\right)e_u^c(x+3h_x^f/2,y,z+h_z^f)
$$

$$
-\frac{1}{2}h_z^c\theta^c\frac{\mu_1-\mu_2}{\langle\mu\rangle}e_{w,x}^c(x-3h_x^f/2,y,z).
$$

In case 2. – the following:

$$
e_u^f(x,y,z) = \left(1 - \frac{1}{2}\frac{\mu_2}{\langle\mu\rangle}\right)e_u^f(x,y,z-h_z^f) + \frac{1}{2}\frac{\mu_2}{\langle\mu\rangle}e_u^f(x,y,z+h_z^f)
$$

$$
+\frac{1}{2}h_z^c(\theta^c-1)\frac{\mu_1-\mu_2}{\langle\mu\rangle}e_{w,x}^c(x-3h_x^f/2,y,z)
$$

$$
= \frac{3}{4}\left(1-\frac{1}{2}\frac{\mu_2}{\langle\mu\rangle}\right)e_u^c(x-h_x^f/2,y,z-h_z^f) + \frac{1}{4}\left(1-\frac{1}{2}\frac{\mu_2}{\langle\mu\rangle}\right)e_u^c(x+3h_x^f/2,y,z-h_z^f)
$$

$$
+\frac{3}{8}\frac{\mu_2}{\langle\mu\rangle}e_u^c(x-h_x^f/2,y,z+h_z^f) + \frac{1}{8}\frac{\mu_2}{\langle\mu\rangle}e_u^c(x+3h_x^f/2,y,z+h_z^f)
$$

$$
+\frac{1}{2}h_z^c(\theta^c-1)\frac{\mu_1-\mu_2}{\langle\mu\rangle}e_{w,x}^c(x-3h_x^f/2,y,z),
$$

where $\langle\mu\rangle = (1-\theta^c)\mu_1 + \theta^c\mu_2$.

The scheme of the interpolation in the cases 1. and 2. is depicted in Figure 4.4.

In case 3., the value in the point (x,y,z) is interpolated linearly:

$$
e^u(x,y,z) = \frac{1}{2}(e^u(x,y,z-h_z^f) + e^u(x,y,z+h_z^f)).
$$

Then, in the rest of the grid points - i.e., in the points belonging to the sub-grids $\omega_f^{u,6}$, $\omega_f^{u,7}$, $\omega_f^{u,8}$ - interpolation is done similarly.

Prolongation operator for the correction ϵ^v is done in a similar way.

Interpolation of the correction ϵ^w differs from the interpolation of ϵ^u and ϵ^v. Staggered grids are located in such a way that for the unknown w, there exist two fine grid points between each two neighboring coarse grid points in z-direction. Suppose we want to calculate the value of e^w in such fine grid point (x,y,z). The structure of the interpolating polynomials implies consideration of the following sub-cases:

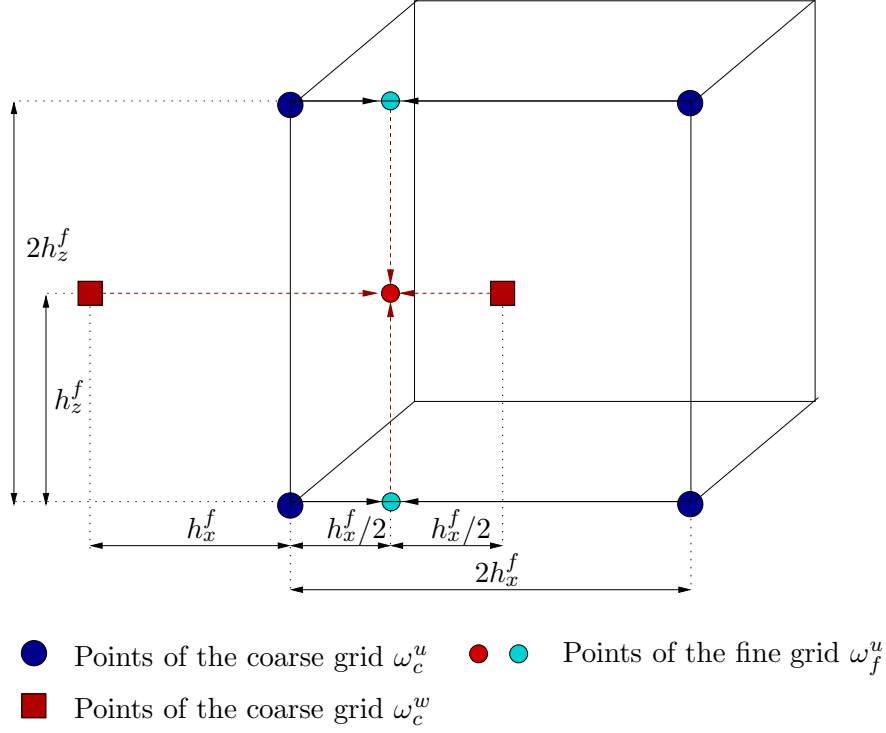1. $z_{k_{int}^c-0.5} < z < z_{k_{int}^c}$, and $\theta^c \leq 1/2$,

Figure 4.4: Problem-dependent interpolation in the point of $\omega_f^{u,5}$.

2. $z_{k_{int}^c} < z < z_{k_{int}^c + 0.5}$, and $\theta^c \leq 1/4$,

3. $z_{k_{int}^c} < z < z_{k_{int}^c + 0.5}$, and $1/4 < \theta^c \leq 1/2$,

4. $z_{k_{int}^c + 0.5} < z < z_{k_{int}^c + 1}$, and $1/2 < \theta^c \leq 3/4$,

5. $z_{k_{int}^c + 0.5} < z < z_{k_{int}^c + 1}$, and $\theta^c > 3/4$,

6. $z_{k_{int}^c + 1} < z < z_{k_{int}^c + 1.5}$, and $\theta^c > 1/2$,

7. $z < z_{k_{int}^c - 0.5}^c$ or $z > z_{k_{int}^c + 1.5}$.

Below, we present the formulae of the problem-dependent interpolation, which correspond to these sub-cases:

in case 1.,

$$e_w^f(x, y, z) = \left(1 - \frac{1}{4} \frac{\lambda_2 + 2\mu_2}{\langle \lambda + 2\mu \rangle_1}\right) e_w^f(x, y, z - h_z^f/2) + \frac{1}{4} \frac{\lambda_2 + 2\mu_2}{\langle \lambda + 2\mu \rangle_1} e_w^f(x, y, z + 3h_z^f/2)$$

$$+ \frac{h_z^c}{4}(\theta^c - 0.5)\frac{(\lambda_1 - \lambda_2)}{\langle \lambda + 2\mu \rangle_1} \left(e_{u,x}^f(x - h_x^f, y, z + h_z^f/2) + e_{v,y}^f(x, y - h_y^f, z + h_z^f/2)\right),$$

in case 2.,

$$e^w(x, y, z) = \frac{1}{4} \frac{\lambda_1 + 2\mu_1}{\langle \lambda + 2\mu \rangle_1} e^w(x, y, z - 3h_z^f/2) + \left(1 - \frac{1}{4} \frac{\lambda_1 + 2\mu_1}{\langle \lambda + 2\mu \rangle_1}\right) e^w(x, y, z + h_z^f/2)$$

$$- \frac{h_z^c}{4}(\theta^c + 0.5)\frac{(\lambda_1 - \lambda_2)}{\langle \lambda + 2\mu \rangle_1} \left(e_x^u(x - h_x^f, y, z - h_z^f/2) + e_y^v(x, y - h_y^f, z - h_z^f/2)\right),$$

in case 3.,

$$e^w(x,y,z) = \left(1 - \frac{3}{4}\frac{\lambda_2 + 2\mu_2}{\langle\lambda + 2\mu\rangle_1}\right)e^w(x,y,z - 3h_z^f/2) + \frac{3}{4}\frac{\lambda_2 + 2\mu_2}{\langle\lambda + 2\mu\rangle_1}e^w(x,y,z + h_z^f/2)$$

$$+ \frac{3}{4}h_z^c(\theta^c - 0.5)\frac{(\lambda_1 - \lambda_2)}{\langle\lambda + 2\mu\rangle_1}\left(e_x^u(x - h_x^f, y, z - h_z^f/2) + e_y^v(x, y - h_y^f, z - h_z^f/2)\right),$$

in case 4.,

$$e^w(x,y,z) = \frac{3}{4}\frac{\lambda_1 + 2\mu_1}{\langle\lambda + 2\mu\rangle_2}w(x,y,z - h_z^f/2) + \left(1 - \frac{3}{4}\frac{\lambda_1 + 2\mu_1}{\langle\lambda + 2\mu\rangle_2}\right)e^w(x,y,z + 3h_z^f/2)$$

$$- \frac{3}{4}h_z^c(\theta^c - 0.5)\frac{(\lambda_1 - \lambda_2)}{\langle\lambda + 2\mu\rangle_2}\left(e_x^u(x - h_x^f, y, z + h_z^f/2) + e_y^v(x, y - h_y^f, z + h_z^f/2)\right),$$

in case 5.,

$$e^w(x,y,z) = \left(1 - \frac{1}{4}\frac{\lambda_2 + 2\mu_2}{\langle\lambda + 2\mu\rangle_2}\right)e^w(x,y,z - h_z^f/2) + \frac{1}{4}\frac{\lambda_2 + 2\mu_2}{\langle\lambda + 2\mu\rangle_2}e^w(x,y,z + 3h_z^f/2)$$

$$+ \frac{h_z^c}{4}(\theta^c - 1.5)\frac{(\lambda_1 - \lambda_2)}{\langle\lambda + 2\mu\rangle_2}\left(e_x^u(x - h_x^f, y, z + h_z^f/2) + e_y^v(x, y - h_y^f, z + h_z^f/2)\right),$$

in case 6.,

$$e^w(x,y,z) = \frac{1}{4}\frac{\lambda_1 + 2\mu_1}{\langle\lambda + 2\mu\rangle_2}e^w(x,y,z - 3h_z^f/2) + \left(1 - \frac{1}{4}\frac{\lambda_1 + 2\mu_1}{\langle\lambda + 2\mu\rangle_2}\right)e^w(x,y,z + h_z^f/2)$$

$$- \frac{1}{4}h_z^c(\theta^c - 0.5)\frac{(\lambda_1 - \lambda_2)}{\langle\lambda + 2\mu\rangle_2}\left(e_x^u(x - h_x^f, y, z - h_z^f/2) + e_y^v(x, y - h_y^f, z - h_z^f/2)\right),$$

where $\langle\lambda + 2\mu\rangle_1 = (1/2 - \theta^c)(\lambda_1 + 2\mu_1) + (1/2 + \theta^c)(\lambda_2 + 2\mu_2)$, and $\langle\lambda + 2\mu\rangle_2 = (3/2 - \theta^c)(\lambda_1 + 2\mu_1) + (\theta^c - 1/2)(\lambda_2 + 2\mu_2)$.

In case 7., the usual linear interpolation in z-direction is applied.

Next, the interpolation of the correction ϵ_w is done linearly in x- and y-directions.

Note that, according to the derived formulae for the problem-dependent interpolation, in order to calculate values of the corrections ϵ_u and ϵ_v on the fine grid, values of ϵ_w from the coarse grid are also used, and in order to calculate values of the correction ϵ_w, coarse grid values of ϵ_u and ϵ_v are used. This means that the interdependence of the variables of the system was automatically taken into account.

We can suppose that, within the Biot system, pressure-to-displacement coupling is weaker than couplings between different displacement components and that it is weak enough to use such prolongation for the pressure correction, which is done separately from the corrections of the displacement components. Moreover, this kind of interpolation naturally follows from the finite volume discretization. From the polynomials $P(\mathbf{x})$, written on the coarse grid, we obtain the formulae for the problem-dependent prolongation of pressure correction in the internal grid points in z-direction. The structure of the polynomials implies consideration of the following sub-cases:
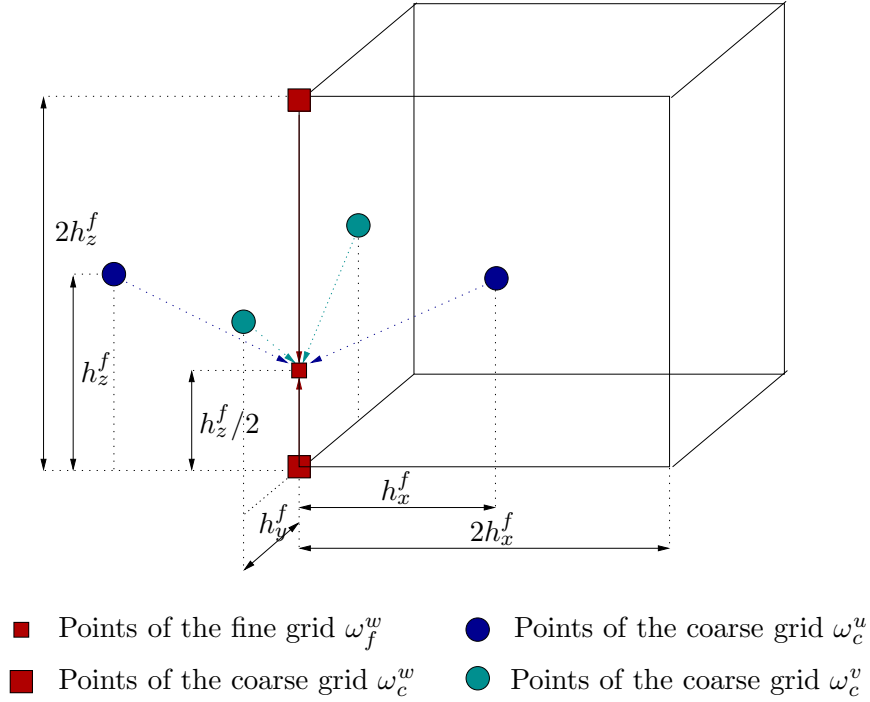
Figure 4.5: Location of the coarse and fine grid points indicating problem-dependent interpolation for the correction ϵ_w.

1. $z_{k^c_{int}} < z < z_{k^c_{int}+1}$, and $\theta^c \leq 1/2$,

2. $z_{k^c_{int}} < z < z_{k^c_{int}+1}$, and $\theta^c > 1/2$,

3. $z < z_{k^c_{int}}$, or $z > z_{k^c_{int}+1}$.

Then, the interpolation is done according to the following formulae:
in case 1.,

$$e^f_p(x,y,z) = \frac{1}{2}\frac{\kappa_1}{\langle\kappa\rangle}e^c_p(x,y,z-h^f_z) + \left(1 - \frac{1}{2}\frac{\kappa_1}{\langle\kappa\rangle}\right)e^c_p(x,y,z+h^f_z),$$

in the case 2.,

$$e^f_p(x,y,z) = \left(1 - \frac{1}{2}\frac{\kappa_2}{\langle\kappa\rangle}\right)e^c_p(x,y,z-h^f_z) + \frac{1}{2}\frac{\kappa_2}{\langle\kappa\rangle}e^c_p(x,y,z+h^f_z),$$

where $\langle\kappa\rangle = (1-\theta^c)\kappa_1 + \theta^c\kappa_2$. In case 3., standard linear interpolation is applied in z-direction.

Note that the formulae for the prolongation of the pressure corrections can be considered as a particular case of the operator dependent prolongation, derived, e.g., in [67, 41] for the diffusion equation.

Often, restriction operator is chosen to be the (properly scaled) transpose of the problem-dependent prolongation. In our case, in order to prevent the overgrowth of the stencil of the restriction operator, we transpose the prolongation

operator, scale it, and apply additional lumping. This lumping is done in x - direction for the restriction of the residual r_1, in y - direction for the restriction of r_2, and in z - direction for the restriction of r_3. The resulting restriction operators have 18-point stencil in the internal grid points.
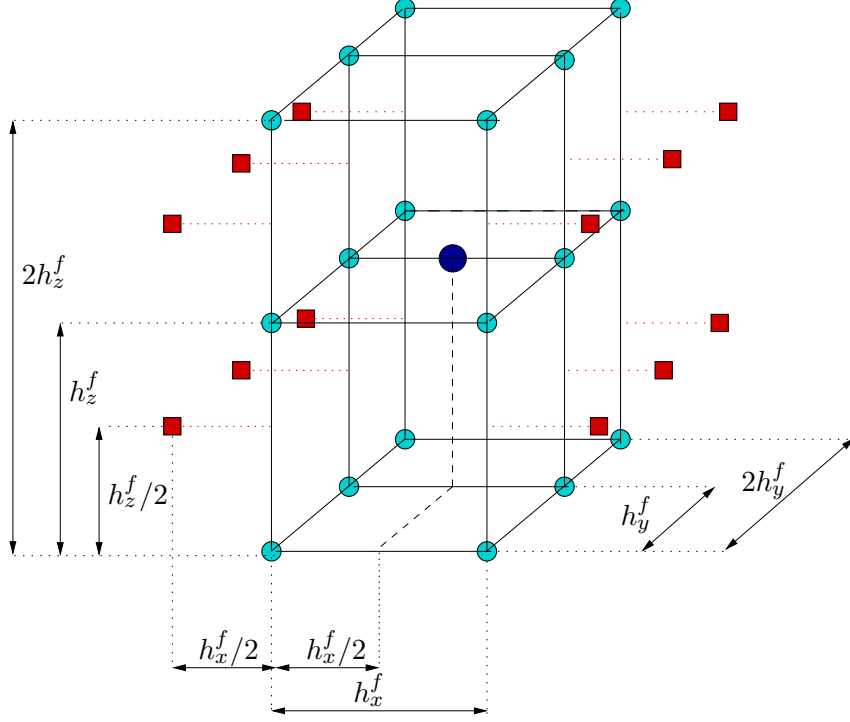
Below, we present, as an example, the formula for the restriction of the correction in the internal coarse grid point (x, y, z) for the case, when $z = z_{k_{int}^c}$ and $\theta^c < 1/4$

$$
\begin{aligned}
r_1^c(x, y, z) &= \frac{1}{8}(r_1^f(x - h_x^f/2, y, z) + r_1^f(x + h_x^f/2, y, z)) \\
&+ \frac{1}{16}(r_1^f(x - h_x^f/2, y - h_y^f, z) + r_1^f(x - h_x^f/2, y + h_y^f, z) \\
&+ r_1^f(x + h_x^f/2, y + h_y^f, z) + r_1^f(x + h_x^f/2, y - h_y^f, z) + r_1^f(y - h_x^f/2, y, z - h_z^f) \\
&+ r_1^f(y + h_x^f/2, y, z - h_z^f)) + \frac{1}{32}(r_1^f(x - h_x^f/2, y + h_y^f, z - h_z^f) \\
&+ r_1^f(x - h_x^f/2, y - h_y^f, z - h_z^f) + r_1^f(x + h_x^f/2, y + h_y^f, z - h_z^f) \\
&+ r_1^f(x + h_x^f/2, y - h_y^f, z - h_z^f)) + \frac{1}{16}\frac{\mu_1}{\langle\mu\rangle_1}(r_1^f(x - h_x^f/2, y, z + h_z^f) \\
&+ r_1^f(x + h_x^f/2, y, z + h_z^f)) + \frac{1}{32}\frac{\mu_1}{\langle\mu\rangle_1}(r_1^f(x - h_x/2, y + h_y, z + h_z^f) \\
&+ r_1^f(x - h_x/2, y - h_y, z + h_z^f) + r_1^f(x + h_x/2, y + h_y, z + h_z^f) \\
&+ r_1^f(x + h_x/2, y - h_y, z + h_z^f)) \\
&+ \frac{1}{16}\frac{h_x^c}{h_z^c}\frac{\lambda_1 - \lambda_2}{\langle\lambda + 2\mu\rangle_1}((\theta^c - 1/2)(r_3^f(x - h_x^f, y, z - h_z^f/2) - r_3^f(x + h_x^f, y, z - h_z^f/2)) \\
&+ (\theta^c + 1/2)(-r_3^f(x - h_x^f, y, z + h_z^f/2) + r_3^f(x + h_x^f, y, z + h_z^f/2))) \\
&+ \frac{(\theta^c - 1/2)}{32}\frac{h_x^c}{h_z^c}\frac{\lambda_1 - \lambda_2}{\langle\lambda + 2\mu\rangle_1}(r_3^f(x - h_x^f, y + h_y^f, z - h_z^f/2) \\
&- r_3^f(x + h_x^f, y + h_y^f, z - h_z^f/2) + r_3^f(x - h_x^f, y - h_y^f, z - h_z^f/2) \\
&- r_3^f(x + h_x^f, y - h_y^f, z - h_z^f/2)) \\
&+ \frac{(\theta^c + 1/2)}{32}\frac{h_x^c}{h_z^c}\frac{\lambda_1 - \lambda_2}{\langle\lambda + 2\mu\rangle_1}(-r_3^f(x - h_x^f, y + h_y^f, z + h_z^f/2) \\
&+ r_3^f(x + h_x^f, y + h_y^f, z + h_z^f/2) - r_3^f(x - h_x^f, y - h_y^f, z + h_z^f/2) \\
&+ r_3^f(x + h_x^f, y - h_y^f, z + h_z^f/2)).
\end{aligned}
$$

The respective location of the coarse and fine grid points for the problem-dependent restriction of the first residual component is depicted in Figure 4.6. For the comparison with the standard restriction, see Figure 4.1.

Similar formulae of the problem-dependent restriction are valid in the other coarse grid points, neighboring the interface. For the other components of the correction e^v, e^w operator-dependent restriction is derived in the same way.

Problem-dependent restriction for the pressure correction is also obtained like transposed prolongation. But, due to the nested coarse and fine grids, the

Figure 4.6: Respective location of the coarse and a fine grid points indicating the operator-dependent restriction into the point of the coarse grid ω_c^u.

stencil of the transposed prolongation does not grow as much as in the case of non-nested grids. Thus, no need for lumping the stencil arises. Below, we present the formula for the restriction of pressure values in the internal coarse grid point (x, y, z), where $z = z_{k_{int}^c}$ and $\theta^c \leq 1/2$

$$
\begin{aligned}
r_4^c(x,y,z) = {} & \frac{1}{8}r_4^f(x,y,z) + \frac{1}{16}(r_4^f(x,y+h_y^f,z) + r_4^f(x,y-h_y^f,z) \\
& + r_4^f(x+h_x^f,y,z) + r_4^f(x-h_x^f,y,z) + r_4^f(x,y,z-h_z^f)) \\
& + \frac{1}{32}(r_4^f(x+h_x^f,y+h_y^f,z) + r_4^f(x+h_x^f,y-h_y^f,z) + r_4^f(x-h_x^f,y+h_y^f,z) \\
& + r_4^f(x-h_x^f,y-h_y^f,z) + r_4^f(x,y+h_y^f,z-h_z^f) + r_4^f(x,y-h_y^f,z-h_z^f) \\
& + r_4^f(h+h_x^f,y,z-h_z^f) + r_4^f(h-h_x^f,y,z-h_z^f)) \\
& + \frac{1}{64}(r_4^f(x+h_x^f,y+h_y^f,z-h_z^f) + r_4^f(x+h_x^f,y-h_y^f,z-h_z^f) \\
& + r_4^f(x-h_x^f,y+h_y^f,z-h_z^f) + r_4^f(x-h_x^f,y-h_y^f,z-h_z^f)) \\
& + \frac{1}{16}\frac{\kappa_1}{\langle\kappa\rangle}r_4^f(x,y,z+h_z^f) + \frac{1}{32}\frac{\kappa_1}{\langle\kappa\rangle}(r_4^f(x,y-h_y^f,z+h_z^f)
\end{aligned}
$$

$$+ r_4^f(x, y - h_y^f, z + h_z^f) + r_4^f(x + h_x^f, y, z + h_z^f) + r_4^f(x - h_x^f, y, z + h_z^f))$$

$$+ \frac{1}{64} \frac{\kappa_1}{\langle \kappa \rangle}(r_4^f(x + h_x^f, y + h_y^f, z + h_z^f) + r_4^f(x + xh_x^f, y - h_y^f, z + h_z^f)$$

$$+ r_4^f(x - h_x^f, y + h_y^f, z + h_z^f) + r_4^f(x - h_x^f, y - h_y^f, z + h_z^f)).$$

As one can see from the formulae, derived problem-dependent restrictions and prolongations satisfy the necessary requirements - account for jumps of coefficients as well as for the couplings of unknowns within the solvable system of PDEs.

4.2 Numerical experiments

Here, we present two sets of numerical experiments. In the first one, we use input data from the Example B of the Chapter 3, and evaluate the convergence of the multigrid method. In the second set, we consider a physical phenomena which is described by the Biot system with discontinuous coefficients. In this case the exact solution is unknown. Within this set of experiments, we calculate the physical characteristics of the process, and also evaluate the convergence of the multigrid solver.

In order to see the advantages of the use of the problem-dependent prolongation and/or problem-dependent restriction, we focus on the following comparison: we consider four multigrid solvers:

1. $M(P^{lin}, R^{lin})$: based on both linear interpolation and restriction,

2. $M(P^{op}, R^{lin})$: based on operator - dependent prolongation and linear restriction,

3. $M(P^{lin}, R^{op})$: based on operator - dependent restriction and linear prolongation,

4. $M(P^{op}, R^{op})$: based on both operator - dependent restriction and prolongation.

Convergence of the multigrid solver was estimated using the convergence factor, which we calculate with the following formula:

$$\rho^n = \sqrt[n]{\frac{\|r^n\|}{\|r^0\|}},$$

where n is the number of multigrid iterations necessary to achieve given tolerance for the residual, and

$$\|r^n\| = \sum_{i=1,4} \|r_i^n\|,$$

where each of $\|r_i^n\|$ is the maximum norm of the residual of i-th equation of the system after the n-th iteration.

4.2.1   Example 1: multigrid convergence test

For this example, we use the data from the Example B of the Chapter 3.

The following values of parameters are chosen for the experiment: $T = 0.1$, $\xi = 0.501$, $\beta = 0$ (fluid is incompressible). Let the coefficients of the problem λ, μ and κ experience jumps of seven orders of magnitude and $\lambda_1 = 1$, $\mu_1 = 1$, $\kappa_1 = 1$, $\lambda_2 = 10^7$, $\mu_2 = 10^7$, $\kappa_2 = 10^7$.

This problem was solved by means of the multigrid method. In the numerical experiments, the F(2,2) cycle was employed based on collective alternating line Gauss-Seidel relaxation.

Comparison of the solvers $M(P^{lin}, R^{lin})$, $M(P^{op}, R^{lin})$, $M(P^{lin}, R^{op})$, and $M(P^{op}, R^{op})$, applied to this problem, was performed. The results of comparison are summarized in Table 4.1. Note that in this table, e.g., grid $16 \times 16 \times 16$ means that in the sub-grids of the staggered grid ω^u, ω^v, ω^w, ω^p values $N_1 = N_2 = N_3 = 17$. As one can see from the results, it is enough to use only problem-

Grid	$M(P^{lin}, R^{lin})$	$M(P^{op}, R^{lin})$	$M(P^{lin}, R^{op})$	$M(P^{op}, R^{op})$
$8 \times 8 \times 8$	*diverges*	0.16(9)	0.13(8)	0.12(8)
$16 \times 16 \times 16$	*diverges*	0.13(9)	0.12(8)	0.11(8)
$32 \times 32 \times 32$	*diverges*	0.09(7)	0.09(7)	0.08(7)
$64 \times 64 \times 64$	*diverges*	0.06(6)	0.07(7)	0.06(6)

Table 4.1: Example 1: Convergence factor ρ^n and number of multigrid iterations (in brackets) for the multigrid solvers.

dependent restriction or only problem-dependent prolongation. In the case of both standard (trilinear) prolongation and restriction, the multigrid solver does not converge (for the comparison of it with $M(R^{op}, P^{op})$ see Figure 4.7).
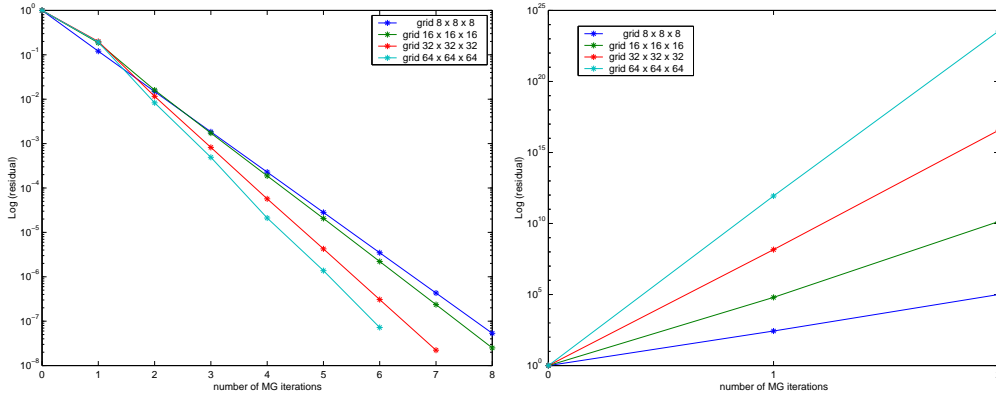

Figure 4.7: Example 1: convergence of the solver $M(R^{op}, P^{op})$ (left), of the solver $M(R^{lin}, P^{lin})$ (right).

Note that multigrid solvers $M(P^{op}, R^{lin})$, $M(P^{lin}, R^{op})$, and $M(P^{op}, R^{op})$ are robust with respect to the size of the jumps in the coefficients, but their convergence can slightly vary for different interface positions.

4.2.2 Example 2: simulation for a real problem

Consider the two-layered porous medium saturated with incompressible fluid ($\beta = 0$). Local load is applied on the upper surface of the medium on the square $[x_1; x_2] \times [y_1; y_2]$. The upper and lower surfaces of the medium are free to drain, and lateral walls are rigid and impermeable. As a result of the applied load, the porous medium deforms and fluid flows through the layers.

The following boundary conditions correspond to this situation: on the lower surface ($z = 0$) $\mathbf{S}^n = 0$ and $p = 0$; on the lateral surfaces ($x = 0$ or $x = 1$ or $y = 0$ or $y = 1$) $\mathbf{u} = 0$ and $\mathbf{V}^n = 0$; on the upper surface ($z = 1$) $S^n = \mathbf{S}^{loc}$, if $(x, y) \in [x_1; x_2] \times [y_1; y_2]$, and $\mathbf{S}^n = 0$ otherwise, and $p = 0$. $\mathbf{S}^n$ and $\mathbf{V}^n$ designate here normal stress tensor component and normal fluid velocity component respectively with respect to the corresponding surfaces, and $\mathbf{S}^{loc}$ is the applied load.

We solve this problem in the domain $[0; 1] \times [0; 1] \times [0; 1]$. The following parameters of the porous layers, separated by the interface $\xi = 0.499$ were considered – the lower layer: $\lambda_1 = 10^4$, $\mu_1 = 10^4$, $\kappa_1 = 10^{-1}$; the upper layer: $\lambda_2 = 1$, $\mu_2 = 1$, $\kappa_2 = 10^{-4}$. As one can see from the parameters, the upper porous layer is softer, but less permeable than the lower one. The vertical local load of the value 5 is applied on the square $[0.15; 0.25] \times [0.15; 0.25]$. The time interval is $[0; 1]$, and we only use one time step.

This problem was solved by the $F(2, 1)$ - cycle on the different grids. Convergence results are presented in Table 4.2.

As in the Example 1, multigrid solver based on both standard restriction and prolongation does not converge. The comparison with $M(R^{op}, P^{op})$ is shown at Figure 4.8. Some of the calculated physical characteristics of the process (in the

Grid	$M(P^{lin}, R^{lin})$	$M(P^{op}, R^{lin})$	$M(P^{lin}, R^{op})$	$M(P^{op}, R^{op})$
$16 \times 16 \times 16$	diverges	0.15(10)	0.21(10)	0.12(9)
$32 \times 32 \times 32$	diverges	0.20(10)	0.23(10)	0.13(9)
$64 \times 64 \times 64$	diverges	0.24(10)	0.32(10)	0.08(8)

Table 4.2: Example 2: Convergence factor ρ^n and number of multigrid iterations (in brackets) for the multigrid solvers.

corresponding cross-sections) are presented in Figures 4.9 - 4.12. The calculations for these figures were done on the grid $32 \times 32 \times 32$.
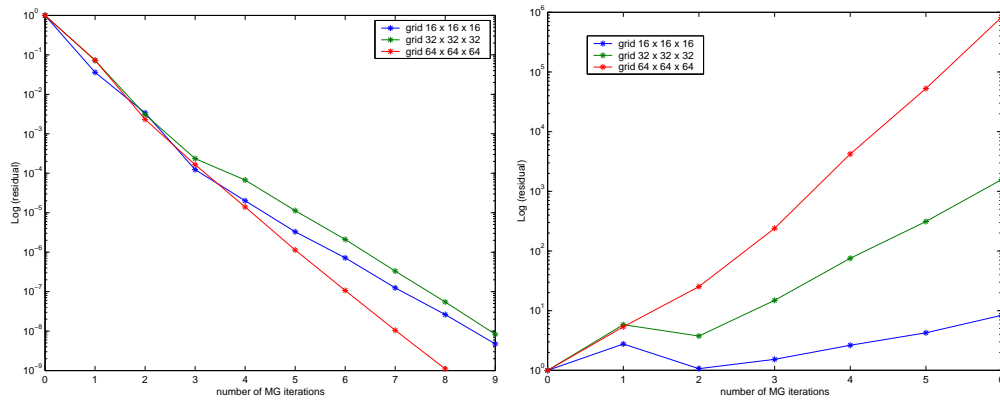
Figure 4.8: Example 2: Convergence of the solver $M(R^{op}, P^{op})$ (left), of the solver $M(R^{lin}, P^{lin})$ (right).

Figure 4.9 shows the fluid pressure values for the different cross-sections: the first cross-section intersects the local load and the second one does not. It is natural that values of the fluid pressure are larger directly under the load, than at some distance from it.
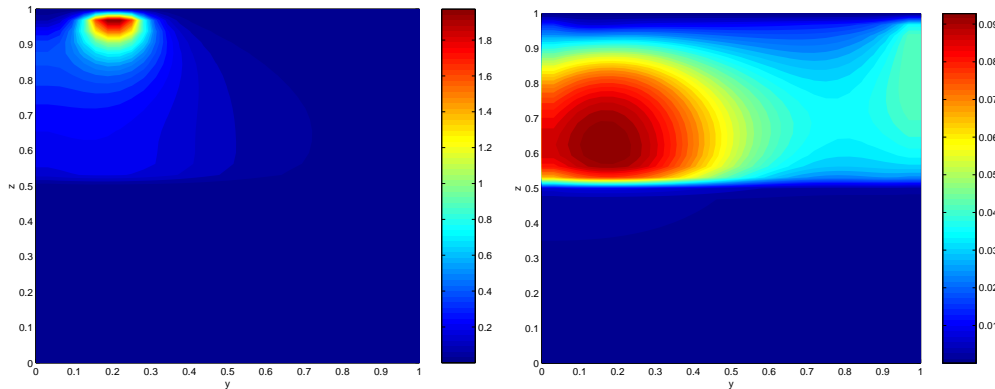

Figure 4.9: Example 2: Pressure of the fluid in the cross-section $x = 0.1875$ (left), in the cross-section $x = 0.53125$ (right).

In Figure 4.10, vertical displacements are shown in the same cross-sections as the fluid pressure. The largest negative values for the vertical displacements are below the load (note that z-axe is oriented upward). Note also that small positive vertical displacement appears in some distance from the load near the upper boundary.

It is well known that values of the stress tensor components are very important in many real problems. Figures 4.11, 4.12 show the tensor stress component $S^{zz} = (\lambda + 2\mu)\, w_z + \lambda\, (u_x + v_y)$ in different vertical and horizontal cross-sections.
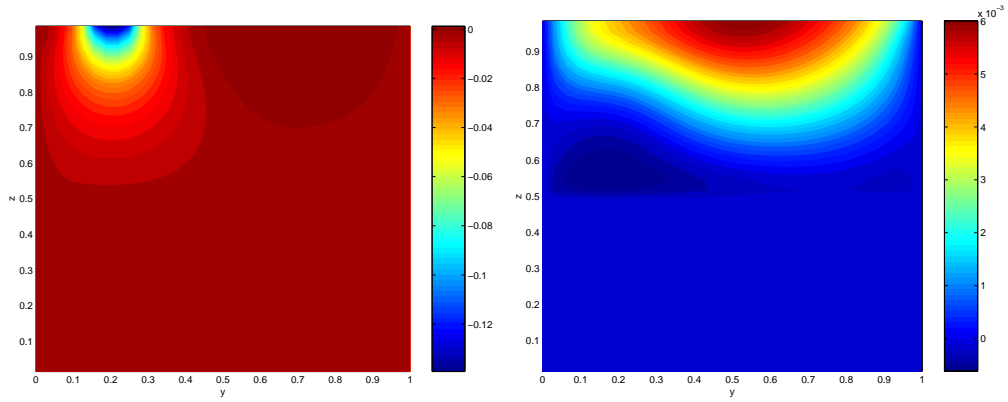
Figure 4.10: Example 2: Vertical displacement component in the cross-section $x = 0.1875$ (left), in the cross-section $x = 0.53125$ (right).
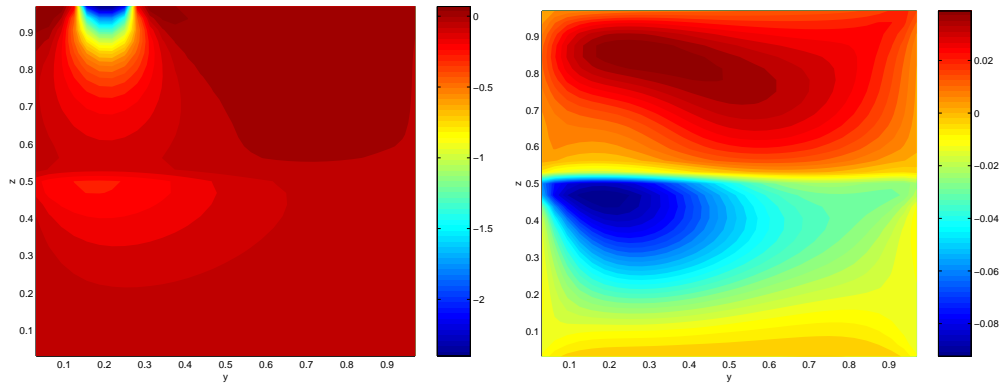

Figure 4.11: Example 2: Stress tensor component S^{zz} in the cross-section $x = 0.1875$ (left), in the cross-section $x = 0.53125$ (right).
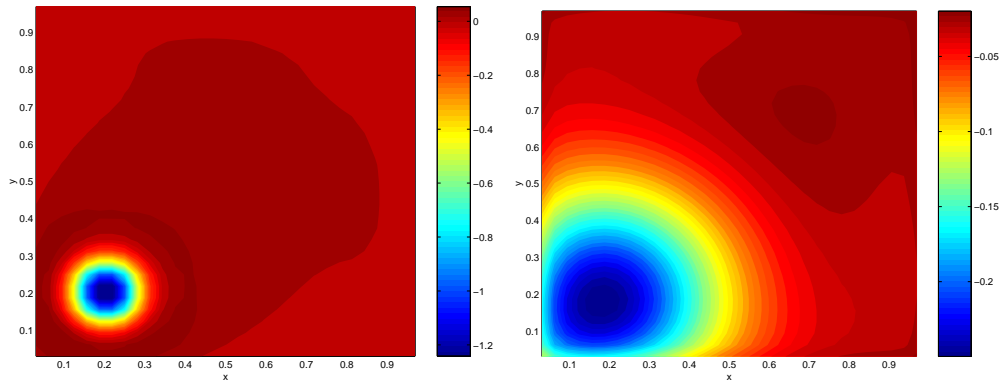

Figure 4.12: Example 2: Stress tensor component S^{zz} in the cross-section $z = 0.90625$ (left), in the cross-section $z = 0.5$ (right).

Conclusions

In this thesis, the quasi-static Biot poroelasticity system in bounded multilayered domain in one and three dimensions was studied.

In more detail, in the one-dimensional case, a finite volume discretization for the Biot system with discontinuous coefficients was derived. The discretization resulted in a difference scheme with harmonic averaging of the coefficients. Detailed theoretical analysis of the obtained discrete model was presented. Error estimates, which established convergence rates for both the pressure and the displacement unknowns were shown. Besides, modified and more accurate discretizations, which can be applied when the interface position coincides with a grid node, were obtained. These discretizations yielded second order convergence of the fluxes of the problem. Finally, a solver for the solution of the produced system of linear equations was developed, and extensively tested. A number of numerical experiments, which confirmed the theoretical considerations were performed.

In the three-dimensional case, the finite volume discretization of the system involved construction of special interpolating polynomials in the dual volumes. These polynomials were derived so that they satisfied the same continuity conditions across the interface, as the original system of PDEs. This technique allowed to obtain such a difference scheme, which provided accurate computation of the primary as well as of the flux unknowns (including the points adjacent to the interface). Numerical experiments, based on the obtained discretization, showed second order convergence for auxiliary problems with known analytical solutions.

A multigrid solver, which incorporated the features of the discrete model, was developed in order to solve efficiently the linear system, produced by the finite volume discretization of the three-dimensional problem. The crucial point was to derive problem-dependent restriction and prolongation operators. Such operators are a well-known remedy for the scalar PDEs with discontinuous coefficients. Here, these operators were derived for system of PDEs, taking into account interdependence of the different unknowns within the system. In the derivation, the interpolating polynomials from the finite volume discretization were employed again, linking thus the discretization and the solution processes.

The developed multigrid solver was tested on several model problems. Numerical experiments showed that, due to the proper problem-dependent prolongation and (or) problem-dependent restriction, the multigrid solver was robust with respect to the discontinuities of the coefficients of the system.

Finally, the poroelasticity system with discontinuous coefficients was used to model a real problem. The Biot model, describing this problem, was treated numerically, i.e., discretized by the developed finite volume techniques and then solved by the constructed multigrid solver. Physical characteristics of the process, such as displacement of the skeleton, pressure of the fluid, components of the stress tensor, were calculated and then presented at certain cross-sections.

List of notations

Below, some the the used notations are listed. They are subdivided into the three groups –namely, notations, which are common throughout the whole manuscript, notations for the one-dimensional case (i.e., for Chapter 2) and notations for the three-dimensional case (i.e., for Chapters 3, 4).

Common notations

f	right hand side of the diffusion equation
n	index indicating discretization in time
M	number of steps in time
L	characteristic length of the domain
p	fluid pressure
$\mathbf{S}$	stress tensor
t	time
T	characteristic size of the time interval
$\mathbf{u}$	displacement vector
$\mathbf{V}$	Darcy velocity vector
$\mathbf{x}$	position vector
β	compressibility of the fluid
Γ	boundary of the domain Ω
Γ_I	interface
ϵ_α	error of the variable α, $\alpha = \{u, v, \text{etc.}\}$
η	viscosity of the fluid
θ	parameter, indicating respective position of the interface
κ	permeability
λ	dilation modulus
μ	shear modulus
ξ	interface position
σ	weight parameter in time discretization

τ discretization time step

ϕ porosity

ω^α grid for the unknown α, $\alpha = \{u, v, w, p\}$

Ω domain of consideration

Notations, used in Chapter 2

A discrete elasticity operator

B discrete diffusion operator

D discrete divergence operator

G discrete gradient operator

h grid step size

i index indicating discretization in space

i_{int} index indicating the relative interface position

N number of grid nodes

ν non-dimensional analogue of $\lambda + 2\mu$.

ψ truncation error

Notations, used in Chapters 3, 4

e_α correction to the unknown α, $\alpha = \{u, v, w, p\}$

h_α grid step size in direction α, $\alpha = \{x, y, z\}$

$\mathbf{I}$ unit tensor

i, j, k indices indicating discratization in x-, y- and z- direction respectively

k_{int} index in z-direction, indicating the interface position

$\mathbf{n}$ normal vector

N_α numer of grid nodes in direction α, $\alpha = \{x, y, z\}$

U, V, W, P interpolating polynomials for unknowns u, v, w and p respectively

P_α prolongation operator for unknown α, $\alpha = \{u, v, w, p\}$

r_α residual of the α-th equation, $\alpha = \{1, 2, 3, 4\}$

R_α restriction operator for the residual r_α, $\alpha = \{1, 2, 3, 4\}$

(u, v, w) components of the displacement vector

$\mathbf{V}^\alpha$ control volume, $\alpha = \{u, v, w, p\}$

(x, y, z) components of the position vector

Bibliography

[1] R. E. Alcouffe, A. Brandt, Jr. J. E. Dendy, and J. W. Painter. *The multi-grid method for the diffusion equation with strongly discontinuous coefficients.* SIAM J. Stat. Comput., pages 430–454, 2(4), 1981.

[2] J-L. Auriault and E. Sanchez-Palencia. *Etude du comportement macroscopique d'un milieu poreux saturé déformable.* Journal de Mécanique, pages 575–603, 16, 1977.

[3] T. Badmus, A. H.-D. Cheng, and S. Grilli. *A Laplace-transform-based three-dimensional BEM for poroelasticity.* Int. J. Numer. Meth. Engng., pages 67–85, 36(1), 1993.

[4] S. I. Barry and G. K. Aldis. *Comparison of models for flow induced deformation of soft biological tissue.* Australian defense force academy, Canberra, 1996.

[5] S. I. Barry and G. N. Mercer. *Deformation and fluid flow due to a source in a poroelastic layer.* Appl. Math. Modelling, pages 681–689, 21, 1997.

[6] S. I. Barry and G. N. Mercer. *Flow and deformation in poroelasticity-II. Numerical method.* Mathematical and computer modelling, pages 31–38, 30, 1999.

[7] S. I. Barry and G. N. Mercer. *Flow and deformation in poroelasticity-I. Unusual exact solutions.* Mathematical and computer modelling, pages 23–29, 30, 1999.

[8] S. I. Barry and G. N. Mercer. *Exact solutions for two dimensional time dependent flow and deformation within a poroelastic medium.* ASME J. Appl. Mechanics, pages 536–540, 66, 1999.

[9] S. I. Barry, G. N. Mercer, and C. Zoppou. *Approximate and analytic solutions for deformation of finite porous filters.* ASME J. Applied Mechanics, pages 929–934, 64, 1997.

[10] J. Bear and Y. Bachmat. *Introduction to modelling of transport Phenomena in Porous Media*. Kluwer Academic, Dordrecht, 1990.

[11] J. Bear and A. Verruijt. *Modelling groundwater flow and pollution*. Kluwer Academic, Dordrecht, 1987.

[12] M. Biot. *General theory of three dimensional consolidation*. J. Appl. Phys., pages 155–169, 12, 1941.

[13] M. Biot. *General solutions of the equations of elasticity and consolidation for a porous material*. J. Appl. Mech., Trans. ASME, pages 91–96, 78, 1956.

[14] J. R. Booker and J. C. Small. *Finite layer analysis of consolidation, part 1*. International Journal for Numerical and Analytical Methods in Geomechanics, pages 151–171, 6, 1982.

[15] R. M. Bowen. *Compressible porous media models by use of the theory of mixtures*. International Journal of Engineering Science, pages 697–735, 1973.

[16] J. H. Bramble. *Multigrid methods*. John Wiley, New York, 1993.

[17] A. Brandt. *Multilevel adaptive technique (MLAT) for fast numerical solution of boundary value problems*. Proc. third Int. Conf. Num. Meth. in Fluid Mech., pages 82–89, 1973.

[18] R. Burridge and J. B. Keller. *Poroelasticity equations derived from microstructure*. J. Acoust. Soc. Am., pages 1140–1146, 70, 1981.

[19] G. J. Chen. *Consolidation of multilayered half space with anisotropic permeability and compressible constituents*. Int. J. Solids Struct., pages 4567–1586, 41, 2004.

[20] A. H.-D. Cheng and E. Detournay. *A direct boundary element method for place strain poroelasticity*. Int. J. Num. Anal. Meth. Geomech., pages 551–572, 12, 1988.

[21] A. H.-D. Cheng and J. A. Liggett. *Boundary integral equation method for linear porous-elasticity with applications to soil consolidation*. Int. J. Numer. Meth. Engng., pages 255–278, 20, 1984.

[22] Y. K. Cheung and L. G. Tham. *Numerical solutions for Biot's consolidation of layered soil*. J. Eng. Mech. Div., ASCE, pages 669–679, 1983.

[23] T. Clees. *AMG Strategies for PDE systems*. PhD Thesis, Univercity of Köln, 2005.

[24] S. C. Cowin. *Bone poroelasticity.* Journal of Biomechanics, pages 217–238, 32, 1999.

[25] G. F. Dargush and P. K. Banerjee. *A time domain boundary element method for poroelasticity.* Int. J. Num. Meth. Eng., pages 2423–2449, 28, 1989.

[26] R. Ewing, O. Iliev, and R. Lazarov. *A modified finite volume approximation of second order elliptic equations with discontinuous coefficients.* SIAM J. Sci. Comp., pages 1334–1350, 23(4), 2001.

[27] R. Ewing, O. Iliev, R. Lazarov, and A. Naumovich. *On convergence of certain finite volume difference discretizations for 1-D poroelasticity interface problems.* Int. J. Num. Meth. PDEs, to appear.

[28] R. Ewing, Zh. Li, T. Lin, and Ya. Lin. *The immersed finite volume element methods for the elliptic interface problems.* Math. Comput. Simul., pages 63–76, 50, 1999.

[29] R. Fedkiw. *The Ghost Fluid Method for Discontinuities and Interfaces.* Godunov Methods, Kluwer, New York, pages 309–317, 2001.

[30] R. P. Fedorenko. *A speed of convergence of one iterative process.* USSR, Comput. Math. and Math. Phys.,, pages 1092–1096, 1964.

[31] A. J. H. Frijns, E. F. Kaasschieter, and J. M. Huyghe. *Numerical modelling of cartilage as a deformable porous medium.* IUTAM symposium on Theoretical and Numerical Methods in Continuum Mechanics of Porous Materials, pages 99–104, 2001.

[32] F. J. Gaspar, F. J. Lisbona, C. W. Oosterlee, and R. Wienands. *A systematic comparison of coupled and distributive smoothing in multigrid for the poroelasticity system.* Num. Lin. Algebra Appl., pages 93–113, 11, 2004.

[33] F. J. Gaspar, F. J. Lisbona, and P. N. Vabischevich. *A numerical model for radial flow through porous and deformable shells.* CMAM, pages 34–47, 1(4), 2004.

[34] F. J. Gaspar, F. J. Lisbona, and P. N. Vabischevich. *A finite difference analysis of Biot's consolidation model.* Appl. Num. Math., pages 487–506, 44, 2003.

[35] M. Griebel, D. Oeltz, and M. A. Schweitzer. *An algebraic multigrid method for linear elasticity.* SIAM J. Sci. Comput., pages 385–407, 2, 2003.

[36] B. Gurevich and M. Schoenberg. *Interface conditions for Biot's equations of poroelasticity.* J. Acoust. Soc. Am., pages 2585–2589, 105(5), 1999.

[37] O. Iliev. *Finite volume discretizations for elliptic problems with discontinuous coefficients.* Habilitation, University of Kaiserslautern, 2002.

[38] S. Jourine, P. P. Valko, , and A. K. Kronenberg. *Modelling poroelastic cylinder experiments with realistic boundary conditions.* Int. J. Numer. Anal. Meth. Geomech., pages 1189–1205, 28, 2004.

[39] E. F. Kaasschieter and A. J. H. Frijns. *Squeezing a sponge: a three-dimensional analytic solution in poroelasticity.* Comp. GeoSc., pages 49–59, 7, 2003.

[40] J.-M. Kim and R. R. Parizek. *Three-dimensional finite element modelling for consolidation due to groundwater withdrawal in a desaturating anisotropic aquifer system.* Int. J. Numer. Anal. Meth. Geomech., pages 549–571, 23, 1999.

[41] S. Knapek. *Matrix-dependent multigrid homogenization for diffusion problems.* SIAM J. Sci. Comput., pages 515–533, 20(2), (1998).

[42] J. Korsawe and G. Starke. *A Least-Squares mixed finite element method for Biot's consolidation problem in porous media.* SIAM Journal on Numerical Analysis, pages 318–339, 43(1), 2005.

[43] R. W. Lewis and B. A. Schrefler. *The finite element method in the static and dynamic deformation and consolidation of porous media.* John Wiley, Chichester, 1998.

[44] Zh. Li and K. Ito. *Maximum principle preserving schemes for interface problems with discontinuous coefficients.* SIAM J. Sci. Comput., pages 339–361, 23, 2001.

[45] K. Lipnikov. *Numerical methods for the Biot model in poroelasticity.* PhD Thesis, Univercity of Houston, 2002.

[46] J. McNamee and R. E. Gibson. *Displacement functions and linear transforms applied to diffusion through porous elastic media.* Q. J. Mech. Appl. Math., pages 98–111, 13, 1960.

[47] M. A. Murad and J. H. Cushman. *Multiscale flow and deformation in hydrophilic swelling porous media.* Internat. J. Engrg. Sci., pages 313–338, 34, 1996.

[48] M. A. Murad and A. F. D. Loula. *On stability and convergence of finite element approximations of Biot's consolidation problem.* Internat. J. Numer. Methods Engrg., pages 645–667, 37, 1994.

[49] A. Naumovich, O. Iliev, F. Gaspar, F. Lisbona, and P. Vabishchevich. *On numerical solution of 1-D poroelasticity equations in a multilayered domain.* Mathematical Modelling and Analysis, pages 287–304, 10(3), 2005.

[50] N. Nishimura and S. Kobayashi. *A boundary integral equation method for consolidation problems.* Int. J. Solids Structures, pages 1–21, 25, 1989.

[51] K. K. Phoon, K. C. Toh, S. H. Chan, and F. H. Lee. *An Efficient Diagonal Preconditioner for Finite Element Solution of Biot's Consolidation Equations.* International Journal for Numerical Methods in Engineering, pages 377–400, 55(4), 2002.

[52] I. C. Pyrah. *One-dimensional consolidation of layered soils.* Geotechnique, pages 555–560, 3(46), 1996.

[53] J. R. Rice and M. P. Cleary. *Some basic stress-diffusion solutions for fluid saturated elastic porous media with compressible constituents.* Rev. Geophys. Space Phys., pages 227–241, 14, 1976.

[54] A. A. Samarskii. *Theory of difference schemes.* Pure and Applied Mathematics, Marcel Dekker, New York, 2001.

[55] A. A. Samarskii, P. N. Vabischevich, and P. P. Matus. *Difference schemes with operator factors.* Minsk, 1998.

[56] M. Schanz. *On the equivalence of linear Biot's theory and the linear theory of porous media.* 16th ASCE Engineering mechanics conference, Seattle, 2003.

[57] A. P. S. Selvadurai. *Mechanics of poroelastic media.* Kluwer academic publishers, Dordrecht, 1996.

[58] R. E. Showalter. *Diffusion in poro-elastic media.* J. Math. Anal. Appl., pages 310–340, 251, 2000.

[59] K. Stüben. *An introduction to algebraic multigrid.* GMD report 70. Fraunhofer SCAI, Sankt Augustin, Germany, Nov. 1999.

[60] X.-W. Tang and K. Onitsuka. *Consolidation of double-layered ground with vertical drains.* Int. J. Numer. Anal. Meth. Geomech., pages 1449–1465, 25, 2001.

[61] K. Terzaghi. *Die berechnung der durchlassigkeitsziffer des tones aus dem verlauf der hydrodynemischen spannungserscheinungen.* Sitz. Akad. Wissen., Wien Math. Naturwiss. Kl., pages 105–124, 132(IIa), 1923.

[62] U. Trottenberg, C. W. Oosterlee, and A. Schüller. *Multigrid.* Academic Press, New York, 2001.

[63] H. F. Wang. *Theory of linear poroelasticity with application to geomechanics and hydrogeology.* Princeton University Press, Princeton, 2000.

[64] P. Wesseling. *An introduction to multigrid methods.* John Wiley, Chichester, 1992.

[65] A. Wiegmann and K. Bube. *The Explicit Jump Immersed Interface Method: Finite Difference Methods for PDE with piecewise smooth solutions.* SIAM J. on Numerical Analysis, pages 827–862, 37, 2000.

[66] R. Wienands, F. J. Gaspar, F. J. Lisbona, and C. W. Oosterlee. *An efficient multigrid solver based on the distributive smoothing for poroelasticity equations.* Computing, pages 99–119, 73(2), 2004.

[67] P. M. De Zeeuw. *Matrix-dependent prolongations and restrictions in a black-box multigrid solver.* J. Comput. Appl. Math., pages 1–27, 33, 1990.

[68] G. Zhu and J.-H. Yin. *Finite element consolidation analysis of soils with vertical drain.* Int. J. Numer. Anal. Meth. Geomech., pages 337–366, 24, 2000.

CURRICULUM VITAE

5 Dec. 1980	Born in Minsk, Belarus
1987 – 1995	Secondary School
1995 – 1998	Lyceum of the Belarussian State University, Department of Mathematics
1998 – 2003	Belarussian State University, Faculty of Applied Mathematics and Computer Science, Department of Applied Mathematics
Jun. 2003	Diploma in Mathematics
2003 – 2006	Doctorate studies at the University of Kaiserslautern, Department of Mathematics and Fraunhofer Institute for Industrial Mathematics (Fraunhofer ITWM)